ÉCOLE DE TECHNOLOGIE SUPÉRIEURE
UNIVERSITÉ DU QUÉBEC

A THESIS SUBMITTED TO
ÉCOLE DE TECHNOLOGIE SUPÉRIEURE

IN FULFILLMENT OF THE REQUIREMENTS
FOR THE DEGREE OF MASTER
IN MECHANICAL ENGINEERING
M. Eng.

BY
JA HO SEO

DEVELOPMENT OF ADVANCED ALGORITHMS FOR DISPLACEMENT, VELOCITY AND PRESSURE CONTROL OF ELECTRO-HYDRAULIC SYSTEMS

MONTRÉAL, APRIL 5, 2006

THIS THESIS HAS BEEN EVALUATED
BY A JURY COMPOSED OF:

M. Jean-Pierre Kenné, director of research
Mechanical Engineering Department at École de technologie supérieure

M. Ravinder Venugopal, co-director of research
President of Sysendes Inc.

M. Antoine Tahan, professor and president of the jury
Mechanical Engineering Department at École de technologie supérieure

M. Martin Viens, member of the jury
Mechanical Engineering Department at École de technologie supérieure

THIS THESIS WAS DEFENDED BEFORE THE JURY AND PUBLIC
ON MARCH 1, 2006
AT ÉCOLE DE TECHNOLOGIE SUPÉRIEURE

ALGORITHMES AVANCÉS DE COMMANDE DU DÉPLACEMENT, DE LA VITESSE ET DE LA PRESSION DES SYSTÈMES ÉLECTROHYDRAULIQUES

Ja Ho Seo

Sommaire

Les systèmes hydrauliques sont largement utilisés dans plusieurs secteurs industriels, particulièrement dans les applications qui exigent des forces ou des couples élevés. Bien que ces systèmes hydrauliques aient des composantes mécaniques relativement simples, ils sont pourtant caractérisés par des dynamiques non linéaires, plus spécifiquement, une relation en racine carrée entre la pression différentielle qui entraîne l'écoulement du fluide hydraulique et la vitesse de l'écoulement ou débit.

La plupart des contrôleurs industriels disponibles sur le marché utilise des commandes de type PID pour contrôler la force, la vitesse et le déplacement dans les systèmes hydrauliques. Cependant, leur performance est limitée à cause de la nature non-linéaire des ces systèmes.

Dans cette étude, nous choisissons la méthode de linéarisation de rétroaction de façon à surmonter les effets non linéaires inhérents au système. En utilisant cette théorie de commande non-linéaire, nous nous proposons de développer des contrôleurs avancés pour la commande du déplacement angulaire, de la vitesse angulaire et de la pression des actuateurs hydrauliques rotationnels. Parallèlement, nous nous proposons de valider la performance élevée des contrôleurs basés sur la linéarisation de rétroaction grâce à des essais de simulation et à des mesures expérimentales sur un banc d'essais hydrauliques.

DEVELOPMENT OF ADVANCED ALGORITHMS FOR DISPLACEMENT, VELOCITY AND PRESSURE CONTROL OF ELECTRO-HYDRAULIC SYSTEMS

Ja Ho Seo

Abstract

Hydraulic motion drives are widely used in several areas of industry, especially in applications that require high forces or torques. While typical hydraulic systems have relatively simple mechanical components, they are characterized by nonlinear dynamics, specifically, a square-root relationship between the differential pressure that drives the flow of the hydraulic fluid and the flow rate.

Most commercially available industrial controllers use PID control for force, velocity and displacement control in hydraulic systems; however, their performance is limited due to the nonlinear nature of these systems.

In this study, we use the technique of feedback linearization method to overcome the effects of the nonlinearity. Using this nonlinear control approach, we develop advanced controllers for angular displacement, angular velocity and pressure control of a rotational hydraulic drive, and test the performance of feedback linearization based controllers through simulation & experimental testing on a hydraulic test-bench.

RÉSUMÉ DU MÉMOIRE EN FRANÇAIS

Les actionneurs hydrauliques ont largement attiré l'attention de beaucoup de chercheurs dans le domaine de la commande en raison des avantages tels que la compacité, le rapport force/masse élevé et la précision. Cependant, la caractéristique non-linéaire du système hydraulique limite la performance du contrôleur, basé sur la méthode linéaire traditionnelle, comme PID, d'où une théorie avancée et robuste considérant la non-linéarité est nécessaire. La méthode de linéarisation de rétroaction pourrait être une alternative pour satisfaire ce besoin.

Dans notre étude, l'objectif principal de ce projet est de développer des algorithmes avancés pour la commande du déplacement, de la vitesse et de la pression des systèmes hydrauliques rotationnels en utilisant la théorie de linéarisation de rétroaction. En même temps, notre projet contribuera à la réalisation des objectifs spécifiques suivants :

- Développer un modèle mathématique décrivant la dynamique du système.
- Développer des algorithmes de commande (c.-à-d. contrôleur PID et contrôleur basé sur la linéarisation de rétroaction) en utilisant le modèle mathématique proposé.
- Implanter les algorithmes de commande du système développé sur un banc d'essai et comparer les performances des contrôleurs développés.

Pour réaliser les objectifs mentionnés ci-dessus, nous avons présenté les séquences et méthodes d'étude dans l'ordre suivant :

1. Description du système électrohydraulique

   Notre système de commande pour cette recherche se compose essentiellement de deux servo-valves électrohydrauliques, qui commandent le mouvement d'actionneur hydraulique et le couple de charge du système respectivement. L'huile est retournée au réservoir d'huile à la pression atmosphérique par la servovalve.

2. Développement d'un modèle mathématique permettant de représenter la dynamique du système étudié.

3. Le contrôleur PID adapté au système linéarisé sera conçu en appliquant la méthode de Ziegler-Nichols. Ce contrôleur PID sera appliqué respectivement au système linéarisé et non-linéaire pour la simulation. La simulation en boucle fermée dans deux conditions d'entrée en échelon unité et sinusoïdale sera faite par MATLAB/ Simulink. Les résultats obtenus par cette simulation en boucle fermée contribueront à identifier la performance limitée du contrôleur PID appliqué au système non-linéaire.

4. Le développement de chaque contrôleur pour la commande du déplacement angulaire, de la vitesse angulaire et de la pression de charge du système non-linéaire en utilisant la technique non-linéaire de type linéarisation de rétroaction. En outre, chaque contrôleur appliqué au système non-linéaire sera validé par la simulation en boucle fermée à l'aide de MATLAB/Simulink et sa comparaison avec le contrôleur PID de l'étape 3 sera effectuée en fonction de sa performance.

5. La commande en temps réel pour l'essai expérimental de chaque algorithme de commande (c.-à-d. commande de type PID et commande par linéarisation de rétroaction) proposé ci-dessus sera faite un utilisant le banc d'essai du LITP (Laboratoire d'intégration des technologies de production). Simultanément, le travail à l'étape 5 inclut la comparaison de la performance entre le contrôleur basé sur la linéarisation de rétroaction et le contrôleur PID.

Dans cette recherche, le principal processus parmi les procédures mentionnées ci-dessus est la comparaison de la performance de chaque contrôleur par les simulations de deux types faites aux étapes 4 et 5. Par cette comparaison, nous avons l'intention d'arriver à la conclusion que la stratégie de linéarisation de rétroaction est très adaptée pour concevoir un contrôleur avec la performance de poursuite plus élevée et stable pour la

commande du déplacement angulaire, de la vitesse angulaire et de la pression de charge du système hydraulique rotationnel en surmontant la limitation du contrôleur PID.

Pour l'organisation de cette thèse, mentionnons que cette recherche se compose de 4 principales parties.

Dans le chapitre 1, à travers une revue de littérature, nous donnons une idée générale et un aperçu sur l'état de l'art dans le domaine de recherche, axé sur la commande des systèmes électrohydrauliques.

Le deuxième chapitre nous permet de comprendre des systèmes asservis par la modélisation et explique comment installer l'environnement expérimental pour notre système électrohydraulique.

Dans le troisième chapitre, nous validerons la réponse de chaque système (c.-à-d. le déplacement angulaire, la vitesse angulaire et la différence de pression de la charge) après la linéarisation par la simulation en boucle ouverte avec MATLAB/Simulink. En outre, nous présentons la procédure pour développer le contrôleur PID par la méthode de Ziegler-Nichols et le contrôleur par la théorie de linéarisation de rétroaction. Les résultats comparatifs concernant la performance de poursuite de chaque contrôleur appliqué au système non-linéaire seront analysés par la simulation en boucle fermée avec MATLAB/Simulink.

Au quatrième chapitre, l'analyse comparative des performances de chaque contrôleur sera faite par la simulation en temps réel en utilisant le banc d'essai du LITP. Finalement, L'évaluation et la conclusion générale pour la stratégie non-linéaire appliquée dans notre étude seront présentées.

ACKNOWLEDGEMENTS

I would like to thank Dr. Jean-Pierre Kenné, my director for his sincere advice, helpful guidance, and devoted endeavor to provide me with the best environment for my research. I am also grateful to Dr. Ravinder Venugopal, my co-director for his systematic instruction and outstanding teaching regarding the theoretical and empirical approach to research. In addition, I thank Mr. Kaddissi who, in spite of his busy schedule, offered advice related to my experiment.

I would also like to thank Mr. Charlot for his friendship and heart felt consideration for my personal affairs as well as my academic studies. I equally give thanks for the camaraderie and help I have received from all members of LITP (Laboratoire d'intégration des technologies de production).

Without the steady understanding, devotion, support and constant love of my wife, Yun Hee Lee, it is needless to say that this accomplishment and honor could not have been imagined.

In addition, I deeply appreciate the encouragement, financial and spiritual support and unflagging trust of my parents, sisters and brother.

Finally, I would sincerely like to express my gratitude for my lord Jesus Christ, my dear Father and two Sisters of the Korean Community Catholic church.

TABLE OF CONTENTS

Page

LIST OF TABLES

Page

LIST OF FIGURES

Page

NOMENCLATURE

A_v	Servo-valve opening area, m^2
$A_{v\max}$	Maximum servo-valve opening area, m^2
B	Viscous damping coefficient, $N \cdot m \cdot s$
C_d	Flow discharge coefficient
C_{im}	Internal leakage coefficient, $(m^3/s)/(N/m^2)$
C_{em}	External leakage coefficient, $(m^3/s)/(N/m^2)$
C_L	Leakage coefficient, $(m^3/s)/(N/m^2)$
D_m	Volumetric displacement, m^3/rad
I	Servo-valve input current, mA
$I_{\max}$	Maximum servo-valve input current, mA
J	Inertia load, $N \cdot m \cdot s^2$
K_a	Servo-valve amplifier gain, V/mA
K_v	Servo-valve area constant, m^2/m
K_x	Servo-valve torque motor constant, m/mA
$P_{1,2}$	Pressures in actuator chambers, N/m^2
P_L	Load pressure difference, N/m^2
P_s	Supply pressure, N/m^2
$Q_{1,2}$	Flow rate in/out of actuator, m^3/s
Q_L	Load flow, m^3/s
Q_s	Maximum supply flow, m^3/s
T_L	Actuator load torque, $N \cdot m$
V	Actuator chamber volume, m^3

θ	Angular displacement, rad
ω	Angular velocity, rad/s
ω_h	Hydraulic natural frequency, rad/s
$\omega_{\max}$	Maximum angular velocity, rad/s
β	Fluid bulk modulus, N/m^2
ρ	Fluid mass density, Kg/m^3
τ_v	Servo-valve time constant, s

Dimensionless Quantities

c_{im}	Internal leakage coefficient
c_{em}	External leakage coefficient
c_L	Leakage load factor
i	Servo-valve input current
$p_{1,2}$	Pressures in actuator chambers
p_L	Load pressure difference
$q_{1,2}$	Flow rate in/out of actuator
q_L	Load flow
t_L	Load torque factor
x_v	Servo-valve opening area
α	Inertia load factor
γ	Viscous load factor
ϕ	Angular velocity

INTRODUCTION

■ Problem statement and objective of research

Hydraulic systems play an indispensable role in motion and force actuation in several fields of application, due to advantages like high power, fast dynamic response and high robustness.

However, in spite of these merits, hydraulic systems have intrinsic control problems. In other words, hydraulic systems include nonlinearities resulting from flow dynamics, as well as hysteresis, friction and leakage, which make the modeling of these systems challenging. We include some of these effects in our modeling for control system design.

Due to the nonlinear nature of these systems, traditional linear methods like PID control have limitations in achieving high precision control of displacement, velocity and force. To overcome these limitations, we formulate an approach based on nonlinear theory.

Among the nonlinear strategies, the technique of feedback linearization is a viable approach to address problems induced by a certain class of system nonlinearities, by transforming a nonlinear system into an equivalent linear system by canceling out nonlinear terms.

In our study, the principal objective is to develop theoretical algorithms for angular displacement, angular velocity and pressure control of a rotational hydraulic drive with this nonlinear control technique. At the same time, our project will achieve the specific objectives of:

- Development of a mathematical model describing the system dynamics

- Development of control algorithms (i.e., PID controller and feedback linearization based controller) using the mathematical model that we develop
- Implementation of the control algorithms on a test bench, and comparison of the performance of each control algorithm

■ Methodology

In this study, the sequence and method are as follows:

1. Description of the electro-hydraulic control system
   The plant essentially consists of two electro-hydraulic servo-valves, one controlling the motion of the hydraulic motor and the other controlling the load torque of system. The oil is returned through the servo-valve to the oil tank at atmospheric pressure.

2. Development of a mathematical model of the electro-hydraulic system (i.e., a fourth order state space model) to represent the system dynamics.

3. Design of a PID controller based on a linearized model of our nonlinear system and application of Ziegler-Nichols tuning rules. This designed PID controller will be applied to both the linearized and nonlinear system for simulation. The closed-loop simulation using unit step and sinusoidal inputs will be performed in MATLAB/ Simulink. The closed-loop simulation results will provide insight into the performance limitations of PID control when it is applied to the nonlinear system.

4. Development of controllers for angular displacement, angular velocity and load pressure control of the nonlinear system based on the nonlinear control-design technique of feedback linearization. To evaluate its performance and compare it with the performance of PID controller, each controller will be tested in a closed-

loop simulation using the nonlinear plant model. MATLAB/Simulink will be used to perform these simulations.

5. Real-time simulation for experimental testing of each control algorithm (i.e., PID control and feedback linearization based control) proposed above will be conducted on a test bench of LITP (Laboratoire d'intégration des technologies de production). The work in this step includes a performance comparison between each feedback linearization based controller and the corresponding PID controller.

The key steps in the procedures outlined above are the performance comparisons of each controller through the simulation and experiment in Steps 4 and 5. Using these comparisons, we show that the feedback linearization based control strategy provides stable and accurate tracking performance for angular displacement, velocity and load pressure control of the nonlinear rotational hydraulic drive, and also overcomes the performance limitations of PID control.

■ Organization of thesis

This thesis is organized in four parts.

In the first chapter, we present a comprehensive literature review, in which we will describe the typical features of electro-hydraulic servo-systems, the need for nonlinear theory and outline the approach for our research.

In the second chapter, we analyze the servo-system through modeling and describe the electro-hydraulic test bench used in our experiments.

In the third chapter, we perform a linearization based analysis of the system with respect to each output (i.e., angular displacement, angular velocity and load pressure difference)

using open-loop simulation in MATLAB/Simulink. We also describe the procedure to tune a PID controller using the Ziegler-Nichols method and then proceed to review feedback linearization theory for controller design. Finally, the comparative results of the tracking performance of each controller applied to the nonlinear system are analyzed using closed-loop simulation in MATLAB/Simulink.

In the fourth chapter, the comparative analysis of the performance of each controller is conducted on a test bench of LITP. We conclude by providing an overall assessment of our nonlinear control strategy.

CHAPTER 1

LITERATURE REVIEW

This chapter will first briefly describe the importance of electro-hydraulic servo-systems in modern industry, as well as the servo-system's unique characteristics from the perspective of control. Secondly, through a comprehensive literature review, we will describe the approach to develop control algorithms for displacement, velocity and differential pressure of electro-hydraulic servo-systems based on our understanding of the typical features of these systems.

1.1 Advantages and disadvantages of Electro-hydraulic servo-system

There are many applications of Electro-hydraulic servo-system (EHSS) in several industries, for example, the automotive, aerospace and industrial automation industries, where large forces and torque are required along with fast dynamic response. The reasons why electro-hydraulic systems play an essential role in modern industrial applications are principally based on specific features of these systems (e.g., a high power/mass ratio, fast response, high stiffness and load capability). To use these advantages of hydraulic systems and to meet current industrial requirements (i.e., robust control with high accuracy and fast response), control design for EHSS has become an active research area. However, the traditional approaches have limitations due to certain inherent characteristics of EHSS.

First, hydraulic systems include nonlinear elements that are difficult to model. Second, nonlinearities and parameter variations result in relatively complex plant behavior. Because of the inherently nonlinear nature of hydraulic systems, traditional linear control approaches cannot properly address the system's dynamics and thus have

limitations in terms of closed-loop performance. Therefore, the focus of our research is to apply a nonlinear control design technique to enhance controller performance.

1.2 Hydraulic drive control approaches

Although the control of a nonlinear system's outputs could be achieved through a general linearization, its control performance is only valid in the vicinity of the equilibrium operating point around which the system's equations are linearized. Thus, diverse approaches appropriate for nonlinear hydraulic systems have been introduced to go beyond traditional linear methods.

Among them, the Variable Structure Control (VSC) technique deals with nonlinear systems through a fast switching control. It forces the original nonlinear system to behave as a stable linear one and achieves accurate servo tracking and consistent performance. But, despite the use of methods such as the reaching law [1] and sliding mode control [2], the discontinuity in switching control of most traditional VSC techniques results in a chattering effect, which may excite undesirable high-frequency dynamics.

The Perturbation Observer based nonlinear control [3] is another method for force control. With this proposed observer, accuracy for force control can be achieved, but it does not require position and velocity feedback. This approach is not suitable for displacement and velocity control. However, it provides a low-cost option for force control, since it does not require displacement and velocity sensors.

In order to address the discontinuity of the system at certain operational boundaries, a force-dependent gain-schedule model and Linear Parameter Varying (LPV) approach are introduced in [4] for velocity and force control. While satisfactory force control can be

achieved using this method, overshoot problems due to dead time are observed for velocity control.

Recently, many approaches have been introduced using Lyapunov functions. The Lyapunov based approach by Liu and Alleyne [5] is focused on reducing parameter uncertainties for force and pressure tracking. Another method based on Lyapunov function analysis, Backstepping Control, is a very robust method which guarantees system stability as well as high output tracking performance. The studies in [6], [7] and [8] describe representative applications of this method.

The main idea of backstepping is to transform the nonlinear system into a chain of integrators, and to construct a candidate Lyapunov function in terms of the error (i.e., difference between a state variable and its desired value). The control signal for the system is calculated by ensuring that the time derivative of the Lyapunov function is negative definite. Thus, the system is made globally asymptotically stable and asymptotic tracking is ensured. The flexibility for design is an important advantage of backstepping, as it makes good use of useful non-linearities.

Reference [7] provides an idea of the procedure for a system's stabilization through backstepping. If internal states that are not directly related to the controlled outputs are stable, we can exclude them from the main procedure for stabilizing a system. This idea can also be applied and be very helpful to our approach using feedback linearization.

However, one major weakness of backstepping is the many complicated procedures required to find the Lyapunov function of the whole system and the system's control signal. Therefore, a great deal of time and the attention during each step is necessary. This is especially so for high-order systems. Moreover, because the method can lead to a relatively large number of control parameters to stabilize the system, the determination of appropriate control parameter values that meet physical constraints such as actuator

performance limits can be challenging. Due to these drawbacks of the backstepping approach, we adopt feedback linearization theory, which is better suited to our study.

The methods outlined here have their own strengths and weakness, but they all demonstrate that the application of nonlinear techniques is required for obtaining high performance control of hydraulic systems.

1.3 Feedback linearization approach

The feedback linearization approach incorporates auxiliary measurements of some system states, which are used in the inverse model for canceling the nonlinearities. In our case, measurements of the load's position, velocity and pressure are required, and since sensors for these variables have been installed in the system, we are able to apply this method. Feedback linearization is also a theoretically rigorous method, utilizing a linearizing control law and state transformation, which transform the open-loop nonlinear system into a linear system in the closed-loop. The ability to use linear control design techniques after transforming the system is one of the advantages of using feedback linearization for control of nonlinear systems.

However, feedback linearization requires some limited conditions to be satisfied by the original nonlinear system. Specifically, the internal dynamics of the system described using a special state transformation need to be stable for the system to be fully linearized by the feedback law. Our electro-hydraulic servo-system satisfies the condition of being feedback linearizable for displacement, velocity and pressure control.

Studies in [6] and [9] for controlling velocity of a servo-system are good examples of the application of feedback linearization, but these studies only consider the case of a positive ramp output reference. In our study, we will diversify the types of output reference (e.g., step and sinusoidal input with various frequency and amplitude).

Noting the strengths and limitations of the various methods described above, we propose the study of feedback linearization theory for control of a nonlinear hydraulic system and provide a performance comparison with the classical linear method, PID control.

1.4 Modeling and experimental setup

The first step of modeling prior to the experiment is to define the servo-system by its physical parameters and values. We base our modeling approach on that of [10] and [11], as the rotational hydraulic drive and experimental equipment used in their studies are identical to ours.

The key components of our servo-system are two servo-valves, of which one valve is for governing the motor of the hydraulics drive and the other is for controlling the load torque or resistance. These servo-valves are driven by the control signal generated from the controller designed in our research and a constant arbitrary load command signal. Detailed information regarding these servo-valves will be provided in section 2.1 and 4.2.

For developing a model to describe the system's characteristics, we use a 4^{th} order nonlinear state space model. The most conspicuous feature in our state space model is that with the exception of angular displacement, other variables, like angular velocity, pressure and servo-valve opening area, are non-dimensionalized. By dividing each variable by its own maximum value, we make all variables dimensionless, and thus reduce numerical errors in the simulation results. A detailed explanation on dimensionless variables follows in section 2.2.

Another point of interest related to modeling is the application of the sigmoid function utilized in [8]. In the state space equation for load pressure difference and the control signal equation obtained by feedback linearization, we replace the sign function with a

sigmoid function, to overcome the issues caused by the discontinuity and nondifferentiability of the sign function.

Although we follow the definition of parameters and use some of the values employed in [10], which describes the same electro-hydraulic system, other values are different from those in [10] because of different experimental conditions. We also use certain mathematical relationships between parameters to obtain precise parameter values instead of the approximated values utilized in [10].

1.5 Simulation and real-time control

As described in the methodology section, the comparison of simulation results between two controllers (i.e., PID and feedback linearization based controller) has significant meaning. Through this exercise, we can show the limited performance of PID control, which is widely utilized for industrial applications, and the excellent tracking ability of a controller designed by feedback linearization, a viable alternative that addresses the nonlinearities of the hydraulic system.

As comparative case studies, two types of simulation are used in our research. They include a fixed-step simulation in MATLAB/ Simulink and a real-time simulation on a test bench of LITP using a commercial real-time system, i.e., RT-LAB.

As presented in [12, 13] and [13], RT-LAB has been used wide for industrial applications (e.g., robot, engine control systems and etc.) because it has several features:

- First, it allows us to execute real-time simulations based on compatibility with MATLAB/Simulink. Therefore, it provides a very convenient environment to design models and run real-time simulations of these models without special learning and training for specific software.

- Second, it provides a graphical user interface that allows us to check the simulation results synchronously.
- Third, during the simulation, we can edit our model design and change parameter values without having to modify C code.

The physical configuration of the RT-LAB system is comprised of a host computer and a real-time target. Using RT-LAB software on the host computer, we design the model for real-time simulation, and control the execution of the simulation on the real-time target. The target executes the real-time code, reads sensor data, generates analog signals that drive the servo-valves and also plays the role of linking the host computer from which we operate the controller, to the hydraulic system.

Execution of RT-LAB real-time simulation models requires the following six steps:

- Creation of Simulink based model for real-time simulation
- Grouping the created model into subsystems (Master, slave and console subsystem)
- Separation of the model groups into sub-models and compilation of the models using the compile option in the RT-LAB Main Control console
- Loading the executable file by using the load option in the RT-LAB Main Control console
- Execution of real-time simulation
- Monitoring results and tuning parameters

CHAPTER 2

MODELING OF ELECTRO-HYDRAULIC SYSTEM

In this chapter, we describe the main components of the electro-hydraulic system and develop a mathematical model (i.e., state space model) representing the system dynamics. We also explain the linearization of the state equations about an equilibrium point from which we create a Simulink model of the linearized system for simulation, and design a PID controller.

2.1 Setup of Electro-Hydraulic System

The electro-hydraulic system for this research is shown in Figure 1. A DC electric motor drives the pump, which induces oil from the oil tank to be delivered to each component of system. The oil is used for the operation of the hydraulic actuator and is returned through the servo-valve to the oil tank at atmospheric pressure. An accumulator and a relief valve are used to maintain a constant pressure supply from the output of the pump. The electro-hydraulic system essentially consists of two servo-valves which control the movement of the hydraulic rotary actuator and the load torque of the system respectively. These servo-valves are operated by signals generated by the real-time target. Additional explanations regarding the operation of the servo-valves are provided in Chapter 4.

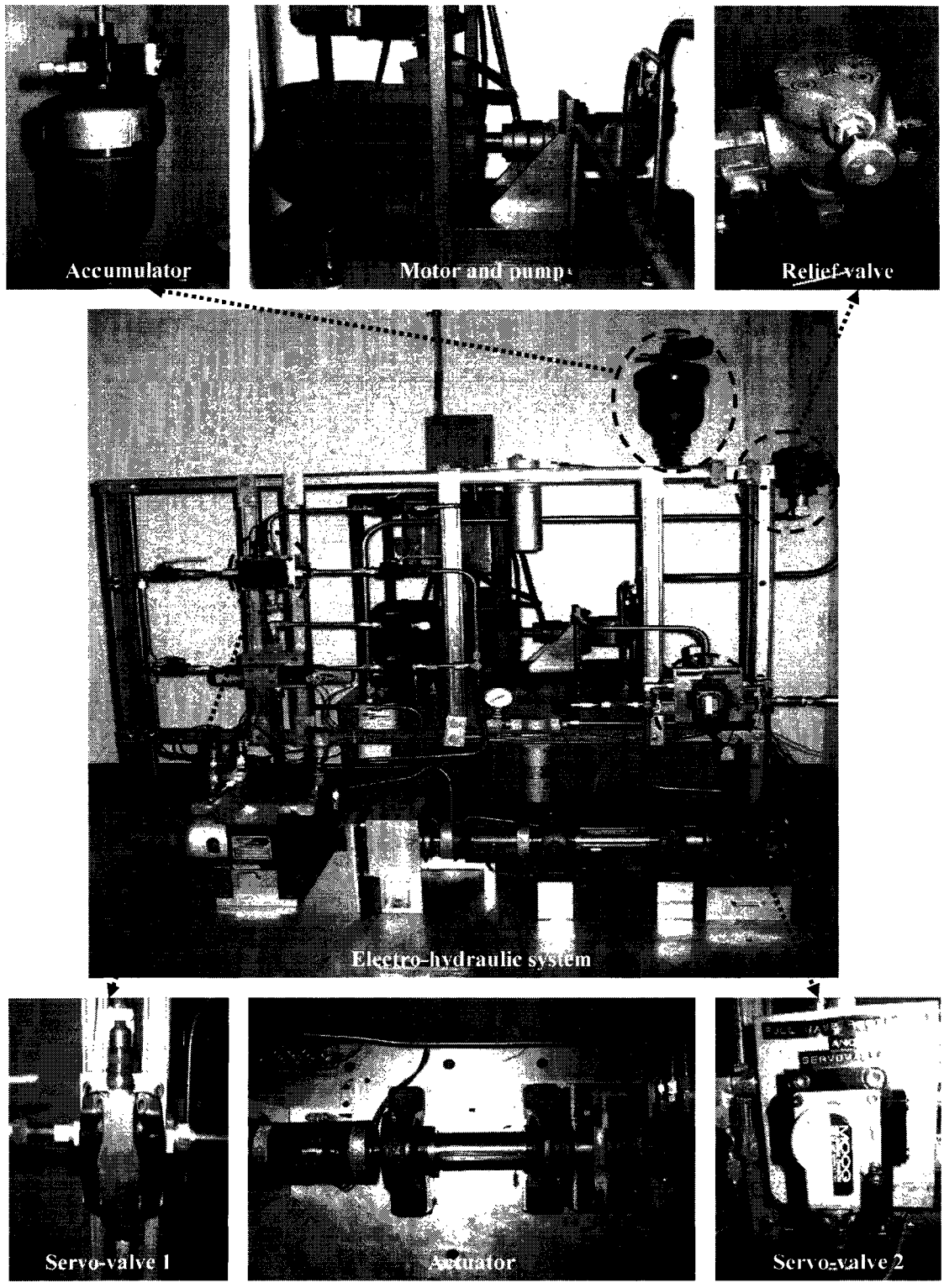

Figure 1 Configuration of Hydraulic System

2.2 Modeling of Electro-Hydraulic System

The modeling of the servo-system is based on the set-up shown in Figure 1 and equations from reference [10]. As discussed briefly in chapter 1, the introduction of several dimensionless variables (i.e., angular velocity, load pressure difference and servo-valve opening area except angular displacement) is needed in the mathematical description for modeling. These dimensionless variables can be obtained by dividing each variable by its own maximum value. Applying them reduces numerical errors during closed-loop simulation. Non-dimensionalizing the variables ensures that they are all in the same numerical range (i.e., 0 < range < 1).

In this section, we develop a mathematical model (i.e., state space model) with dimensionless variables, which describe the dynamics of our hydraulic system.

2.2.1 Servo-valve opening area and input command variables

All terms used for our modeling are defined in the nomenclature of this thesis.

For the input command required for simulation, a dimensionless current to the servo-valve is defined as follows:

$$i = \frac{I_i}{I_{\max}} .$$

The first-order differential equation for the actuator servo-valve is given by [10]

$$\tau_v \left(\frac{dA_v}{dt} \right) + A_v = K_x \cdot K_v \cdot I \ .$$

Dividing both sides of this equation by $K_x \cdot K_v \cdot I_{\max} (= A_{v\max})$, we arrive at an equation presenting the relationship between the dimensionless servo-valve opening area and input command variable,

$$\tau_v \left(\frac{dx_v}{dt} \right) + x_v = i \quad \text{where} \quad x_v = \frac{A_v}{A_{\max}}. \tag{2.1}$$

2.2.2 Load pressure difference variable

First, we need to define the dimensionless load pressure difference between the servomotor chamber pressures.

By definition,

$$p_L = p_1 - p_2 \quad \text{where} \quad p_L = \frac{P_L}{P_s}, \; p_{1,2} = \frac{P_{1,2}}{P_s} \tag{2.2}$$

From reference [10], as well as the assumption that the servo-valve is critically centered, and the orifices are matched and symmetrical, we define the dimensionless flow rate in each actuator chamber as

$$q_1 = \begin{cases} \sqrt{2} x_v \sqrt{1 - p_1} & \text{if} \quad x_v > 0 \\ \sqrt{2} x_v \sqrt{p_1} & \quad\;\; x_v < 0 \end{cases} \tag{2.3}$$

$$q_2 = \begin{cases} \sqrt{2} x_v \sqrt{p_2} & \text{if} \quad x_v > 0 \\ \sqrt{2} x_v \sqrt{1 - p_2} & \quad\;\; x_v < 0 \end{cases} \tag{2.4}$$

$$\text{Where} \quad q_{1,2} = \frac{Q_{1,2}}{Q_s}, \quad Q_s = C_d A_{v\max} \sqrt{P_s / \rho}$$

If the internal leakage inside the servo-valve can be neglected, we can assume $q_1 = q_2$ at steady-state. Because of the fact that servo-valves are matched and symmetric, this assumption can be applied in our model. Moreover, if the external leakage of the servomotor can also be neglected, we are able to set $q_1 = q_2$ even in the transient state. Such a condition is usually considered true, because the external leakage is practically negligible.

Therefore, using equations of (2.3) and (2.4), and the assumption, $q_1 = q_2$, it follows that

$$p_1 + p_2 = 1 \tag{2.5}$$

Using (2.2) and (2.5), we obtain

$$\begin{cases} p_1 = \dfrac{1 + p_L}{2} \\ p_2 = \dfrac{1 - p_L}{2} \end{cases} \tag{2.6}$$

Substituting the result of (2.6) into (2.3) and (2.4) yields

$$q_1 = \begin{cases} \sqrt{2} x_v \sqrt{\dfrac{1 - p_L}{2}} & \text{if} \quad x_v > 0 \\ \sqrt{2} x_v \sqrt{\dfrac{1 + p_L}{2}} & \quad x_v < 0 \end{cases}$$

$$q_2 = \begin{cases} \sqrt{2}x_v\sqrt{\dfrac{1-p_L}{2}} & \text{if} \quad x_v > 0 \\ \sqrt{2}x_v\sqrt{\dfrac{1+p_L}{2}} & \quad x_v < 0 \end{cases}$$

Therefore,

$$q_L = \begin{cases} x_v\sqrt{1-p_L} & \text{if} \quad x_v > 0 \\ x_v\sqrt{1+p_L} & \quad x_v < 0 \end{cases} \qquad \text{where} \quad q_L = \frac{Q_L}{Q_s} \quad \text{or} \quad q_L = \frac{q_1+q_2}{2}$$

or, for all conditions (i.e., positive and negative) of x_v

$$\begin{aligned} q_L &= x_v\sqrt{1-p_L(\frac{x_v}{|x_v|})} \\ &= x_v\sqrt{1-p_L sign(x_v)} \end{aligned} \tag{2.7}$$

From [10], the fluid dynamic equation in each actuator chamber can be expressed as follows.

For the first chamber:

$$Q_1 = \frac{V}{\beta}\frac{dP_1}{dt} + D_m\omega + C_{im}(P_1 - P_2) + C_{em}P_1$$

or,

$$\frac{V}{\beta}\frac{dP_1}{dt} = Q_1 - D_m\omega - C_{im}(P_1 - P_2) - C_{em}P_1$$

Re-arranging this equation, we obtain

$$\begin{aligned}\frac{dp_1}{dt} &= \frac{\omega_h \cdot \alpha}{2}(q_1 - \phi - \frac{c_{im}}{\alpha}(p_1 - p_2) - \frac{c_{em}}{\alpha} p_1) \\ &= \frac{\omega_h \cdot \alpha}{2}(\sqrt{2} x_v \sqrt{1 - p_1} - \phi - \frac{c_{im}}{\alpha}(p_1 - p_2) - \frac{c_{em}}{\alpha} p_1)\end{aligned} \tag{2.8}$$

$$\text{Where } \omega_h = \sqrt{2\beta D_m{}^2 / JV}, \quad c_{im} = \frac{JC_{im}\omega_h}{D_m{}^2}, \quad c_{em} = \frac{JC_{em}\omega_h}{D_m{}^2}$$

For the second chamber:

$$Q_2 = -\frac{V}{\beta}\frac{dP_2}{dt} + D_m\omega + C_{im}(P_1 - P_2) - C_{em}P_2$$

Using the same arrangement,

$$\frac{dp_2}{dt} = \frac{\omega_h \cdot \alpha}{2}(-\sqrt{2} x_v \sqrt{p_2} + \phi + \frac{c_{im}}{\alpha}(p_1 - p_2) - \frac{c_{em}}{\alpha} p_2) \tag{2.9}$$

Next, from equations (2.2), (2.3), (2.4), (2.7), (2.8) and (2.9), it follows that

$$\frac{dp_L}{dt} = \alpha\omega_h(q_L - \phi - \frac{c_L}{\alpha} p_L) \tag{2.10}$$

$$\frac{dp_L}{dt} = \alpha\omega_h(x_v \sqrt{1 - p_L sign(x_v)} - \phi - \frac{c_L}{\alpha} p_L) \tag{2.11}$$

$$\text{Where } c_L = c_{im} + \frac{c_{em}}{2} \quad \text{or} \quad c_L = \frac{JC_L\omega_h}{D_m{}^2}$$

2.2.3 Angular velocity variable

The torque-acceleration relationship of the actuator is given by [10]. Neglecting the frictional torque, the relationship is

$$J\frac{d\omega}{dt} = D_m(P_1 - P_2) - B\omega - T_L$$

By dividing the above equation by $J \cdot \omega_{\max}$, we obtain

$$\frac{d\phi}{dt} = \frac{\omega_h}{\alpha}(p_1 - p_2 - \gamma\phi - t_L) \tag{2.12}$$

Where $\phi = \frac{\omega}{\omega_{\max}}$, $\gamma = \frac{B\omega_{\max}}{P_s D_m}$, $t_L = \frac{T_L}{P_s D_m}$, $\alpha = \frac{J\omega_h\omega_{\max}}{P_s D_m}$, $\omega_{\max} = \frac{Q_s}{D_m}$

From equations (2.2) and (2.12), the dimensionless angular velocity is given by

$$\frac{d\phi}{dt} = \frac{\omega_h}{\alpha}(p_L - \gamma\phi - t_L) \tag{2.13}$$

2.2.4 Sigmoid function

In order to address the discontinuity introduced by the sign (x_v) function (Figure 2),

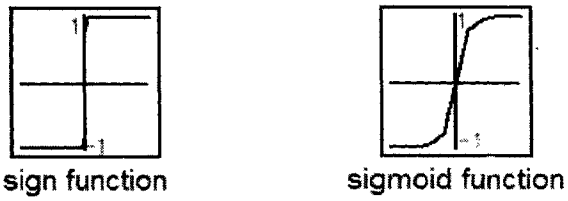

Figure 2 Comparison between sign and sigmoid function

We replace it with a sigmoid function, defined as

$$sigm(x) = \frac{1 - e^{-ax}}{1 + e^{-ax}} \tag{2.14}$$

From equation (2.14), we note that the sigmoid function is a continuously differentiable function, which has the following properties,

$$sigm(x) = \begin{cases} 1 & \text{if} \quad ax \to \infty \\ 0 & \text{if} \quad x = 0 \\ -1 & \text{if} \quad ax \to -\infty \end{cases} \qquad \text{where } a > 0 \tag{2.15}$$

Its derivative is given by

$$\frac{dsigm(x)}{dx} = \frac{2ae^{-ax}}{(1 + e^{-ax})^2} \tag{2.16}$$

Based on equations (2.15) and (2.16), we can plot the characteristic of the sigmoid function with the following graph,

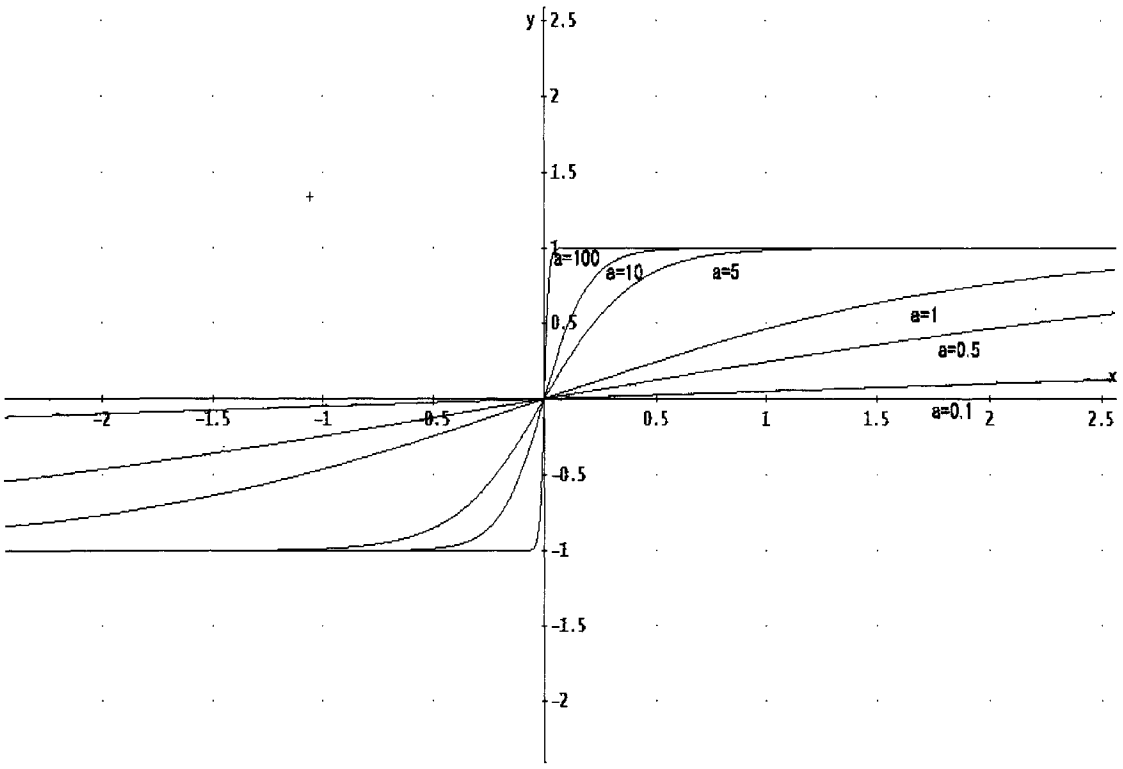

Figure 3 Graph of sigmoid function according to the variation of 'a' value

Here, we arbitrarily choose a=700 as a slope factor in order to approximate the sign function by the sigmoid function for simulation and experiment.

2.2.5 State Space Model

A state space model represents a physical system as n first order coupled differential equations. This form is better suited for computer simulation than an n^{th} order input-output differential equation and is an effective way to analyze the system's nonlinearities. These merits are the main reasons for a state space model to be chosen as a mathematical model to describe the dynamics of our system.

Here, we express our system using a state space model with the four first order differential equations derived earlier and the sigmoid function.

For the state space model, we set $x_1 = \theta$, $x_2 = \phi$, $x_3 = p_L$, $x_4 = x_v$ as state variables.

First, by rearranging equation (2.1), we obtain

$$\dot{x}_4 = -\frac{1}{\tau_v} x_4 + \frac{i}{\tau_v}$$

Next, by the applying equation (2.14) to (2.11) to replace the sign (x_v) function, we get

$$\dot{x}_3 = \alpha \omega_h x_4 \sqrt{1 - x_3 sigm(x_4)} - \alpha \omega_h x_2 - \omega_h c_L x_3$$

From equation (2.13), it follows that

$$\dot{x}_2 = \frac{\omega_h}{\alpha} x_3 - \gamma \frac{\omega_h}{\alpha} x_2 - \frac{\omega_h}{\alpha} t_L$$

Finally, using the relation between x_1 and x_2 yields

$$\dot{x}_1 = \omega_{\max} x_2$$

$$\text{Where } \phi = \frac{\omega}{\omega_{\max}} = \frac{\frac{d\theta}{dt}}{\omega_{\max}} \text{ or } x_2 = \frac{\dot{x}_1}{\omega_{\max}}$$

From the four state equations above, we obtain the following state space model:

$$\dot{X} = \begin{bmatrix} \dot{x}_1 \\ \dot{x}_2 \\ \dot{x}_3 \\ \dot{x}_4 \end{bmatrix} = \begin{bmatrix} f_1(x_1, x_2, x_3, x_4) \\ f_2(x_1, x_2, x_3, x_4, t_L) \\ f_3(x_1, x_2, x_3, x_4) \\ f_4(x_1, x_2, x_3, x_4, i) \end{bmatrix} = \begin{bmatrix} \omega_{\max} x_2 \\ -\gamma \frac{\omega_h}{\alpha} x_2 + \frac{\omega_h}{\alpha} x_3 - \frac{\omega_h}{\alpha} t_L \\ -\alpha\omega_h x_2 - \omega_h c_L x_3 + \alpha\omega_h x_4 \sqrt{1 - x_3 sigm(x_4)} \\ -\frac{1}{\tau_v} x_4 + \frac{i}{\tau_v} \end{bmatrix} \quad (2.17)$$

Where

For the state variable x

$$x_1 = \theta,\ x_2 = \frac{\omega}{\omega_{\max}} = \phi,\ x_3 = \frac{P_L}{P_S} = p_L,\ x_4 = \frac{A_{v\max}}{A_v} = x_v$$

For the command variable u

$$u_1 = i,\ u_2 = t_L$$

In (2.17), all variables except x_1 are dimensionless.

2.3 Linearization

From the state space model (2.17), we note that this system has a nonlinear characteristic because of the square root factor in the equation for $\dot{x}_3$.

Even though the system has a nonlinear characteristic, if the system operates around an equilibrium point, it is possible to approximate the nonlinear system by a linearized system.

In control engineering, the equilibrium point is typically considered to be a nominal operating point of the system. Therefore, the existence of the equilibrium point for the nonlinear system has a clear significance.

The first step in linearizing the nonlinear system is to determine its equilibrium point(s).

Let the equilibrium points be denoted by x_{10}, x_{20}, x_{30} and x_{40}.

At the equilibrium point, $\dot{x}$ must be 0.

From (2.17)

$$\dot{X} = \begin{bmatrix} \dot{x}_1 \\ \dot{x}_2 \\ \dot{x}_3 \\ \dot{x}_4 \end{bmatrix} = \left[\begin{array}{c} \omega_{\max} x_2 \\ -\gamma \dfrac{\omega_h}{\alpha} x_2 + \dfrac{\omega_h}{\alpha} x_3 - \dfrac{\omega_h}{\alpha} t_L \\ -\alpha\omega_h x_2 - \omega_h c_L x_3 + \alpha\omega_h x_4 \sqrt{1 - x_3 sigm(x_4)} \\ -\dfrac{1}{\tau_v} x_4 + \dfrac{i}{\tau_v} \end{array} \right]_{\substack{x_1 = x_{10} \\ x_2 = x_{20} \\ x_3 = x_{30} \\ x_4 = x_{40}}} = \begin{bmatrix} 0 \\ 0 \\ 0 \\ 0 \end{bmatrix}$$

From the equations above, we can easily find the equilibrium point of X (i.e., x_{10}, x_{20}, x_{30} and x_{40}).

$$X_{\text{equilibrium point}} = X_0 = \begin{bmatrix} x_{10} \\ x_{20} \\ x_{30} \\ x_{40} \end{bmatrix} = \begin{bmatrix} 0 \\ 0 \\ 0 \\ 0 \end{bmatrix} = 0$$

We now need the following Jacobian matrices in terms of x and u using Equation (2.17) to get a linearized system.

The Jacobian matrix in terms of x is given by

$$J_x = \left[\begin{array}{cccc} \frac{\partial f_1}{\partial x_1} & \frac{\partial f_1}{\partial x_2} & \frac{\partial f_1}{\partial x_3} & \frac{\partial f_1}{\partial x_4} \\ \frac{\partial f_2}{\partial x_1} & \frac{\partial f_2}{\partial x_2} & \frac{\partial f_2}{\partial x_3} & \frac{\partial f_2}{\partial x_4} \\ \frac{\partial f_3}{\partial x_1} & \frac{\partial f_3}{\partial x_2} & \frac{\partial f_3}{\partial x_3} & \frac{\partial f_3}{\partial x_4} \\ \frac{\partial f_4}{\partial x_1} & \frac{\partial f_4}{\partial x_2} & \frac{\partial f_4}{\partial x_3} & \frac{\partial f_4}{\partial x_4} \end{array}\right]_{\substack{x_1=x_{10} \\ x_2=x_{20} \\ x_3=x_{30} \\ x_4=x_{40}}} = \left[\begin{array}{cccc} 0 & \omega_{\max} & 0 & 0 \\ 0 & -\gamma\frac{\omega_h}{\alpha} & \frac{\omega_h}{\alpha} & 0 \\ 0 & -\alpha\omega_h & -\omega_h c_L & \alpha\omega_h \\ 0 & 0 & 0 & -\frac{1}{\tau_v} \end{array}\right]$$

Where

$$\left.\frac{\partial f_3}{\partial x_3}\right|_{\substack{x_1=x_{10} \\ x_2=x_{20} \\ x_3=x_{30} \\ x_4=x_{40}}} = \left[-\omega_h c_L + \frac{\alpha\omega_h x_4}{2}\frac{-sigm(x_4)}{\sqrt{1-x_3 sigm(x_4)}}\right]_{\substack{x_1=x_{10} \\ x_2=x_{20} \\ x_3=x_{30} \\ x_4=x_{40}}}$$

$$= \left[-\omega_h c_L - \frac{\alpha\omega_h x_{40}}{2}\frac{sigm(x_{40})}{\sqrt{1-x_{30} sigm(x_{40})}}\right]$$

$$= \left[-\omega_h c_L - \frac{\alpha\omega_h x_{40}}{2}\frac{\frac{1-e^{-a\cdot x_{40}}}{1+e^{-a\cdot x_{40}}}}{\sqrt{1-x_{30}\frac{1-e^{-a\cdot x_{40}}}{1+e^{-a\cdot x_{40}}}}}\right] \text{ by } x_{10}=x_{20}=x_{30}=x_{40}=0$$

$$= -\omega_h c_L$$

$$\left.\frac{\partial f_3}{\partial x_4}\right|_{\substack{x_1=x_{10} \\ x_2=x_{20} \\ x_3=x_{30} \\ x_4=x_{40}}} = \left[\alpha\omega_h\sqrt{1-x_3 sigm(x_4)} - \frac{\alpha\omega_h x_4\cdot x_3}{2}\frac{(sigm(x_4))'}{\sqrt{1-x_3 sigm(x_4)}}\right]_{\substack{x_1=x_{10} \\ x_2=x_{20} \\ x_3=x_{30} \\ x_4=x_{40}}}$$

$$= \left[\alpha\omega_h\sqrt{1-x_{30}\frac{1-e^{-a\cdot x_{40}}}{1+e^{-a\cdot x_{40}}}} - \frac{\alpha\omega_h x_{40}\cdot x_{30}}{2\sqrt{1-x_{30}\frac{1-e^{-a\cdot x_{40}}}{1+e^{-a\cdot x_{40}}}}}\frac{2a\cdot e^{-a\cdot x_{40}}}{(1+e^{-a\cdot x_{40}})^2}\right] \text{ by } x_{10}=x_{20}=x_{30}=x_{40}=0$$

$$= \alpha\omega_h$$

The Jacobian matrix in terms of u is given by

$$J_u = \begin{bmatrix} \frac{\partial f_1}{\partial u_1} & \frac{\partial f_1}{\partial u_2} \\ \frac{\partial f_2}{\partial u_1} & \frac{\partial f_2}{\partial u_2} \\ \frac{\partial f_3}{\partial u_1} & \frac{\partial f_3}{\partial u_2} \\ \frac{\partial f_4}{\partial u_1} & \frac{\partial f_4}{\partial u_2} \end{bmatrix} = \begin{bmatrix} 0 & 0 \\ 0 & -\frac{\omega_h}{\alpha} \\ 0 & 0 \\ \frac{1}{\tau_v} & 0 \end{bmatrix}$$

Where $u_1 = i$ and $u_2 = t_L$

The mathematical model for the linearization of the nonlinear system in the neighborhood of the normal operating condition is then given by

$$\dot{X}_{linear} = J_x \times (X - X_0) + J_u \times (U - U_0)$$

U is the control signal; therefore, for the purpose of linearization, we can assume $U_0 = 0$ (or $\Delta U = U$).

Thus,

$$\begin{aligned} \dot{X}_{linear} &= J_x \times (X - X_0) + J_u \times (U - U_0) \\ &= J_x \times \Delta X + J_u \times \Delta U \\ &= J_x \times \Delta X + J_u \times U \end{aligned} \tag{2.18}$$

As X_0(Equilibrium point) $= 0$, it follows that

$$\Delta X = X_{linear} - X_0 = X_{linear} \Rightarrow \Delta \dot{X} = \dot{X}_{linear} \tag{2.19}$$

Now, we can compactly express the linearized system using equations (2.18) and (2.19) as:

$$\Delta\dot{X} = \dot{X}_{linear} = J_x \times \Delta X + J_u \times U$$

$$\Delta\dot{X} = \begin{bmatrix} \Delta\dot{x}_1 \\ \Delta\dot{x}_2 \\ \Delta\dot{x}_3 \\ \Delta\dot{x}_4 \end{bmatrix} = \begin{bmatrix} 0 & \omega_{\max} & 0 & 0 \\ 0 & -\gamma\dfrac{\omega_h}{\alpha} & \dfrac{\omega_h}{\alpha} & 0 \\ 0 & -\alpha\omega_h & -\omega_h c_L & \alpha\omega_h \\ 0 & 0 & 0 & -\dfrac{1}{\tau_v} \end{bmatrix} \begin{bmatrix} \Delta x_1 \\ \Delta x_2 \\ \Delta x_3 \\ \Delta x_4 \end{bmatrix} + \begin{bmatrix} 0 & 0 \\ 0 & -\dfrac{\omega_h}{\alpha} \\ 0 & 0 \\ \dfrac{1}{\tau_v} & 0 \end{bmatrix} \begin{bmatrix} i \\ t_L \end{bmatrix}$$

$$= \mathrm{A} \cdot \Delta X + \mathrm{B} \cdot U \qquad (2.20)$$

Next, we define a Y matrix to convert the dimensionless variables into variables with dimension in order to get actual outputs.

$$Y = \begin{bmatrix} 1 & 0 & 0 & 0 \\ 0 & \omega_{\max} & 0 & 0 \\ 0 & 0 & P_s & 0 \\ 0 & 0 & 0 & A_{v\max} \end{bmatrix} \begin{bmatrix} x_1 \\ x_2 \\ x_3 \\ x_4 \end{bmatrix}$$

$$= \begin{bmatrix} 1 & 0 & 0 & 0 \\ 0 & \omega_{\max} & 0 & 0 \\ 0 & 0 & P_s & 0 \\ 0 & 0 & 0 & A_{v\max} \end{bmatrix} \begin{bmatrix} \Delta x_1 + x_{10} \\ \Delta x_2 + x_{20} \\ \Delta x_3 + x_{30} \\ \Delta x_4 + x_{40} \end{bmatrix} \quad \because\ x_{10} = x_{20} = x_{30} = x_{40} = 0$$

$$= \begin{bmatrix} 1 & 0 & 0 & 0 \\ 0 & \omega_{\max} & 0 & 0 \\ 0 & 0 & P_s & 0 \\ 0 & 0 & 0 & A_{v\max} \end{bmatrix} \begin{bmatrix} \Delta x_1 \\ \Delta x_2 \\ \Delta x_3 \\ \Delta x_4 \end{bmatrix}$$

$$= \mathrm{C} \cdot \Delta X + D \cdot U \quad (D = 0) \qquad (2.21)$$

Finally, by replacing all elements in the matrices above by their values listed in ANNEX 1, we obtain

$$A = \begin{bmatrix} 0 & 173.45 & 0 & 0 \\ 0 & -15.889 & 29.253 & 0 \\ 0 & -657.45 & -10.684 & 657.45 \\ 0 & 0 & 0 & -100 \end{bmatrix} \qquad B = \begin{bmatrix} 0 & 0 \\ 0 & -29.253 \\ 0 & 0 \\ 100 & 0 \end{bmatrix}$$

$$C = \begin{bmatrix} 1 & 0 & 0 & 0 \\ 0 & 173.45 & 0 & 0 \\ 0 & 0 & 8.73\times10^{6} & 0 \\ 0 & 0 & 0 & 7.94\times10^{-6} \end{bmatrix} \qquad D = \begin{bmatrix} 0 & 0 \\ 0 & 0 \\ 0 & 0 \\ 0 & 0 \end{bmatrix}$$

These matrices A, B, C and D will be used to build a model of the linearized system for MATLAB/Simulink based simulation and to design a PID controller.

CHAPTER 3

CONTROL ALGORITHMS AND VALIDATION

In this chapter, we compare our nonlinear system with the linearized system and describe the limitations of approximating a nonlinear system by a linear system. We also design a PID controller using the Ziegler-Nichols method and a feedback linearization based controller for the nonlinear system and verify the performance of each controller.

3.1 Open-loop simulation of nonlinear and linearized system

First, we intend to study the characteristics of angular displacement, angular velocity, load pressure difference and servo-valve opening area in the nonlinear system, using an open-loop simulation. Following that study, we want to compare the outputs of the nonlinear and linearized systems, and characterize how changes in the current input (i.e., high and low amplitude) impact the outputs of the two systems.

For the open-loop simulation study, the linear system matrices (i.e., A, B, C and D) and the state space model (2.17) were used for the linearized (Figure 4) and nonlinear system (Figure 5) respectively.

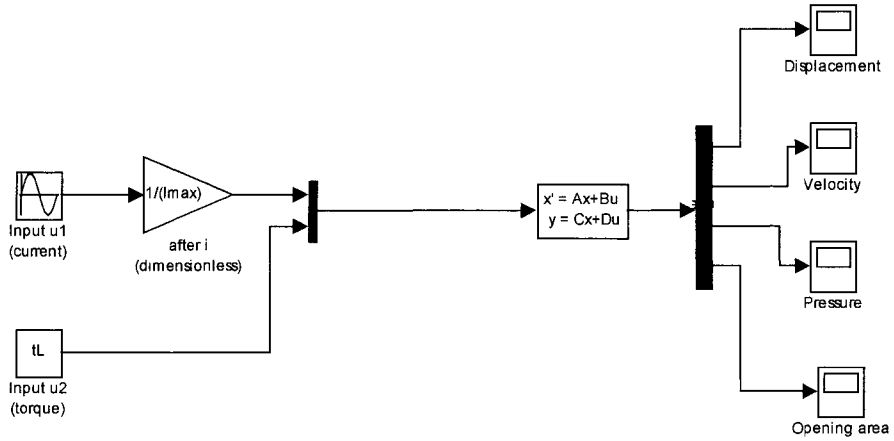

Figure 4 Linearized open-loop system

All required simulations in this chapter were done using MATLAB/Simulink. We used a sine wave for current input ($u_1 = i$) that has two different amplitudes (low: 1mA and high: 10mA) and the same frequency of π (rad/sec). We also set the torque input ($u_2 = t_L$) to be 0 and the initial conditions of the nonlinear system were set to zero as in the case of the linearized system.

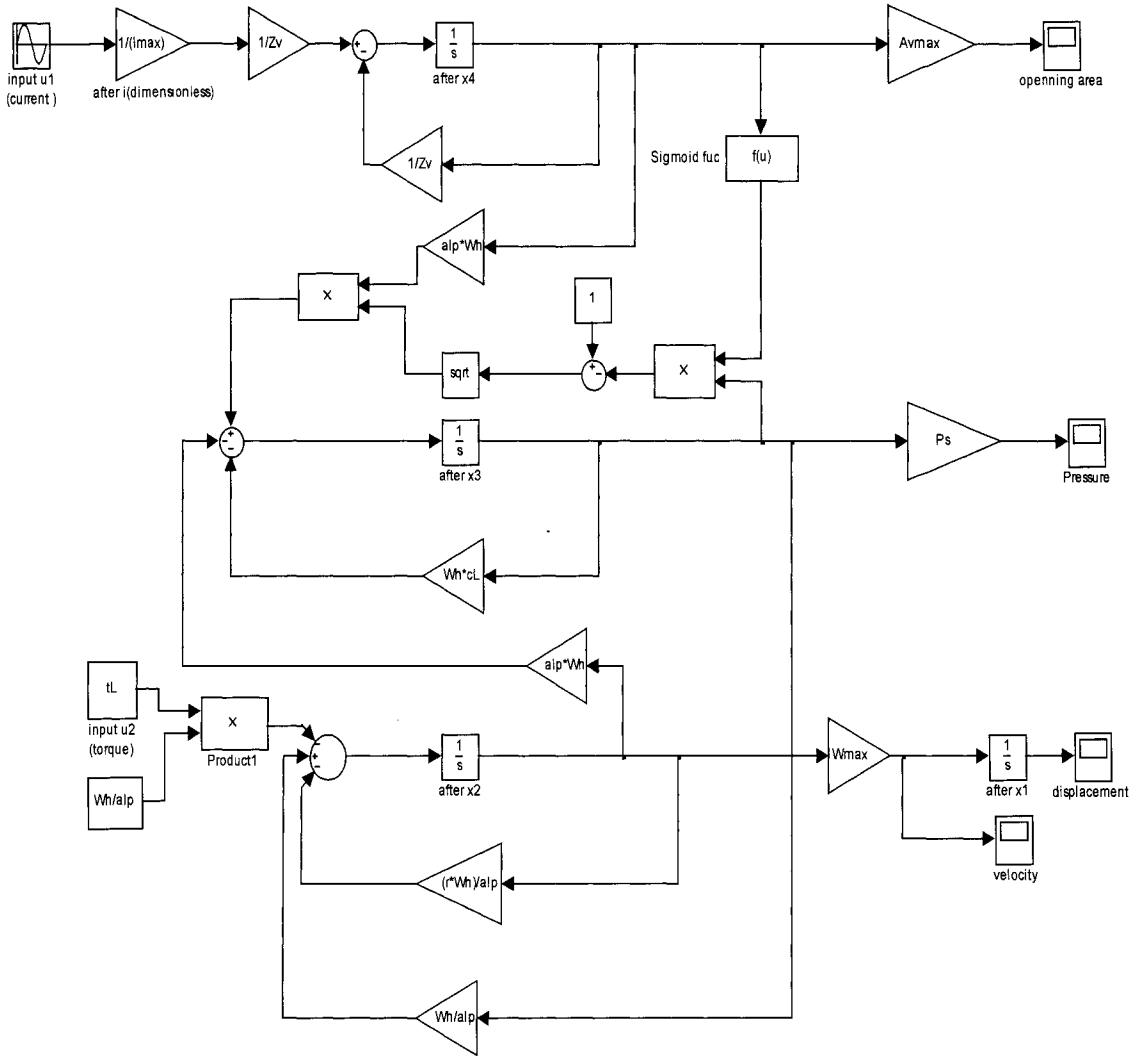

Figure 5 Nonlinear open-loop system

The following Figures provide a comparison of simulation results between the linearized and nonlinear systems in terms of each output variable.

■ Simulation results

▪ Angular displacement

▫ Input current with 10mA amplitude

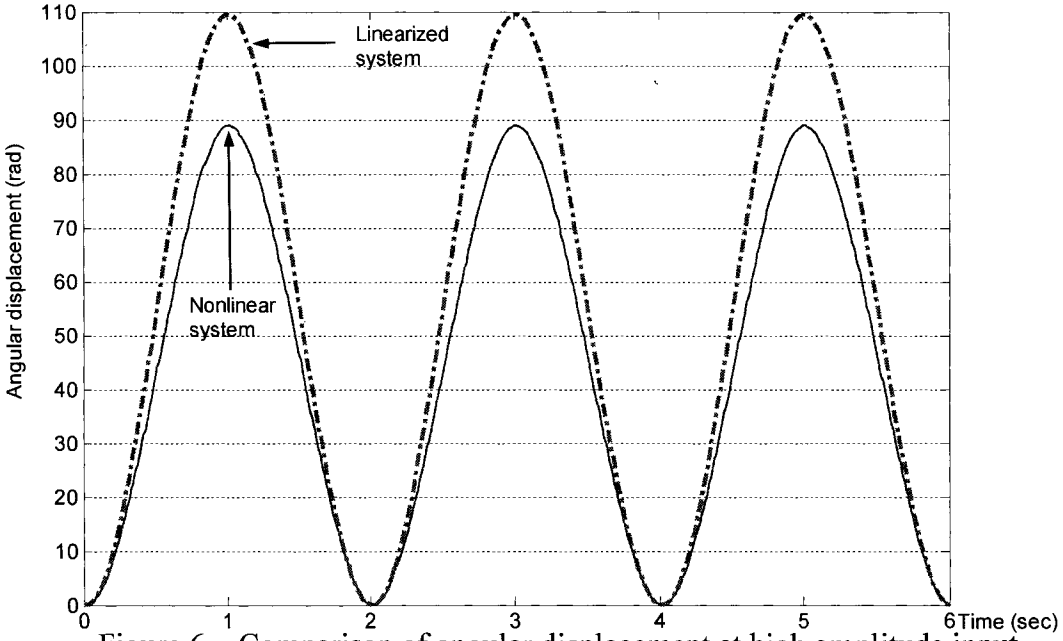

Figure 6 Comparison of angular displacement at high amplitude input

▫ Input current with 1mA amplitude

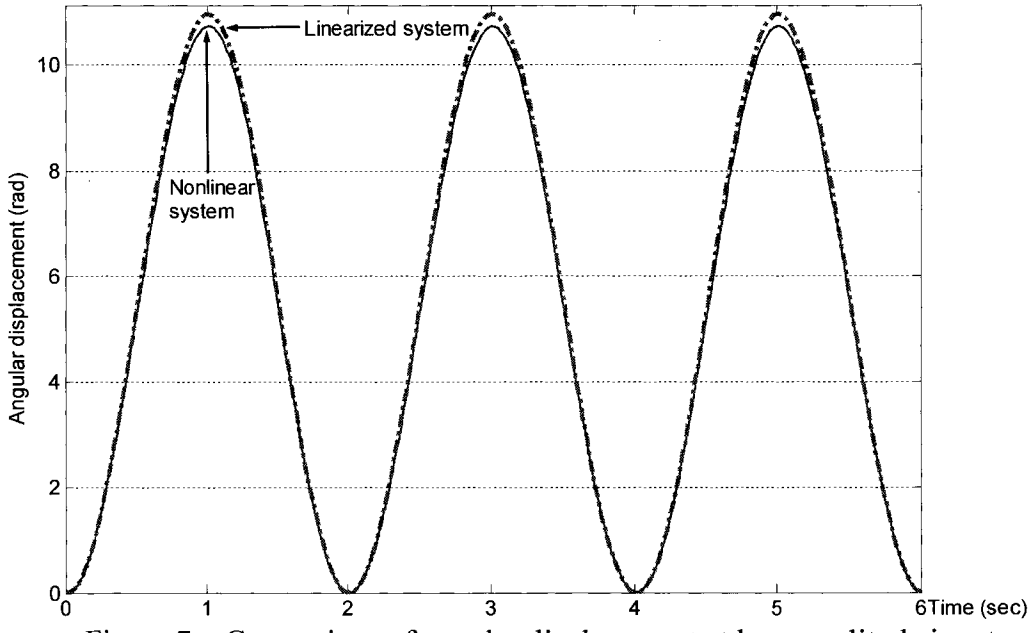

Figure 7 Comparison of angular displacement at low amplitude input

- **Angular velocity**

  - Input current with 10mA amplitude

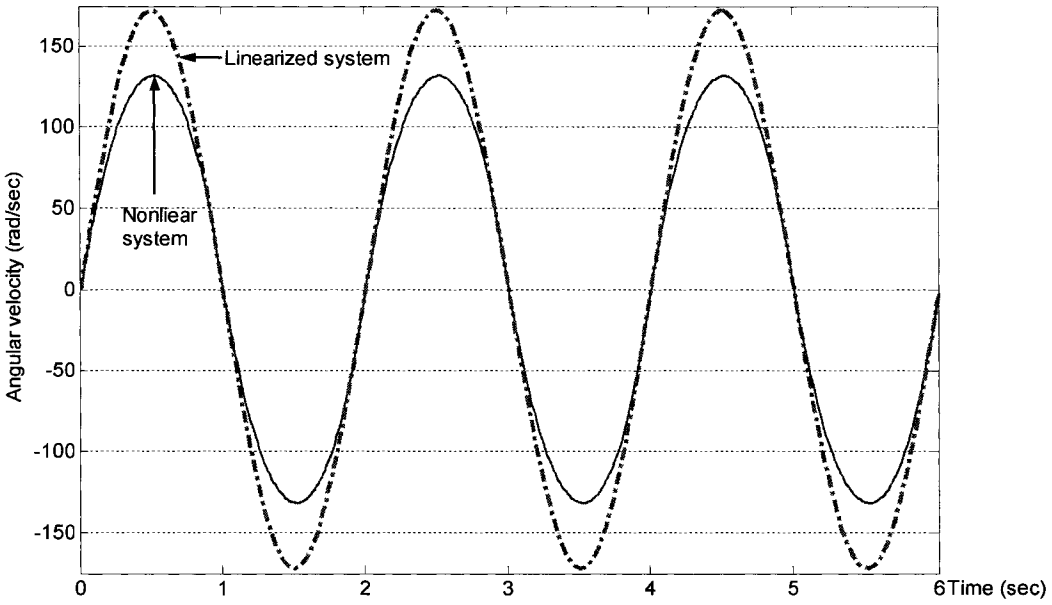

Figure 8 Comparison of angular velocity at high amplitude input

  - Input current with 1mA amplitude

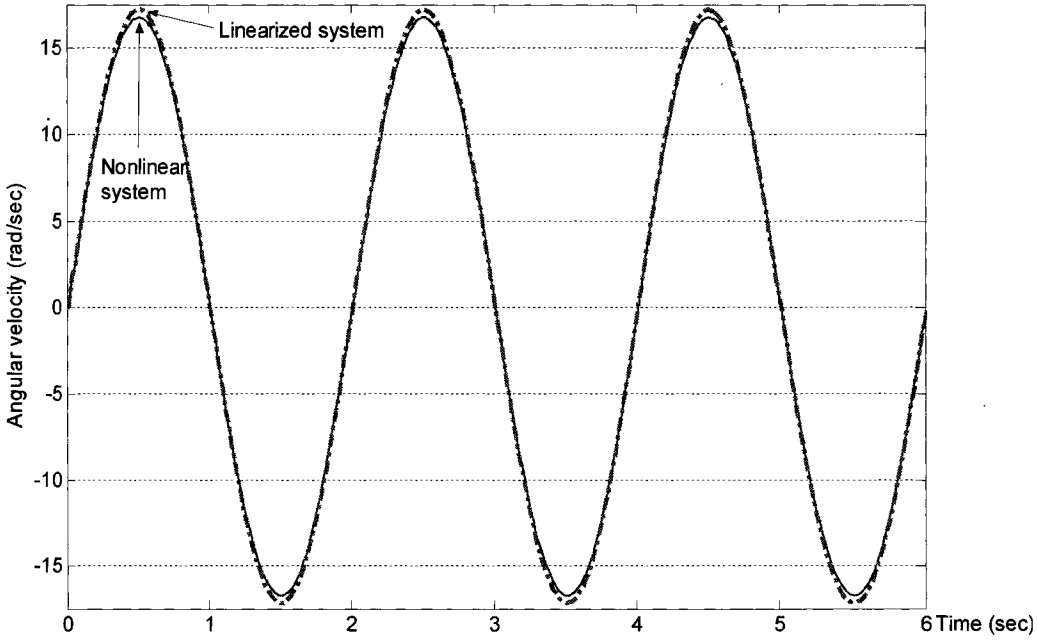

Figure 9 Comparison of angular velocity at low amplitude input

- **Load pressure difference**

  - Input current with 10mA amplitude

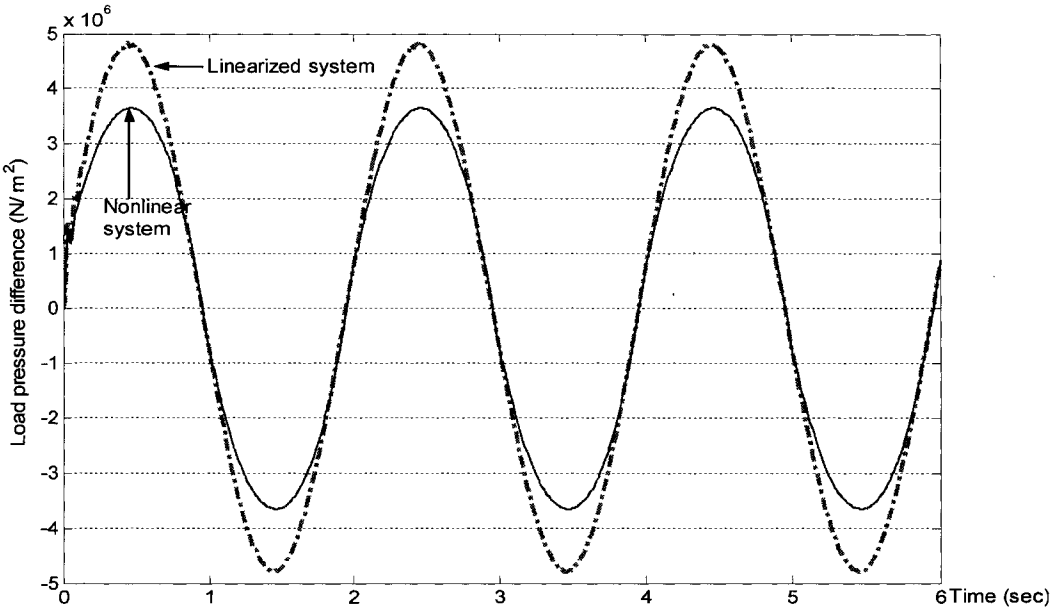

Figure 10 Comparison of load pressure difference at high amplitude input

  - Input current with 1mA amplitude

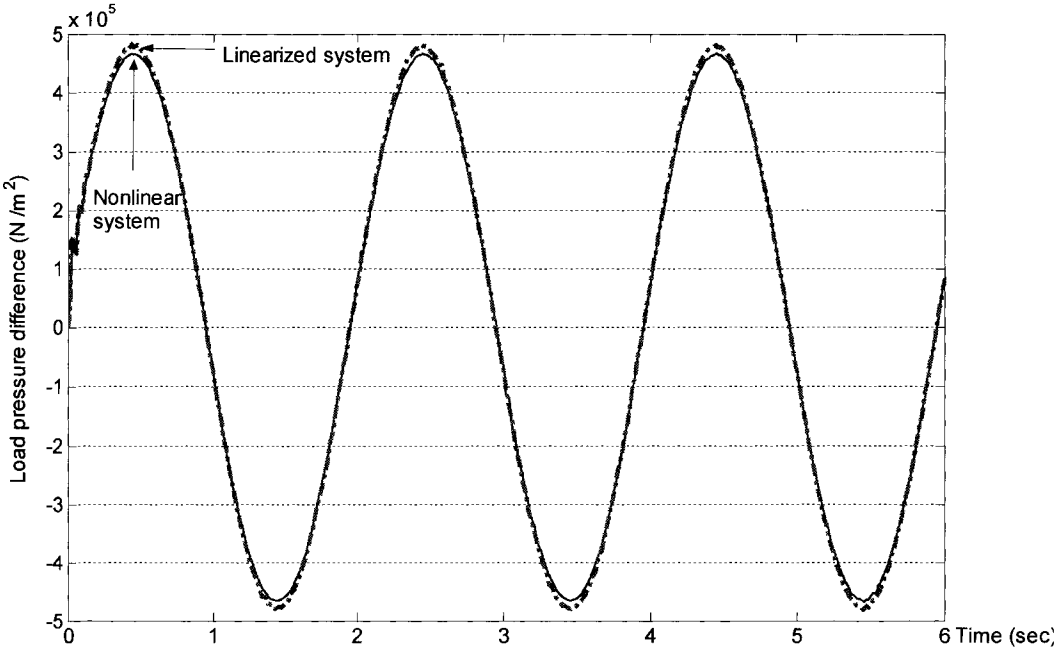

Figure 11 Comparison of load pressure difference at low amplitude input

- **Servo-valve opening area**

  - Input current with 10mA amplitude

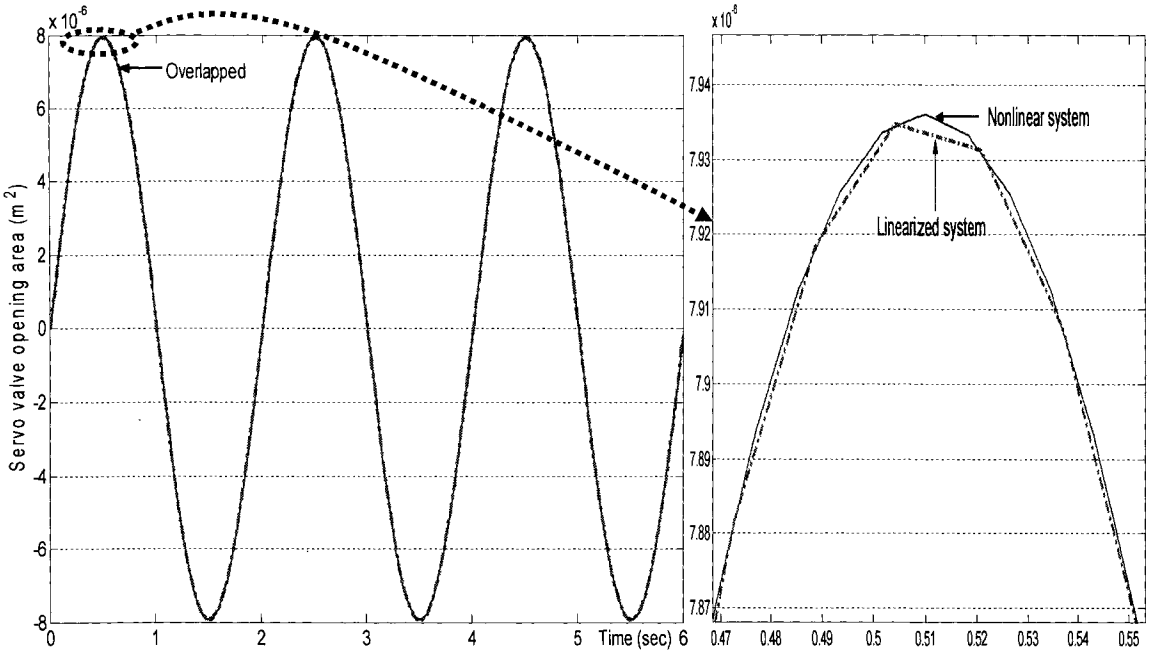

Figure 12 Comparison of servo-valve opening area at high amplitude input

  - Input current with 1mA amplitude

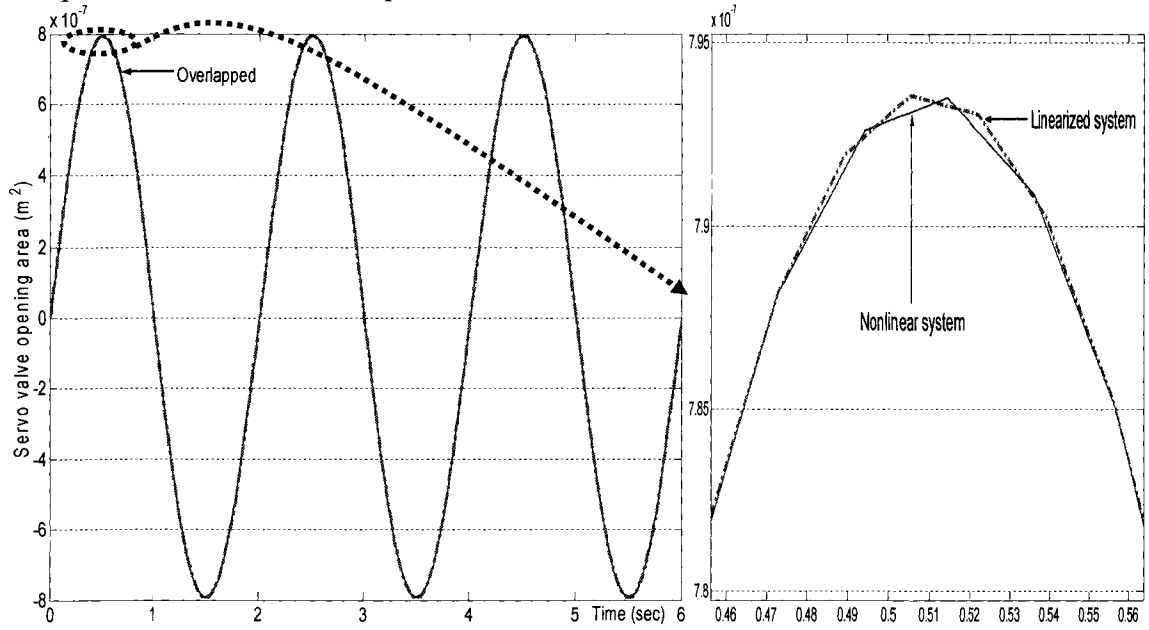

Figure 13 Comparison of servo-valve opening area at low amplitude input

■ **Simulation results analysis**

From the previous simulation results, the positive peak point value of each output is presented in the following tables.

Table I

Positive peak point value of angular displacement in relation to amplitude of current input

Current amplitude	Linearized system	Nonlinear system	Difference rate $(=\frac{\text{Value of linear.-value of nonlinear.}}{\text{value of nonlinear.}}\times 100)$
1 mA	10.94 rad	10.71 rad	2.14 %
10 mA	109.4 rad	88.8 rad	23.19 %
Increase rate (From 1mA to 10 mA)	10 times	8.29 times	–

Table II

Positive peak point value of angular velocity in relation to amplitude of current input

Current amplitude	Linearized system	Nonlinear system	Difference rate $(=\frac{\text{Value of linear.-value of nonlinear.}}{\text{value of nonlinear.}}\times 100)$
1 mA	17.18 rad/s	16.73 rad/s	2.68 %
10 mA	171.8 rad/s	131.6 rad/s	30.54 %
Increase rate (From 1mA to 10 mA)	10 times	7.86 times	–

Table III

Positive peak point value of load pressure difference in relation to amplitude of current input

Current amplitude	Linearized system	Nonlinear system	Difference rate $(= \frac{\text{Value of linear.-value of nonlinear.}}{\text{value of nonlinear.}} \times 100)$
1 mA	4.82×10^{5} N/m^2	4.65×10^{5} N/m^2	3.22 %
10 mA	4.82×10^{6} N/m^2	3.65×10^{6} N/m^2	32.05 %
Increase rate (From 1mA to 10 mA)	10 times	7.84 times	–

Table IV

Positive peak point value of servo-valve opening area in relation to amplitude of current input

Current amplitude	Linearized system	Nonlinear system	Difference rate $(= \frac{\text{Value of linear.-value of nonlinear.}}{\text{value of nonlinear.}} \times 100)$
1 mA	7.935×10^{-7} m^2	7.935×10^{-7} m^2	0 %
10 mA	7.934×10^{-6} m^2	7.934×10^{-6} m^2	0 %
Increase rate (From 1mA to 10 mA)	10 times	10 times	–

As noted from the figures, all outputs except angular displacement are symmetric with respect to the x axis in the open-loop nonlinear system. The asymmetry is explained as

follows: The velocity has a sine wave form (e.g., $A\sin bt$), therefore the angular displacement is the integral of the angular velocity (i.e., $-\frac{A}{b}\left[\cos bt\right]_0^t = -\frac{A}{b}\left[\cos(bt)-1\right]$) and is biased because by the constant term (i.e., $\frac{A}{b}$).

From the tables, all outputs are directly affected by the change of current amplitude. Specifically, a factor of 10 increase of amplitude amplifies each output value by a factor of 7.84 to 10 times. As compared to the pattern of the linearized system, where the amplification factor (i.e., 10 times) of all outputs is equal to the change in amplitude (i.e., 10 times) of the input, the nonlinear system does not show such regularity in the relationship between output and input amplitude.

We also note that whereas the approximation of the nonlinear system by linearization is accurate for low amplitude (1 mA) current, the difference between each output value of the linearized and nonlinear systems is large at high amplitude (10 mA). (However, for the servo-valve opening area, there is no distinctive difference between the outputs of the two systems. This result can be explained by the fact that in contrast to the other outputs, the servo-valve opening has a linear relationship with the current as seen in equation (2.17).)

We are thus able to conclude that although the operation of system may be around equilibrium point, it is not possible to approximate the nonlinear system by the linear system unless the current input has small amplitude.

From these open-loop simulation results, we see that there are limitations to the use of linearization and traditional methods based on linearization are only effective in a narrow operating range, and thus, a nonlinear approach is required to provide high performance for the whole operating range.

3.2 PID controller

3.2.1 Introduction

Based on the mathematical model of the system that has been derived, various controllers can be designed to control the outputs of the rotational hydraulic system.

Among the various types of controllers, PID control is widely used due to its clear, simple structure, relatively good performance and low cost. Besides, PID controllers can be easily modified, updated and auto tuned.

To design a PID controller to control our system, we choose the Ziegler-Nichols method, because it provides a convenient rule for controller tuning based on experimental response, and because it does not require a specific process model or plant dynamic model.

In this section, we will apply the same PID controller obtained by the Ziegler Nichols method to both the linearized system and nonlinear system simultaneously and compare the results of simulation for each system to verify that the PID controller has limited control performance when applied to the nonlinear system, in terms of precision and response.

3.2.2 PID controller and Ziegler-Nichols method

Ziegler-Nichols tuning rules aim to limit maximum overshoot to 10~25%. Even though it does not guarantee extremely optimized tuning, it provides good control performance and has real usefulness when the plant dynamics are not known and analytical or graphical approaches to the design of controllers cannot be used. For example, the Ziegler-Nichols method does not need specific characteristics of plant dynamics like the damping ratio and natural frequency of the system, since this method extracts the required information from experimental system response data. However, since we have a dynamic model of the plant, we will use that model for the design of the PID controller.

The Ziegler- Nichols procedure is described briefly below:

Ziegler-Nichols rules (First and second method) are basically used to determine values of K_p (Proportional gain), T_i (Integral time) and T_d (Derivative time), which are the basic elements of a PID controller.

When we follow the second method, the first step is to set $T_i = \infty$ and $T_d = 0$ for designing a controller.

Next, applying Routh's stability criterion to the denominator of the closed-loop transfer function, we find K_{cr}, the critical gain.

Finally, we use the experimentally determined tuning relationships based on ω (Frequency of the sustained oscillation), P_{cr} (Critical period) and K_{cr}, to obtain the required parameters for a tuned PID controller.

We now present all the steps to design a PID controller using the Ziegler-Nichols second method for angular displacement control in the linearized system.

Using the matrices obtained through linearization in Chapter 2 and the "ss2tf" function of MATLAB, we obtain a transfer function $G(s)$ for the linearized system from current input to angular displacement output.

We first define new state matrices relating the current input and angular displacement output as follows:

$$A_{des}=A,\quad B_{des}=B(:,1)=\begin{bmatrix}0\\0\\0\\314.465\end{bmatrix},\quad C_{des}=C^{*}(1,:)=\begin{bmatrix}1 & 0 & 0 & 0\end{bmatrix},\quad D_{des}=\begin{bmatrix}0\end{bmatrix}$$

To reduce numerical errors in simulation, we take $C^{*}=eye(4)$ instead of C.

Using the MATLAB command, "[num,den]=ss2tf(A_{des}, B_{des} , C_{des}, D_{des})", we obtain the transfer function $G(s)$ given as

$$G(s)=\frac{-4.263\times10^{-14}s^{3}-1.455\times10^{-11}s^{2}-5.355\times10^{-9}s+3.336\times10^{8}}{s^{4}+126.6s^{3}+2.206\times10^{4}s^{2}+1.94\times10^{6}s}$$

We now use the second method of Ziegler-Nichols for designing a PID controller, $G_c(s)$ with

$$G_c(s)=K_p(1+\frac{1}{T_i s}+T_d s)$$

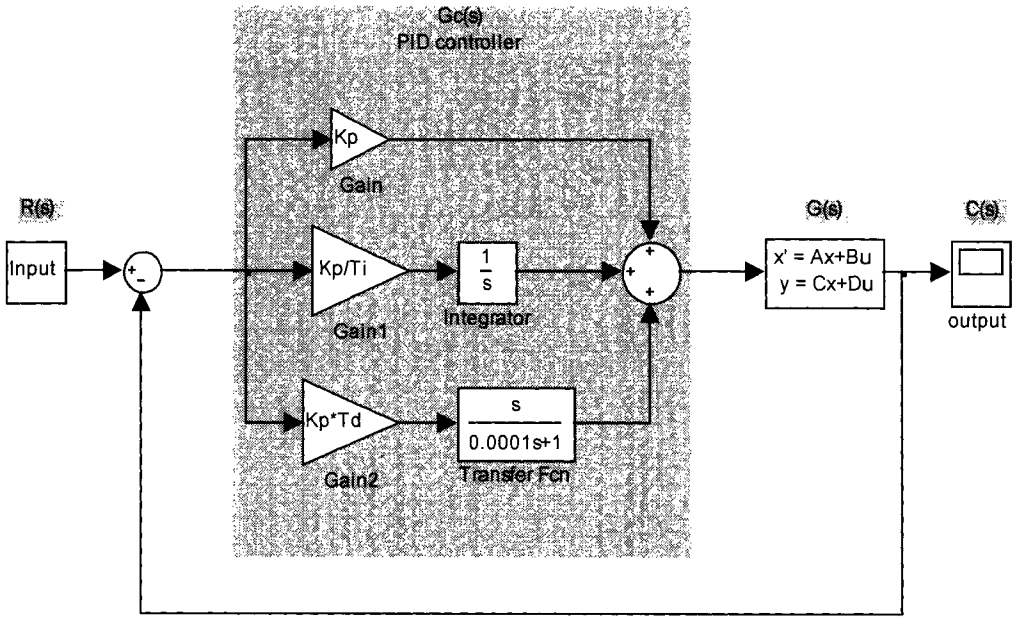

Figure 14 PID Controller applied to a linearized system

By setting $T_i = \infty$ and $T_d = 0$, we obtain the closed-loop transfer function with the PID controller, using $G(s)$ and K_p of $G_c(s)$.

$$\frac{C(s)}{R(s)} = \frac{G(s)\cdot K_P}{1+G(s)\cdot K_P} = \frac{a_1 \cdot K_P(s^3 + a_2 \cdot s^2 + a_3 \cdot s + a_4)}{s^4 + b_1(K_P + b_2)s^3 + b_3(K_P + b_4)\cdot s^2 + b_5(K_P + b_6)s + b_7 \cdot K_P}$$

Where

$a_1 = -4.263\times10^{-14}$, $a_2 = 341.309$, $a_3 = 125616$, $a_4 = -7.82548\times10^{21}$

$b_1 = -4.263\times10^{-14}$, $b_2 = -2.96974\times10^{15}$, $b_3 = -1.455\times10^{-11}$, $b_4 = -1.51615\times10^{15}$

$b_5 = -5.355\times10^{-9}$, $b_6 = -3.62278\times10^{14}$, $b_7 = 3.336\times10^{8}$

The value of K_P that makes the system marginally stable can be obtained by using Routh's stability criterion. Since the characteristic equation of the entire closed-loop system is

$$s^4 + b_1(K_P + b_2)s^3 + b_3(K_P + b_4)\cdot s^2 + b_5(K_P + b_6)s + b_7 \cdot K_P = 0$$

The first column of the Routh array is:

$$\begin{array}{ll} s^4 & 1 \\ s^3 & -4.263\times10^{-14}(K_P - 2.96974\times10^{15}) \\ s^2 & \dfrac{-1.455\times10^{-11}(K_P^2 + 4.14749\times10^{15}K_P + 1.37489\times10^{30})}{K_P - 2.96974\times10^{15}} \\ s^1 & \dfrac{-977414\cdot(K_P^3 - 5.93948\times10^{15}K_P^2 + 8.81935\times10^{30}K_P - 2.72892\times10^{30})}{K_P^2 + 4.14749\times10^{15}K_P + 1.37489\times10^{30}} \\ s^0 & 3.336\times10^{8}K_P \end{array}$$

For the system to be stable, all elements in the first column of the Routh array must be positive. We now determine the value of K_P to satisfy this condition as follows:

$K_P > 0$ from (5,1) of Routh array

$K_P < 2.96\times10^{15}$ from (2,1) of Routh array

$K_P < -3.78\times10^{15}$ or $K_P > -3.63\times10^{14}$ from (3,1) of Routh array

$K_P < 0.309424$ or $2.96\times10^{15} < K_P < 2.97\times10^{15}$ from (4,1) of Routh array

$\therefore 0 < K_P < 0.309424$: Common range obtained from the conditions above

Therefore, sustained oscillations will occur if $K_P = 0.309424$.

Thus, the critical gain $K_{cr} = K_P = 0.309424$

Using the value of 0.309424 for K_{cr}, the characteristic equation becomes

$$s^4 + 126.6s^3 + 22060s^2 + 1.94\times10^6 s + 1.03224\times10^8 = 0$$

To find the frequency of the sustained oscillation, we substitute s by $j\omega$ in the characteristic equation.

$$(j\omega)^4 + 126.6(j\omega)^3 + 22060(j\omega)^2 + 1.94\times10^6(j\omega) + 1.03224\times10^8 = 0$$
$$\omega^4 - 22060\omega^2 + 1.03224\times10^8 + (1.94\times10^6\omega - 126.6\omega^3)j = 0$$

The imaginary part of the above equation should be zero at the frequency of sustained oscillation. Accordingly, $1.94\times10^6\omega - 126.6\omega^3 = 0 \Leftrightarrow \omega = 123.79$

Hence, the period of sustained oscillation is

$$P_{cr} = \frac{2\pi}{\omega} = \frac{2\pi}{123.79} = 0.050757$$

Finally, we find the values for the PID controller using the tuning relationships.

$$K_p = 0.6K_{cr} = 0.6\times0.309424 = 0.185654$$
$$T_i = 0.5P_{cr} = 0.5\times0.050757 = 0.025379$$
$$T_d = 0.125P_{cr} = 0.125\times0.050757 = 0.006345$$

Thus, the PID controller designed using the Zeigler-Nichols second method is given by

$$G_c(s) = K_p(1 + \frac{1}{T_i s} + T_d s)$$
$$= 0.185654(1 + \frac{1}{0.025379s} + 0.006345s)$$

Applying the same method to the cases of angular velocity and load difference pressure control, we can design PID controllers for each of these outputs. The parameters for these controllers are given in Table V.

Table V

Tuning parameters by Ziegler Nichols method

	Angular velocity	Load difference pressure
Matrix	A_{des}=A, B_{des} = B(:,1), $C_{des} = C^*(2,:)$, $D_{des} = [0]$	A_{des}=A, B_{des} = B(:,1), $C_{des} = C^*(3,:)$, $D_{des} = [0]$
$G(s)$	$\frac{a_1 s^2 + a_2 s + a_3}{s^3 + b_1 s^2 + b_2 s + b_3}$ where $a_1 = 1.421\times10^{-14}$, $a_2 = 2.91\times10^{-11}$ $a_3 = 1.923\times10^{6}$, $b_1 = 126.6$ $b_2 = 2.206\times10^{4}$, $b_3 = 1.94\times10^{6}$	$\frac{a_1 s^2 + a_2 s + a_3}{s^3 + b_1 s^2 + b_2 s + b_3}$ where $a_1 = -1.421\times10^{-14}$, $a_2 = 6.575\times10^{4}$ $a_3 = 1.045\times10^{6}$, $b_1 = 126.6$ $b_2 = 2.206\times10^{4}$, $b_3 = 1.94\times10^{6}$
K_{cr}	0.443474	0.4
ω	148.526	219.909
P_{cr}	0.042304	0.028572
K_P	0.266084	0.24
T_i	0.021152	0.014286
T_d	0.005288	0.003572
$G_c(s)$	$0.266084(1+\frac{1}{0.021152s}+0.005288s)$	$0.24(1+\frac{1}{0.014286s}+0.003572s)$

Where $C^* = eye(4)$

$G(s)$: Transfer function of a linearized system

$G_c(s)$: Function of PID controller

3.2.3 PID controller for linearized system

For each $G_c(s)$, the corresponding responses of the linearized system for constant and sinusoidal references can be obtained by simulation with Matlab/Simulink. Since x_2 and x_3 are non-dimensional, we have to restrict the reference's maximum value for these states to be less than 1. The reference amplitudes used for simulation are as follows:

- Reference for angular displacement: 1 and $1 \cdot \sin \pi t$
- Reference for angular velocity: 0.35 and $0.35 \cdot \sin \pi t$
- Reference for load pressure difference: 0.2 and $0.2 \cdot \sin \pi t$

■ Simulation results

▪ Angular displacement

▫ Constant reference for displacement: 1

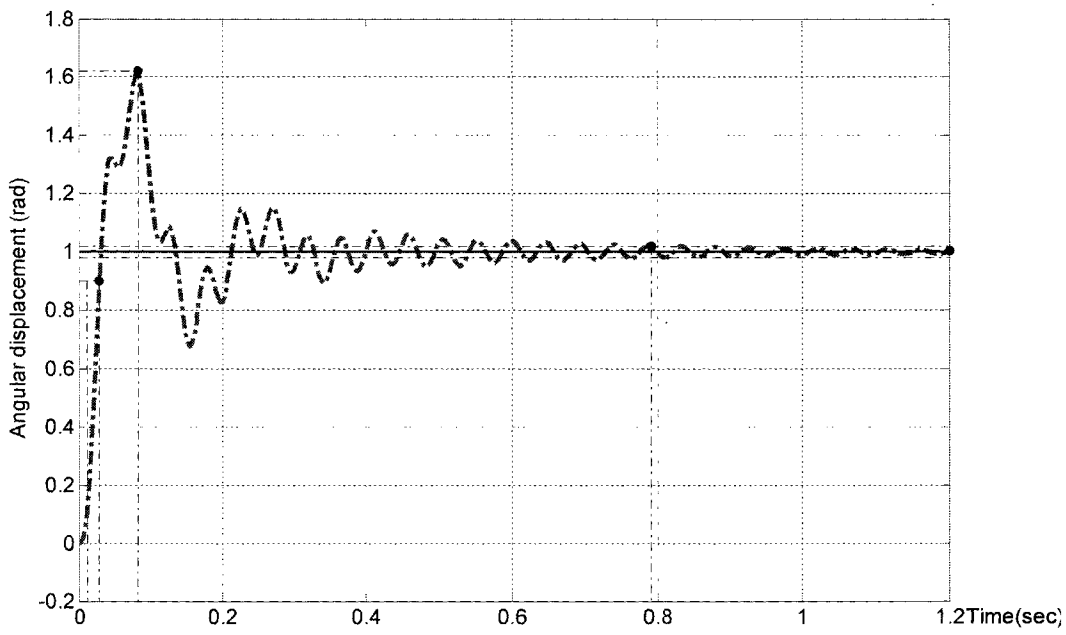

Figure 15 Unit step response of angular displacement by PID controller applied to linearized closed-loop system

The resulting unit-step response curve is shown in Figure 15. The maximum overshoot for the unit-step response is approximately 62%. The 2% setting time is 0.79 sec.

▫ Sinusoidal reference of displacement: $1 \cdot \sin \pi t$

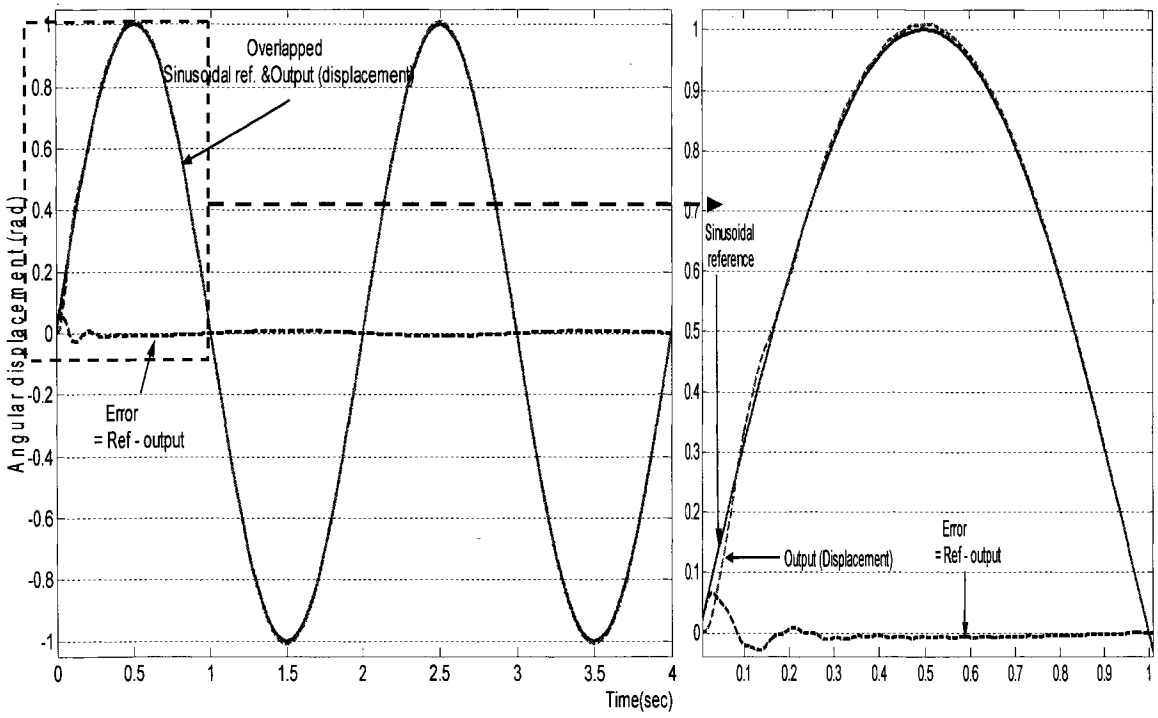

Figure 16 Sinusoidal response of angular displacement by PID controller applied to linearized closed-loop system

From Figure 16, we note that the error between the sinusoidal reference and the output (angular displacement) is negligible (around 0 %). Therefore, this controller, designed by using the Ziegler-Nichols method, provides high-precision tracking of sinusoidal inputs for the linearized system.

- **Angular velocity**

The non-dimensional variable x_2 calculated by dividing the angular velocity by the maximum angular velocity (ω_{max}) is used as the feedback variable for the closed-loop system. As mentioned before, the reason for using a non-dimensional quantity is to reduce the output error as much as possible, as shown in Figure 17. x_2 is always less than 1 (i.e., the angular velocity is always less than ω_{max}), and we choose 0.35 and $0.35 \cdot \sin \pi t$ as reference commands for non-dimensional angular velocity to satisfy the range of x_2.

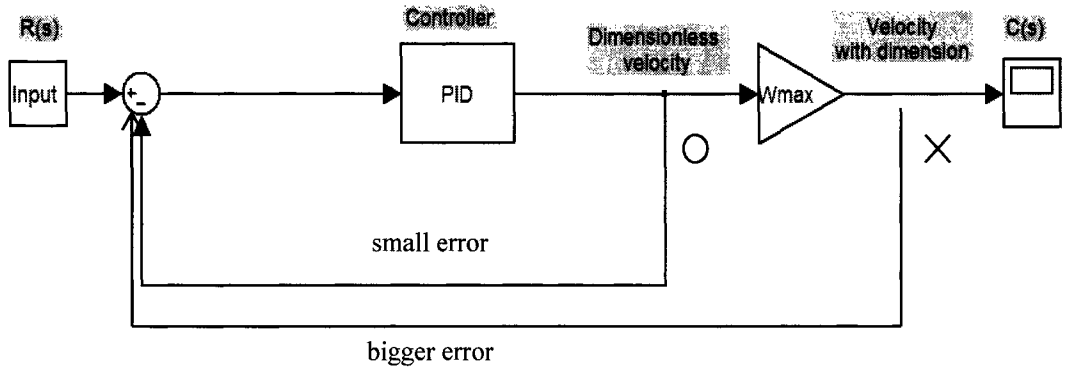

Figure 17 Comparison between variable with dimension and dimensionless variable as outputs for the feedback control system

▫ Constant reference of angular velocity: 0.35

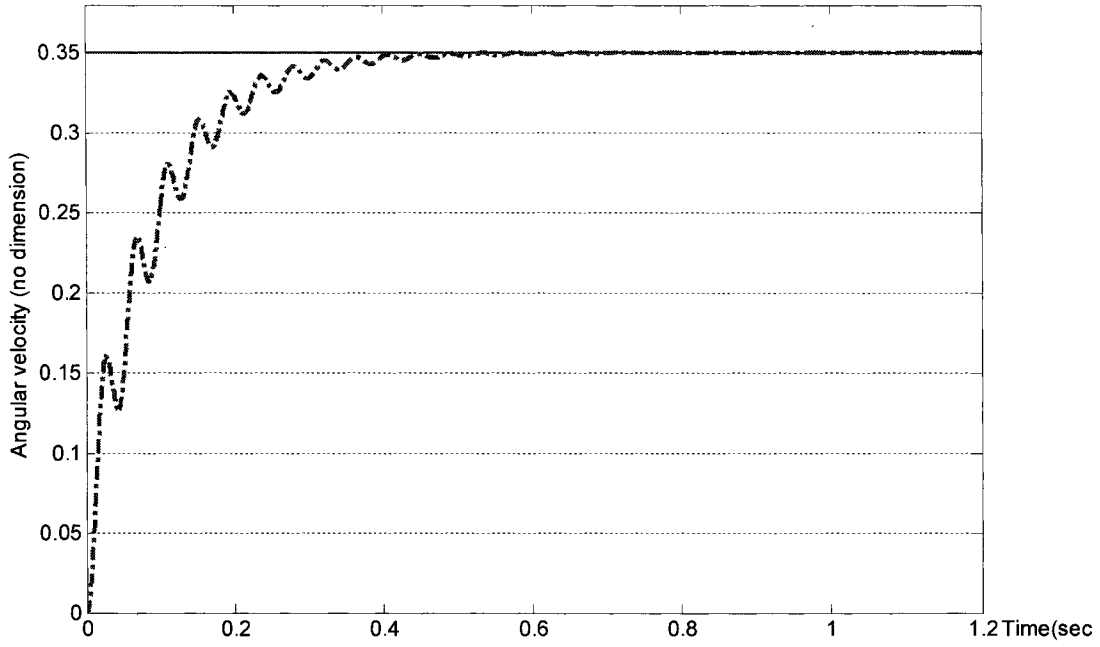

Figure 18 Constant response of dimensionless angular velocity by PID controller applied to linearized closed-loop system

Figure 18 presents the angular velocity response for a constant reference. There is no overshoot and the 2% settling time is 0.315 sec. Therefore, this PID controller is acceptable for control of the linearized system's angular velocity with constant reference commands.

We note the sinusoidal oscillation from the beginning of the simulation to 0.6 sec. The reason for this phenomenon is related to the poles in the transfer function of the closed-loop system. Using $G(s)$ (the transfer function of the linearized system) and $G_c(s)$ (the transfer function of the PID controller) in table V, the following transfer function, $T_{CL}(s)$ of the entire closed-loop system is obtained:

$$T_{CL}(s) = \frac{G(s) \cdot G_C(s)}{1 + G(s) \cdot G_C(s)}$$

$$T_{CL}(s) = \frac{a_1 s^4 + a_2 s^3 + a_3 s^2 + a_4 s + a_5}{b_1 (s - c_1)(s - c_2)(s - c_3)(s - c_4)}$$

Where

$a_1 = 4.229 \times 10^{-19}$, $a_2 = 9.462 \times 10^{-16}$, $a_3 = 57.24$, $a_4 = 1.082 \times 10^4$, $a_5 = 5.117 \times 10^5$

$b_1 = 0.02115$, $c_{1,2} = -7.784 \pm 147.89j$, $c_3 = -11.03$, $c_4 = -99.97$

From the denominator of $T_{CL}(s)$, we see that the two complex poles (c_1 and c_2) create a damped sinusoidal response with an exponential (i.e., underdamped response) and two real poles (c_3 and c_4) generate a natural (i.e., overdamped) response consisting of two different exponentials. The superposition (Figure 19) of each response generates the output response of the entire closed system identical to the one seen in Figure 18. Thus, the occurrence of the sinusoidal oscillation shown in Figure 18 can be explained by this superposition.

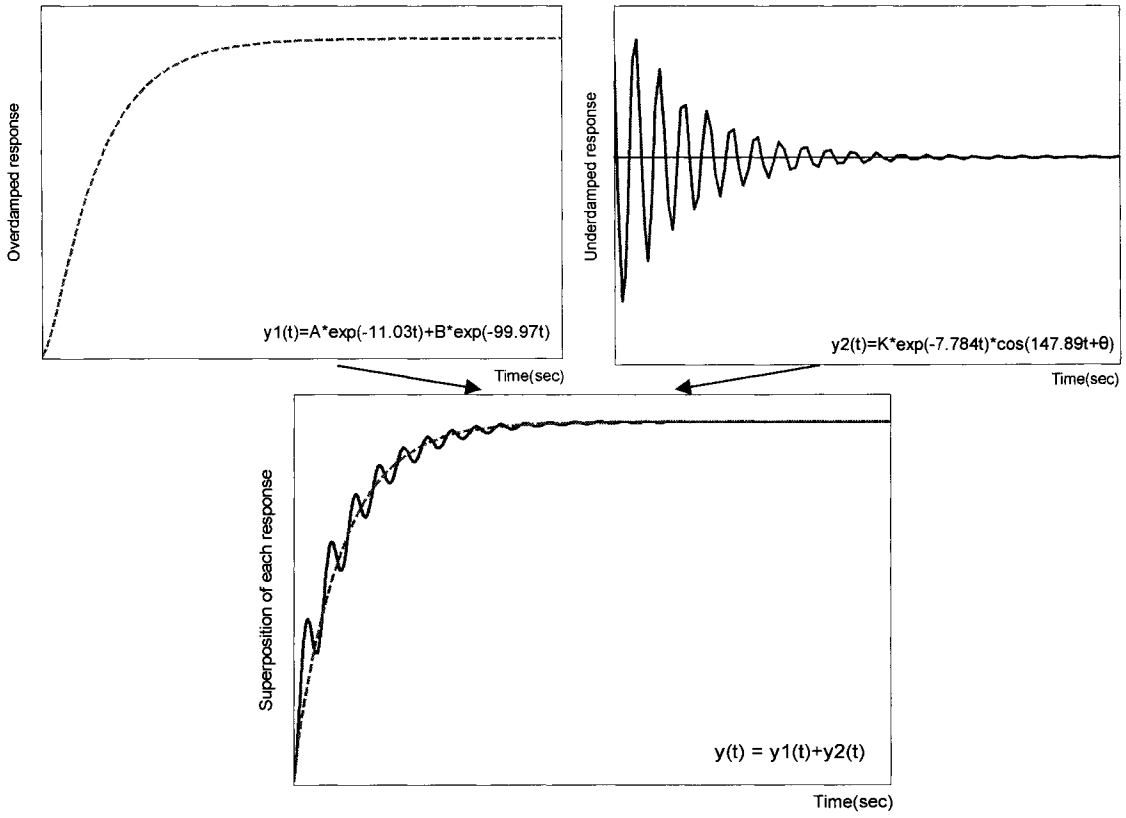

Figure 19 Superposition of each response

▫ Sinusoidal reference of angular velocity: $0.35 \cdot \sin \pi t$

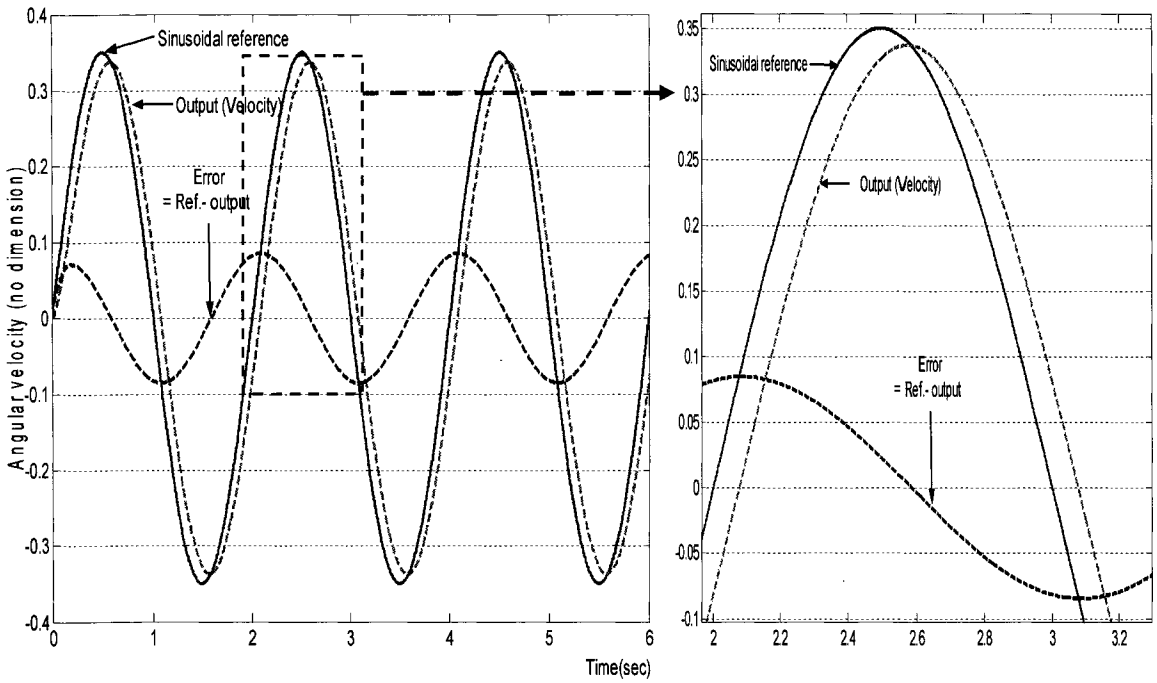

Figure 20 Sinusoidal response of dimensionless angular velocity by PID controller applied to linearized closed-loop system

Even though there is a delay of 0.0785 sec and a maximum error of ± 0.0848 between reference and output, we can consider that this PID controller for angular velocity control in the linear system is acceptable because the response is extremely fast and the error is slight.

▪ **Load pressure difference**

Again, to reduce numerical errors in simulation, we designate the dimensionless variable x_3 as the variable for feedback control, and thus, the maximum value of the reference for x_3 is always less than 1. To fulfill this condition for x_3, we choose 0.2 and $0.2 \cdot \sin \pi t$ as references for closed-loop simulation of load pressure difference.

▫ Constant reference of load pressure difference: 0.2

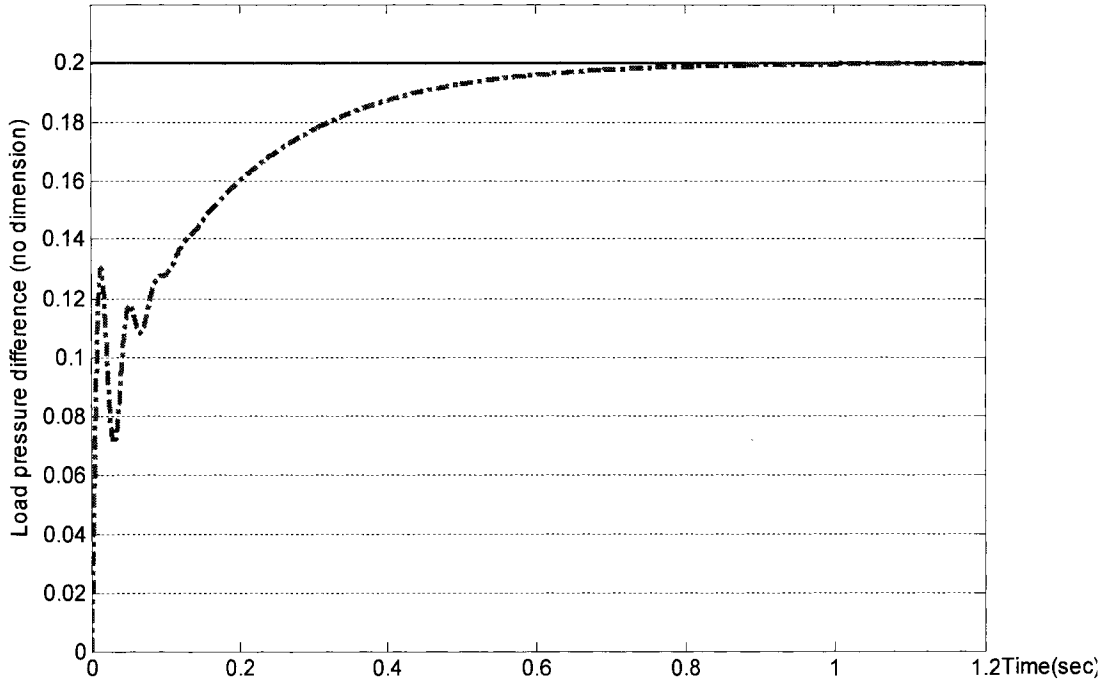

Figure 21 Constant response of dimensionless load pressure difference by PID controller applied to linearized closed-loop system

Considering that there is no overshoot and the 2% settling time is 0.605 sec, this PID controller is acceptable for control of load pressure difference in the linearized system for constant reference commands.

▫ Sinusoidal reference of load pressure difference: $0.2 \cdot \sin \pi t$

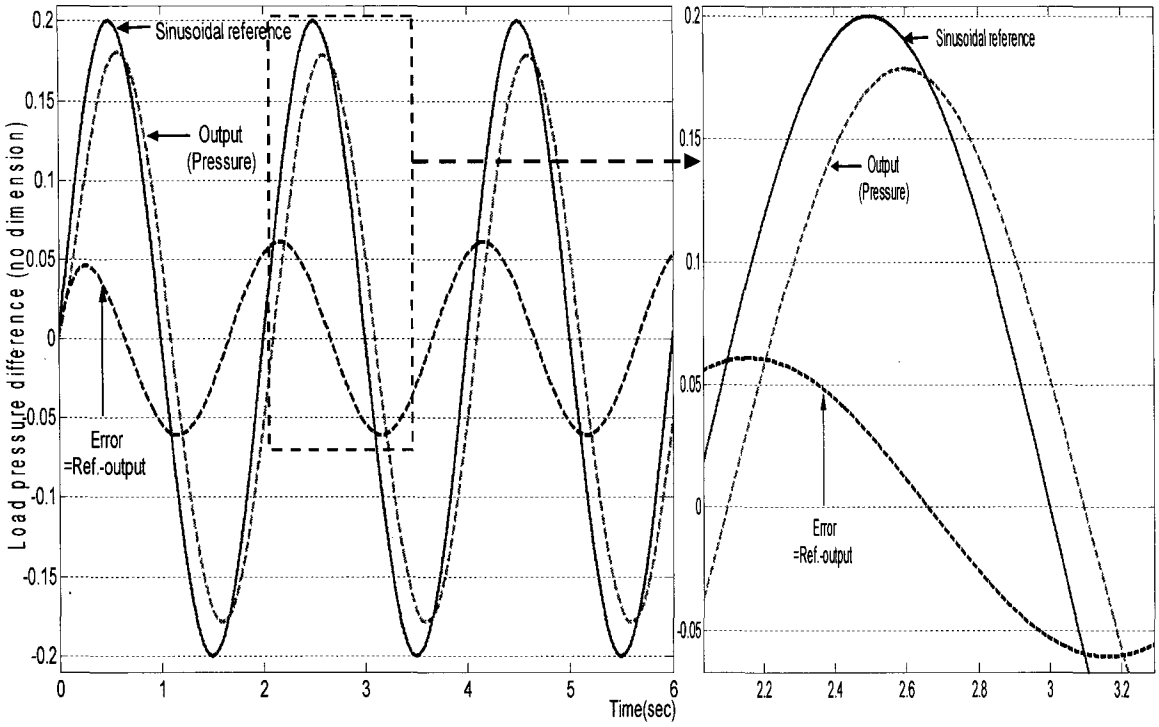

Figure 22 Sinusoidal response of dimensionless load pressure difference by PID controller applied to linearized closed-loop system

Because the delay of 0.1 sec and maximum error of ± 0.0608 are small, the PID controller can be considered to have acceptable performance for load pressure control in the linear system.

■ Simulation results analysis

For the linearized closed-loop system, the PID controllers designed using the Ziegler-Nichols method show acceptable performance for controlling the angular displacement, velocity and load pressure of the actuator, for sinusoidal and constant reference commands.

3.2.4 PID controller for nonlinear system

Typically, PID control is effective for a linear system, but it is not always capable of controlling a nonlinear system. To study the limitations of PID control, we intend to apply the same PID controllers to the nonlinear electro-hydraulic system model for Simulink based simulation (Figure 23), and investigate the error range of each output in the nonlinear system, with the same initial conditions as the linearized system.

By comparing each simulation results for the linearized and nonlinear closed-loop systems, we will show that PID control performance is limited when applied to the nonlinear system. Based on these results, we will argue that we require an alternative control strategy that is more suited for control of nonlinear systems.

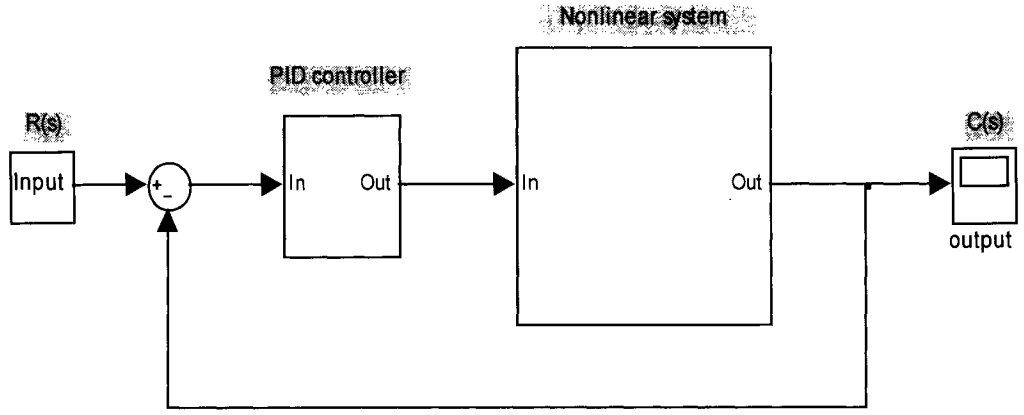

Figure 23 PID Controller in nonlinear system

■ Simulation results

▪ Angular displacement

▫ Constant reference of displacement: 1

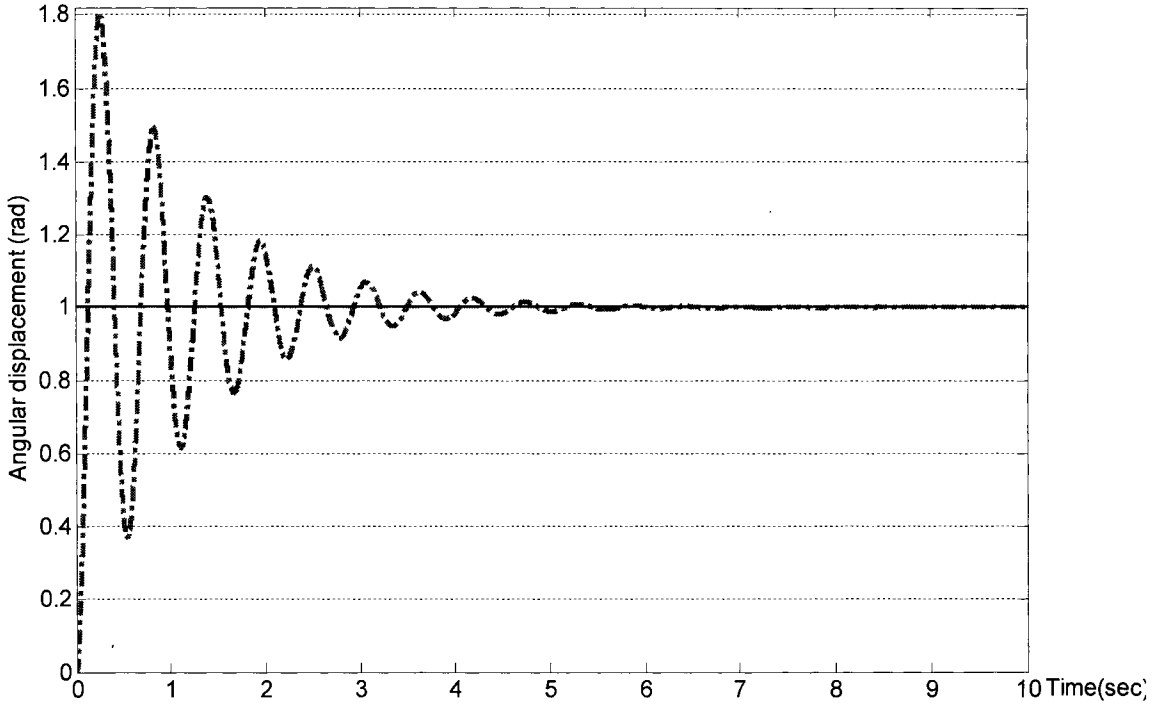

Figure 24 Unit step response of angular displacement by PID controller applied to nonlinear closed-loop system

As seen from the graph above, the value of the maximum overshoot is 1.803 and the 2% settling time is 4.25 sec. Compared with the simulation result for the linearized system (Figure 15), the maximum overshoot value increases by 11.29 % and the 2% settling time also shows an increase of 4.37 times that of the linearized system. Thus, we note that the performance of the PID controller is significantly reduced for angular displacement control in the nonlinear system with a constant reference command.

▫ Sinusoidal reference of displacement: $1 \cdot \sin \pi t$

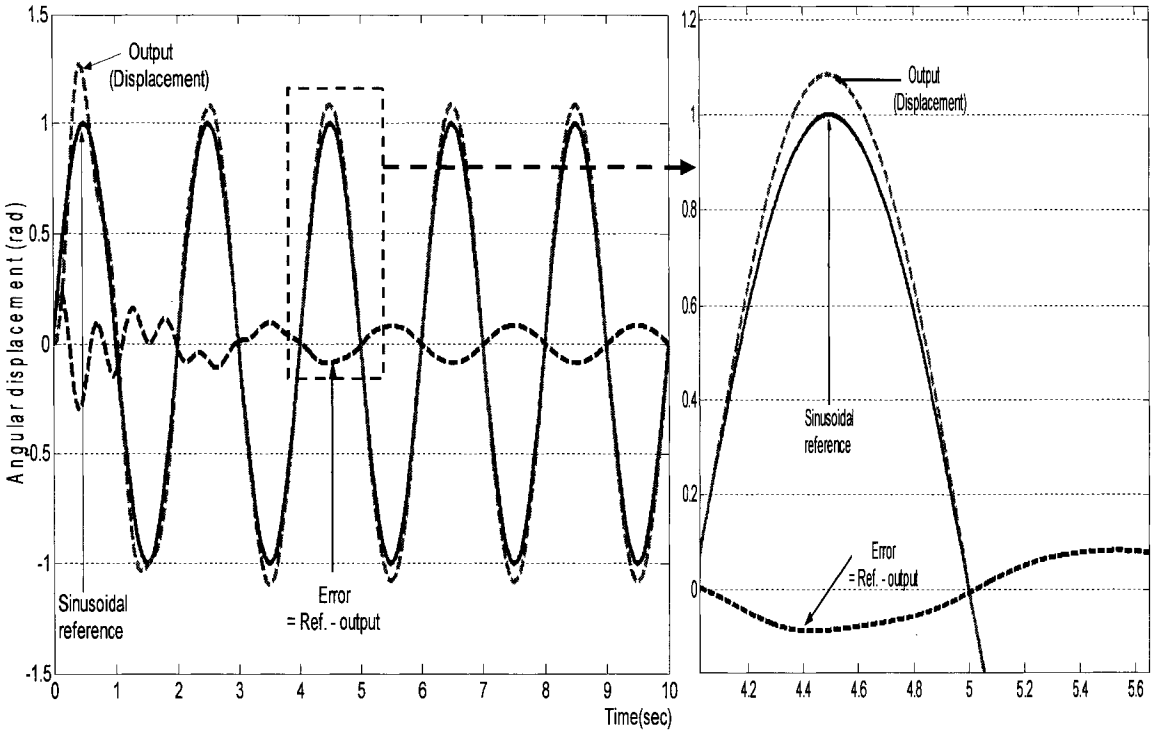

Figure 25 Sinusoidal response of angular displacement by PID controller applied to nonlinear closed-loop system

The angular displacement shows a regular pattern after 4 sec. We choose the interval of 4.0 ~ 5.6 sec in order to magnify and investigate in detail the response characteristics. From this investigation, we can see that the maximum error between the sinusoidal reference and the output becomes a constant of ± 0.0826 after 4 sec and the delay is minimal. Although this result is reasonable in terms of nonlinear system control, this PID controller is still less effective with the nonlinear system as compared to the linear system based on the simulation result for the linearized system (Figure 16). The error between reference and output is negligible in the latter and there is no delay as well.

▪ **Angular velocity**

For the same reason mentioned in 3.2.3, we use the non-dimensional variable x_2 as the variable for feedback control in simulation. We also choose the same references for angular velocity, 0.35 and $0.35 \cdot \sin \pi t$.

▫ Constant reference of angular velocity: 0.35

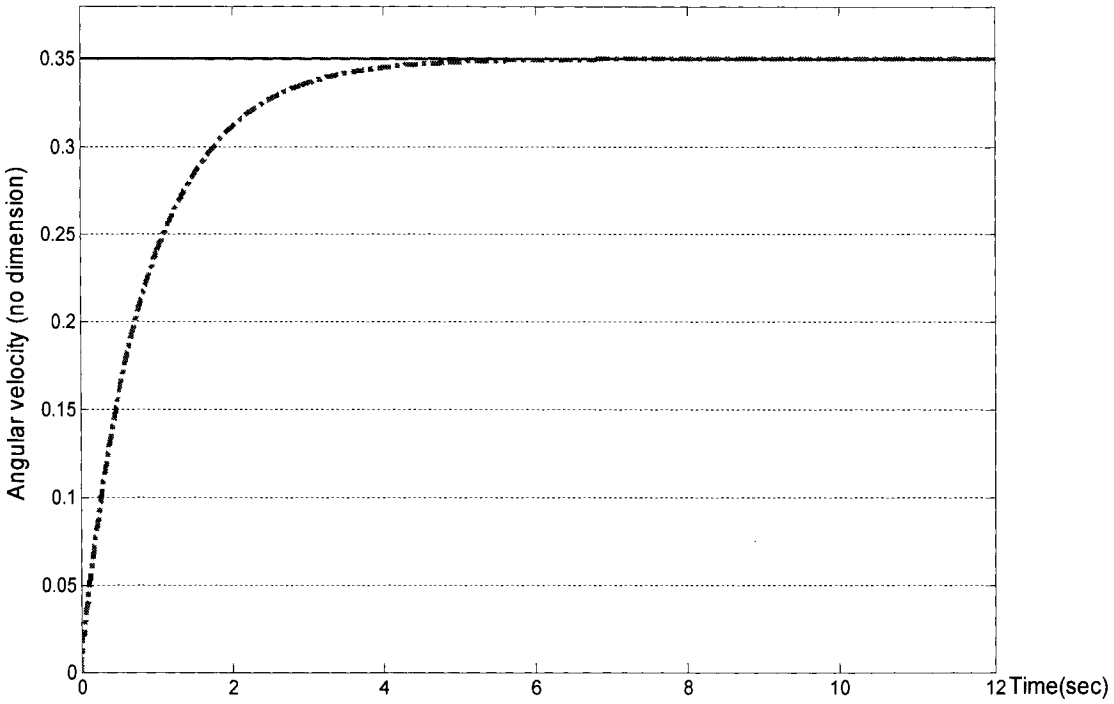

Figure 26 Constant response of dimensionless angular velocity by PID controller applied to nonlinear closed-loop system

From Figure 26, the constant response displays the characteristic that there is no overshoot and the 2% settling time is approximately 3.7 sec. Comparing the result with that of Figure 18, we see that the 2% settling time is 10.74 times as long as that for the linearized system. So this PID controller of angular velocity control is less effective for the nonlinear system as compared to the linearized one.

▫ Sinusoidal reference of angular velocity: $0.35 \cdot \sin \pi t$

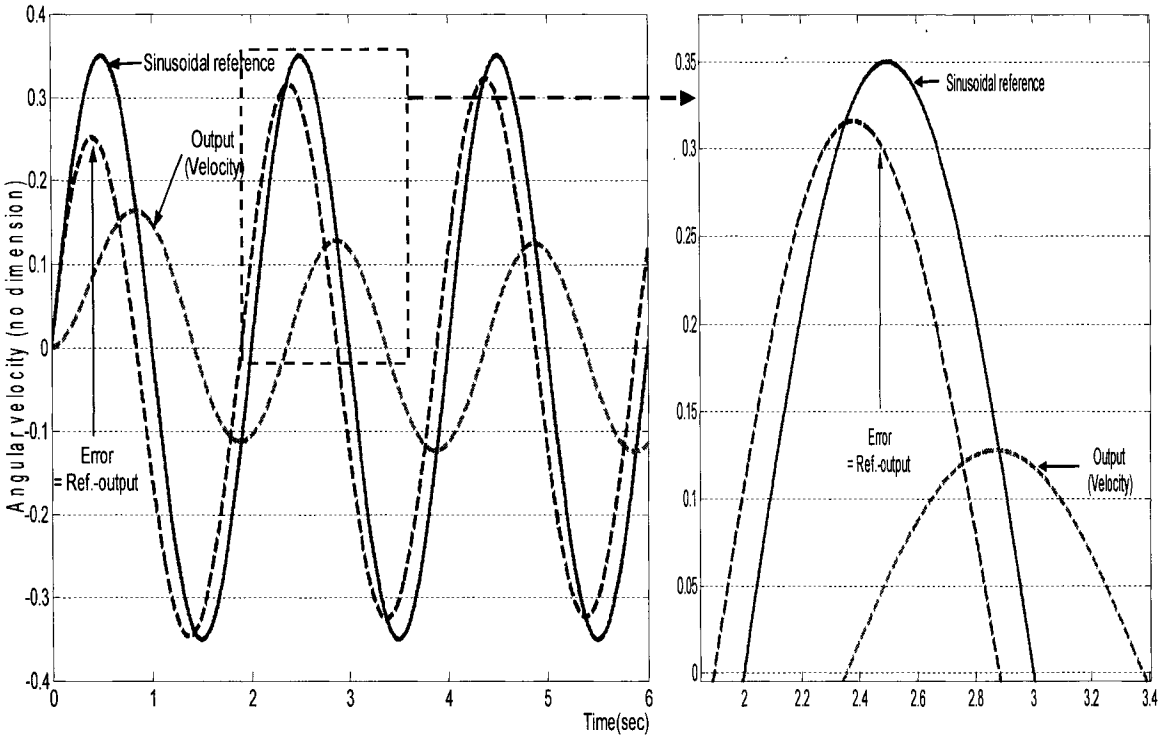

Figure 27 Sinusoidal response of dimensionless angular velocity by PID controller applied to nonlinear closed-loop system

Here, after 2 sec, the output shows regular behavior with a constant delay of 0.373 sec, and a uniform error between the sinusoidal reference and the output is within the range of $\pm$ 0.323. Referring to the case of the linearized system (Figure 20), where the delay is 0.0785 sec and the maximum error is $\pm$ 0.0848, the use of PID control for the nonlinear system brings about increases of 375 % for the delay and 280 times for the maximum error. Thus, we note that PID control is not well suited for angular velocity control of the nonlinear system.

▪ **Load pressure difference**

As a condition of simulation for load pressure, we use the same non-dimensional variable x_3 and references (0.2 and $0.2 \cdot \sin \pi t$) as in the case of the linearized system.

▫ Constant reference of load pressure difference: 0.2

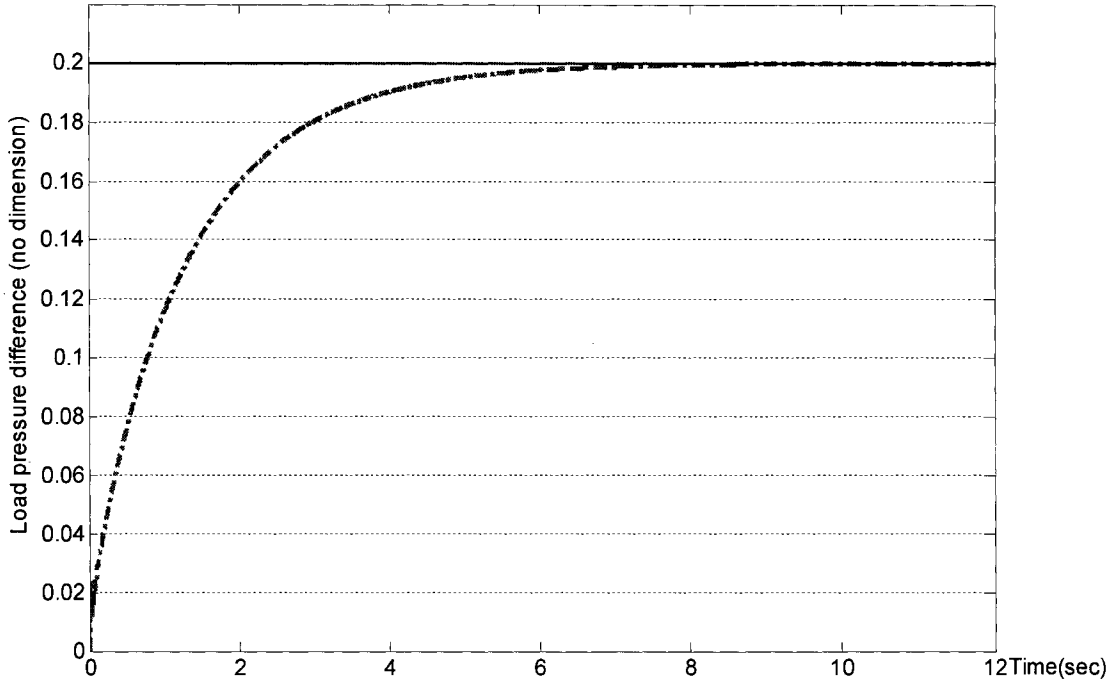

Figure 28 Constant response of dimensionless load pressure difference by PID controller applied to nonlinear closed-loop system

Comparing these results with the results for the linearized system, we see that the 2% settling time increases to 7.76 times as much as that in Figure 21. (The 2% settling times of the nonlinear and linear systems are 5.3 sec and 0.605 sec respectively). Thus, PID control is not well suited for load pressure control in the nonlinear system.

▫ Sinusoidal reference of load pressure difference: $0.2 \cdot \sin \pi t$

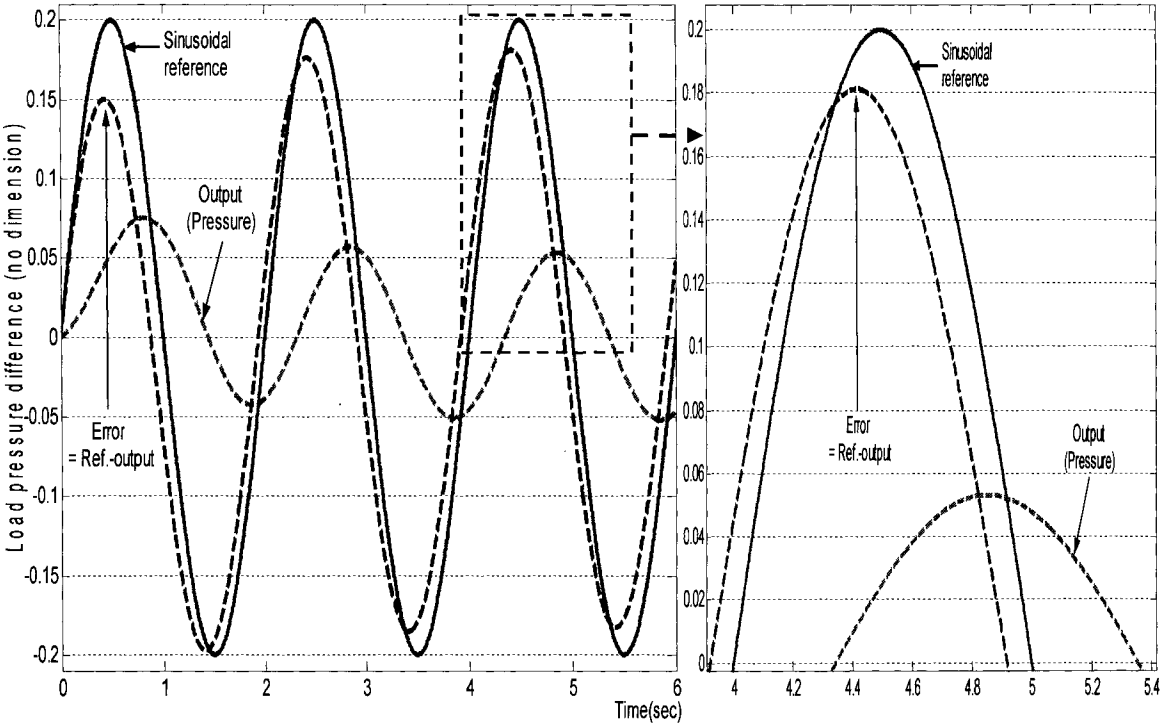

Figure 29 Sinusoidal response of dimensionless load pressure difference by PID controller applied to nonlinear closed-loop system

In comparison with Figure 22, , we see that the delay increases radically from 0.1 sec (linear system) to 0.34 sec (nonlinear system) and the maximum error increases from $\pm$ 0.0608 (linear system) to $\pm$ 0.1813 (nonlinear system). Thus, PID control is inadequate for load pressure control in the nonlinear system for sinusoidal reference commands as well.

■ **Simulation results analysis**

As seen from the simulation results for angular displacement, velocity and pressure control of the nonlinear system, PID control has limitations in coping with the nonlinear hydraulic dynamics and these limitations are seen in the considerable delay and error in tracking performance.

Accordingly, instead of using a traditional linearization based method, we suggest a new control approach which considers the nonlinear nature of the system, and this will be our focus in the next section.

3.3 Feedback linearization theory

3.3.1 Introduction

In spite of its advantages, the PID controller has shown its limitations for hydraulic control, given that the dynamics of hydraulic servo-systems are complex and nonlinear. These limitations of PID control for our hydraulic system have been shown in simulations in 3.2.4.

Therefore, the necessity of designing a controller suited for the nonlinear system is clear. Among the many nonlinear control design techniques described in the literature , we feel that feedback linearization provides a powerful framework for control design which addresses the nonlinear nature of the hydraulic systems and overcomes the drawbacks that PID control has shown.

Feedback linearization is a theoretically rigorous method whose distinctive feature is the use of a state variable transformation (diffeomorphism) to transform the nonlinear

system model into a linear system in the new coordinate basis, through cancellation of nonlinear terms.

In this section, we review the concept of feedback linearization and its application. We will then develop a feedback linearization based controller with high tracking performance for the nonlinear system.

3.3.2 Feedback linearization based controller

First, we describe the basics of feedback linearization.
Consider a nonlinear SISO (single-input single output) system

$$\begin{aligned} \dot{x} &= f(x) + g(x)u \\ y &= h(x) \end{aligned} \tag{3.1}$$

Where u is the control input

We find the dimension (n) of the state vector based on $f(x)$ and $g(x)$, and the relative degree (ρ), defined as the number of integrators between the input u and the output y. After the differentiation of output y, if the n th order derivative of the output y has nonzero coefficients for the control input u, the relative degree ρ is equal to n.

If $\rho = n$, the system is full state feedback linearizable, and we can find a new set of coordinate variables. As our hydraulic system satisfies the condition $\rho = n$, an input-output linearizing state feedback controller can be designed for system control.

Now, define

$$\begin{aligned}
\varepsilon_1 &= h(x) \\
\varepsilon_2 &= \dot{\varepsilon}_1 = L_f h(x) \\
\varepsilon_3 &= \dot{\varepsilon}_2 = L_f{}^2 h(x) \\
&\vdots \\
\varepsilon_n &= \dot{\varepsilon}_{n-1} = L_f{}^{n-1} h(x)
\end{aligned} \tag{3.2}$$

$$\text{Where } L_f h(x) = \sum_{i=1}^{n} \frac{\partial h(x)}{\partial x_i} f_i(x)$$

The next step is to make the change of variables for tracking control using ε found in the previous step. Define

$$e = \begin{bmatrix} \varepsilon_1 - r \\ \varepsilon_2 - r^{(1)} \\ \vdots \\ \varepsilon_n - r^{(n-1)} \end{bmatrix} \tag{3.3}$$

Where r = reference signal

For stabilization, we need the following form:

$$\dot{e} = A_C e + B_c \left[\gamma(x)\left(u - \alpha(x)\right) - r^{(\rho)} \right] \tag{3.4}$$

Where A_c, B_c are canonical forms

The controller is given by

$$u = \alpha(x) + \frac{1}{\gamma(x)}\left[\nu + r^{(\rho)}\right]$$

Where (3.5)

$$\gamma(x) = L_g L_f{}^{\rho-1} h(x),\ \alpha(x) = -\frac{L_f{}^{\rho} h(x)}{L_g L_f{}^{\rho-1} h(x)}$$

Substituting (3.5) in (3.4), we cancel the nonlinear terms and obtain a linear system given by

$$\begin{aligned} \dot{e} &= A_C e + B_c \nu \qquad \text{Where } \nu = -Ke \\ &= \left[A_C - B_c K\right] \cdot e \end{aligned} \tag{3.6}$$

$$\text{Where } K = \begin{bmatrix} k_1 & \cdots & k_n \end{bmatrix},\ e = \begin{bmatrix} e_1 \\ \vdots \\ e_n \end{bmatrix}$$

As a final step, we design the vector K such that the matrix $A_C - B_c K$ of the closed-loop system is Hurwitz, thus guaranteeing closed-loop stability. With K obtained through the Routh-Hurwitz criterion, we create a linearized system that guarantees asymptotic tracking of the reference command.

■ **Design of a controller for angular displacement control by feedback linearization theory**

From the state space model

$$x_1 = \theta,\ x_2 = \Phi,\ x_3 = p_L,\ x_4 = x_v$$

$$\begin{aligned}
\dot{x}_1 &= \omega_{\max} x_2 \\
\dot{x}_2 &= \frac{\omega_h}{\alpha} x_3 - \gamma \frac{\omega_h}{\alpha} x_2 - \frac{\omega_h}{\alpha} t_L \\
\dot{x}_3 &= \alpha \omega_h x_4 \sqrt{1 - x_3 sigm(x_4)} - \alpha \omega_h x_2 - \omega_h c_L x_3 \\
\dot{x}_4 &= -\frac{1}{\tau_v} x_4 + \frac{i}{\tau_v}
\end{aligned} \tag{3.7}$$

We can define the nonlinear system as

$$\begin{aligned}
\dot{x} &= f(x) + g(x)u \\
y &= h(x) = x_1
\end{aligned} \tag{3.8}$$

Where

$$f(x) = \begin{bmatrix} f_1(x) \\ f_2(x) \\ f_3(x) \\ f_4(x) \end{bmatrix} = \begin{bmatrix} \omega_{\max} x_2 \\ \frac{\omega_h}{\alpha} x_3 - \gamma \frac{\omega_h}{\alpha} x_2 \\ \alpha \omega_h x_4 \sqrt{1 - x_3 sigm(x_4)} - \alpha \omega_h x_2 - \omega_h c_L x_3 \\ -\frac{1}{\tau_v} x_4 \end{bmatrix}, \quad g(x) = \begin{bmatrix} g_1(x) \\ g_2(x) \\ g_3(x) \\ g_4(x) \end{bmatrix} = \begin{bmatrix} 0 \\ 0 \\ 0 \\ \frac{1}{\tau_v} \end{bmatrix}$$

Assuming $t_L = 0$

Because the dimension n is 4, we need the 4th order derivative of y to find the relative degree (ρ).

$$y^{(1)} = \dot{x}_1 = \omega_{\max} x_2 \tag{3.9}$$

$$y^{(2)} = \omega_{\max}\dot{x}_2 = \omega_{\max}\left(\frac{\omega_h}{\alpha}x_3 - \gamma\frac{\omega_h}{\alpha}x_2\right) \tag{3.10}$$

$$\begin{aligned} y^{(3)} &= \omega_{\max}\left(\frac{\omega_h}{\alpha}\dot{x}_3 - \gamma\frac{\omega_h}{\alpha}\dot{x}_2\right) \\ &= \omega_{\max}\begin{bmatrix} \frac{\omega_h}{\alpha}\left(\alpha\omega_h x_4\sqrt{1-x_3 sigm(x_4)} - \alpha\omega_h x_2 - \omega_h c_L x_3\right) \\ -\gamma\frac{\omega_h}{\alpha}\left(\frac{\omega_h}{\alpha}x_3 - \gamma\frac{\omega_h}{\alpha}x_2\right) \end{bmatrix} \quad \text{by (4.7)} \\ &= \omega_{\max}\left[\omega^2{}_h x_4 \underbrace{\sqrt{1-x_3 sigm(x_4)}}_{J(x_3,x_4)=J(\cdot)} - \omega^2{}_h\left(1-\frac{\gamma^2}{\alpha^2}\right)x_2 - \frac{\omega^2{}_h}{\alpha}\left(c_L+\frac{\gamma}{\alpha}\right)x_3\right] \end{aligned} \tag{3.11}$$

$$\begin{aligned} y^{(4)} &= \omega_{\max}\left[\omega^2{}_h\left(x_4 J(\cdot)\right)' - \omega^2{}_h\left(1-\frac{\gamma^2}{\alpha^2}\right)\dot{x}_2 - \frac{\omega^2{}_h}{\alpha}\left(c_L+\frac{\gamma}{\alpha}\right)\dot{x}_3\right] \\ &= \omega_{\max}\begin{bmatrix} \omega^2{}_h\left(x_4 J(\cdot)\right)' - \underbrace{\omega^2{}_h\left(1-\frac{\gamma^2}{\alpha^2}\right)}_{a_1}\left(\frac{\omega_h}{\alpha}x_3 - \gamma\frac{\omega_h}{\alpha}x_2\right) \\ -\underbrace{\frac{\omega^2{}_h}{\alpha}\left(c_L+\frac{\gamma}{\alpha}\right)}_{a_2}\left(\alpha\omega_h x_4\underbrace{\sqrt{1-x_3 sigm(x_4)}}_{J(\cdot)} - \alpha\omega_h x_2 - \omega_h c_L x_3\right) \end{bmatrix} \\ &= \omega_{\max}\left[\omega^2{}_h\left(x_4 J(\cdot)\right)' + \left(\frac{a_1\gamma}{\alpha}+a_2\alpha\right)\omega_h x_2 + \left(\frac{-a_1}{\alpha}+a_2 c_L\right)\omega_h x_3 - a_2\alpha\omega_h x_4 J(\cdot)\right] \end{aligned} \tag{3.12}$$

Where

$$\begin{aligned} \left(x_4 J(\cdot)\right)' &= \left(x_4\sqrt{1-x_3 sigm(x_4)}\right)' \\ &= \left(\frac{J(\cdot)}{\tau_v} - \frac{x_4}{2J(\cdot)}x_3\frac{2ae^{-ax_4}}{(1+e^{-ax_4})^2}\cdot\frac{1}{\tau_v}\right)i - \frac{1}{\tau_v}x_4 J(\cdot) \\ &\quad -\frac{x_4}{2J(\cdot)}\begin{pmatrix}\alpha\omega_h x_4 J(\cdot) \\ -\alpha\omega_h x_2 - \omega_h c_L x_3\end{pmatrix}\times sigm(x_4) + \frac{x_4}{2J(\cdot)}x_3\frac{2ae^{-ax_4}}{(1+e^{-ax_4})^2}\cdot\frac{x_4}{\tau_v} \end{aligned} \tag{3.13}$$

From (3.12) and (3.13), it follows that

$$y^{(4)}=\omega_{\max}\left[\begin{array}{l}\omega^2{}_h\cdot\left\{\begin{array}{l}\left(\dfrac{J(\cdot)}{\tau_v}-\dfrac{x_4}{2J(\cdot)}x_3\dfrac{2ae^{-ax_4}}{(1+e^{-ax_4})^2}\cdot\dfrac{1}{\tau_v}\right)i-\dfrac{1}{\tau_v}x_4J(\cdot)\\ -\dfrac{x_4}{2J(\cdot)}\left(\alpha\omega_h x_4J(\cdot)-\alpha\omega_h x_2-\omega_h c_L x_3\right)\times sigm(x_4)\\ +\dfrac{x_4}{2J(\cdot)}x_3\dfrac{2ae^{-ax_4}}{(1+e^{-ax_4})^2}\cdot\dfrac{x_4}{\tau_v}\end{array}\right\}\\ +(\dfrac{a_1\gamma}{\alpha}+a_2\alpha)\omega_h x_2+(\dfrac{-a_1}{\alpha}+a_2c_L)\omega_h x_3-a_2\alpha\omega_h x_4J(\cdot)\end{array}\right] \tag{3.14}$$

From (3.14) we note that the 4th order derivative of the output $y=x_1$ has a nonzero coefficient for the input i. Accordingly, ρ (relative degree) $= n = 4$.

The condition $\rho = n$ ensures that the system is full state feedback linearizable, and we can employ the following change of coordinates:

$$\begin{aligned}\varepsilon_1 &= h(x)\\ \varepsilon_2 &= \dot{\varepsilon}_1 = L_f h(x)\\ \varepsilon_3 &= \dot{\varepsilon}_2 = L_f{}^2 h(x)\\ \varepsilon_4 &= \dot{\varepsilon}_3 = L_f{}^3 h(x)\end{aligned} \tag{3.15}$$

So,

$$\varepsilon_1 = h(x) = x_1 \tag{3.16}$$

$$\begin{aligned}\varepsilon_2 = L_f h(x) &= \frac{\partial h(x)}{\partial x}\cdot f(x) = \frac{\partial x_1}{\partial x}\cdot f(x)\\ &= \frac{\partial x_1}{\partial x_1}\cdot f_1(x)+\frac{\partial x_1}{\partial x_2}\cdot f_2(x)+\frac{\partial x_1}{\partial x_3}\cdot f_3(x)+\frac{\partial x_1}{\partial x_4}\cdot f_4(x)\\ &= f_1(x) = \omega_{\max}x_2\end{aligned} \tag{3.17}$$

$$\begin{aligned}\varepsilon_3 = L_f{}^2 h(x) &= \frac{\partial\left(L_f h(x)\right)}{\partial x}\cdot f(x) = \frac{\partial \omega_{\max} x_2}{\partial x}\cdot f(x) \\ &= \frac{\partial\left(\omega_{\max} x_2\right)}{\partial x_1}\cdot f_1(x) + \frac{\partial\left(\omega_{\max} x_2\right)}{\partial x_2}\cdot f_2(x) + \frac{\partial\left(\omega_{\max} x_2\right)}{\partial x_3}\cdot f_3(x) \\ &+ \frac{\partial\left(\omega_{\max} x_2\right)}{\partial x_4}\cdot f_4(x) \\ &= \omega_{\max} f_2(x) = \omega_{\max}\left(\frac{\omega_h}{\alpha} x_3 - \gamma\frac{\omega_h}{\alpha} x_2\right)\end{aligned} \tag{3.18}$$

$$\begin{aligned}\varepsilon_4 = L_f{}^3 h(x) &= \frac{\partial\left(L_f{}^2 h(x)\right)}{\partial x}\cdot f(x) = \frac{\partial\left(\omega_{\max}\left(\frac{\omega_h}{\alpha} x_3 - \gamma\frac{\omega_h}{\alpha} x_2\right)\right)}{\partial x}\cdot f(x) \\ &= \left(\omega_{\max}\gamma^2\frac{\omega_h{}^2}{\alpha^2} - \omega_{\max}\omega_h{}^2\right)x_2 + \left(-\omega_{\max}\gamma\frac{\omega_h{}^2}{\alpha^2} - \omega_{\max}\frac{\omega_h{}^2}{\alpha} c_L\right)x_3 \\ &+ \omega_{\max}\omega_h{}^2 x_4\sqrt{1 - x_3 sigm(x_4)}\end{aligned} \tag{3.19}$$

The following change of variables is necessary for tracking control.

$$e = \begin{bmatrix} \varepsilon_1 - r \\ \varepsilon_2 - r^{(1)} \\ \varepsilon_3 - r^{(2)} \\ \varepsilon_4 - r^{(3)} \end{bmatrix} \tag{3.20}$$

Using equations (3.16), (3.17), (3.18) and (3.19), we get

$$e=\begin{bmatrix} x_1-r \\ \omega_{\max}x_2-r^{(1)} \\ \omega_{\max}(\frac{\omega_h}{\alpha}x_3-\gamma\frac{\omega_h}{\alpha}x_2)-r^{(2)} \\ (\omega_{\max}\gamma^2\frac{\omega^2{}_h}{\alpha^2}-\omega_{\max}\omega^2{}_h)x_2+(-\omega_{\max}\gamma\frac{\omega^2{}_h}{\alpha^2}-\omega_{\max}\frac{\omega^2{}_h}{\alpha}c_L)x_3 \\ +\omega_{\max}\omega^2{}_h x_4\sqrt{1-x_3 sigm(x_4)}-r^{(3)} \end{bmatrix} \tag{3.21}$$

Where r is a reference signal vector

The following form is used for the stabilization problem:

$$\dot{e}=A_C e+B_c\left[\gamma(x)\left(u-\alpha(x)\right)-r^{(4)}\right] \tag{3.22}$$

Where A_c, B_c are canonical forms

$$\text{(i.e.) } A_c=\begin{bmatrix} 0 & 1 & 0 & 0 \\ 0 & 0 & 1 & 0 \\ 0 & 0 & 0 & 1 \\ 0 & 0 & 0 & 0 \end{bmatrix} \quad B_c=\begin{bmatrix} 0 \\ 0 \\ 0 \\ 1 \end{bmatrix}$$

From Equation (3.5), the controller is given by

$$u=\alpha(x)+\frac{1}{\gamma(x)}\left[v+r^{(4)}\right] \tag{3.23}$$

Where

$$\begin{aligned}\gamma(x) &= L_g L_f{}^{\rho-1} h(x) \\ &= L_g L_f{}^{3} h(x) \\ &= \frac{\partial\left(L_f{}^{3} h(x)\right)}{\partial x} g(x) \\ &= \left\{ \omega_{\max} \omega_h{}^{2} \sqrt{1 - x_3 sigm(x_4)} + \frac{\omega_{\max} \omega_h{}^{2} x_4}{2\sqrt{1 - x_3 sigm(x_4)}} \cdot \left(-x_3 \cdot \frac{2ae^{-ax_4}}{(1+e^{-ax_4})^2} \right) \right\} \cdot \frac{1}{\tau_v}\end{aligned} \tag{3.24}$$

$$\alpha(x) = -\frac{L_f{}^{\rho} h(x)}{L_g L_f{}^{\rho-1} h(x)} = -\frac{L_f{}^{4} h(x)}{L_g L_f{}^{3} h(x)} = -\frac{L_f{}^{4} h(x)}{\gamma(x)}$$

$$= \frac{\left[\begin{array}{l} \left(\omega_{\max} \gamma^2 \frac{\omega_h{}^{2}}{\alpha^2} - \omega_{\max} \omega_h{}^{2} \right) \left(\frac{\omega_h}{\alpha} x_3 - \gamma \frac{\omega_h}{\alpha} x_2 \right) \\ + \left\{ \begin{array}{l} \left(-\omega_{\max} \gamma \frac{\omega_h{}^{2}}{\alpha^2} - \omega_{\max} \frac{\omega_h{}^{2}}{\alpha} c_L \right) \\ + \omega_{\max} \omega_h{}^{2} x_4 \cdot \frac{1}{2\sqrt{1 - x_3 sigm(x_4)}} \left(-sigm(x_4) \right) \end{array} \right\} \times \begin{pmatrix} \alpha \omega_h x_4 \sqrt{1 - x_3 sigm(x_4)} \\ -\alpha \omega_h x_2 - \omega_h c_L x_3 \end{pmatrix} \\ + \left\{ \begin{array}{l} \omega_{\max} \omega_h{}^{2} \sqrt{1 - x_3 sigm(x_4)} \\ + \frac{\omega_{\max} \omega_h{}^{2} x_4}{2\sqrt{1 - x_3 sigm(x_4)}} \cdot \left(-x_3 \cdot \frac{2ae^{-ax_4}}{(1+e^{-ax_4})^2} \right) \end{array} \right\} \cdot \left(-\frac{1}{\tau_v} x_4 \right) \end{array} \right]}{\left\{ \omega_{\max} \omega_h{}^{2} \sqrt{1 - x_3 sigm(x_4)} + \frac{\omega_{\max} \omega_h{}^{2} x_4}{2\sqrt{1 - x_3 sigm(x_4)}} \cdot \left(-x_3 \cdot \frac{2ae^{-ax_4}}{(1+e^{-ax_4})^2} \right) \right\} \cdot \frac{1}{\tau_v}} \tag{3.25}$$

Using (3.22) and (3.23), it follows that

$$\begin{aligned}\dot{e} &= A_C e + B_c\left[\gamma(x)\left(u-\alpha(x)\right)-r^{(4)}\right] \\ &= A_C e + B_c v \\ &= \left[A_C - B_c K\right]\cdot e\end{aligned} \tag{3.26}$$

Where $v = -Ke$, $K = [k_1 \quad k_2 \quad k_3 \quad k_4]$ and $e = \begin{bmatrix} e_1 \\ e_2 \\ e_3 \\ e_4 \end{bmatrix}$

To stabilize the system, we have to design K such that $A_C - B_c K$ is Hurwitz.

The characteristic polynomial is

$$\begin{aligned}&\det(\lambda I - (A_C - B_c K)) \\ &= \begin{vmatrix} \lambda & -1 & 0 & 0 \\ 0 & \lambda & -1 & 0 \\ 0 & 0 & -1 & -1 \\ k_1 & k_2 & k_3 & k_4 \end{vmatrix} = \lambda^4 + k_4\lambda^3 + k_3\lambda^2 + k_2\lambda^1 + k_1\end{aligned} \tag{3.27}$$

By using the Routh-Hurwitz criterion, we can find conditions on all coefficients (k_1, k_2, k_3, k_4).

$$\begin{array}{c|cc} s^4 & 1 & k_3 \quad k_1 \\ s^3 & k_4 & k_2 \quad 0 \\ s^2 & \dfrac{-(k_2 - k_3\cdot k_4)}{k_4} & k_1 \quad 0 \\ s^1 & \dfrac{k_1\cdot k_4{}^2 + k_2\cdot(k_2 - k_3\cdot k_4)}{k_2 - k_3\cdot k_4} & \\ s^0 & k_1 & \end{array} \tag{3.28}$$

$$k_4 > 0, \quad \frac{-(k_2 - k_3\cdot k_4)}{k_4} > 0, \quad \frac{k_1\cdot k_4{}^2 + k_2\cdot(k_2 - k_3\cdot k_4)}{k_2 - k_3\cdot k_4} > 0, \quad k_1 > 0$$

We now choose values for k_1, k_2, k_3 and k_4 satisfying the conditions for the Routh-Hurwitz criterion as

$$\begin{aligned} k_1 &= 2\times 10^8 \\ k_2 &= 2\times 10^7 \\ k_3 &= 5\times 10^5 \\ k_4 &= 1\times 10^2 \end{aligned} \tag{3.29}$$

Using (3.23), (3.29) and $v = -Ke$, we can rearrange the expression for u.

$$\begin{aligned} u &= \alpha(x) + \frac{1}{\gamma(x)}\left[-Ke + r^{(4)}\right] \\ &= \alpha(x) + \frac{1}{\gamma(x)}\left[-k_1 e_1 - k_2 e_2 - k_3 e_3 - k_4 e_4 + r^{(4)}\right] \end{aligned} \tag{3.30}$$

Equation (3.30) describes the feedback linearization based controller for angular displacement control of the actuator in the nonlinear system.

■ **Design of a controller for angular velocity control by feedback linearization theory**

Let us now consider the case of angular velocity control. Through inspection of the system in Equation (3.7), we can verify the stability of the internal state x_1 in the first equation of (3.7). By assuming $x_2 = 0$ in the first equation of (3.7), we note that the state x_1 is stable as

$$\dot{x}_1 = \omega_{\max} x_2 = 0 \tag{3.31}$$

Therefore, it is not necessary to stabilize x_1, and thus the feedback linearization procedure uses only x_2, x_3 and x_4.

The nonlinear SISO system excluding x_1 is as follows:

$$\dot{x} = f(x) + g(x)u$$
$$y = h(x) = x_2$$

Where

$$f(x) = \begin{bmatrix} f_1(x) \\ f_2(x) \\ f_3(x) \end{bmatrix} = \begin{bmatrix} \frac{\omega_h}{\alpha} x_3 - \gamma \frac{\omega_h}{\alpha} x_2 \\ \alpha\omega_h x_4 \sqrt{1 - x_3 sigm(x_4)} - \alpha\omega_h x_2 - \omega_h c_L x_3 \\ -\frac{1}{\tau_v} x_4 \end{bmatrix}, g(x) = \begin{bmatrix} g_1(x) \\ g_2(x) \\ g_3(x) \end{bmatrix} = \begin{bmatrix} 0 \\ 0 \\ \frac{1}{\tau_v} \end{bmatrix} \quad (3.32)$$

The dimension n of the system is 3 and therefore the 3rd order derivative of y has to be calculated.

$$y^{(1)} = \dot{x}_2 = (\frac{\omega_h}{\alpha} x_3 - \gamma \frac{\omega_h}{\alpha} x_2) \quad (3.33)$$

$$y^{(2)} = -\omega^2{}_h (1 - \frac{\gamma^2}{\alpha^2}) x_2 - \frac{\omega^2{}_h}{\alpha}(c_L + \frac{\gamma}{\alpha}) x_3 + \omega^2{}_h x_4 \sqrt{1 - x_3 sigm(x_4)} \quad (3.34)$$

$$y^{(3)} = \underbrace{-\omega^2{}_h (1 - \frac{\gamma^2}{\alpha^2})}_{L_1(\bullet)} \dot{x}_2 \underbrace{- \frac{\omega^2{}_h}{\alpha}(c_L + \frac{\gamma}{\alpha})}_{L_2(\bullet)} \dot{x}_3 \underbrace{- \frac{\omega^2{}_h x_4 \dot{x}_3 sigm(x_4)}{2\sqrt{1 - x_3 sigm(x_4)}}}_{L_3(\bullet)}$$
$$\underbrace{+ \left(\omega^2{}_h \sqrt{1 - x_3 sigm(x_4)} - \frac{\omega^2{}_h x_4 x_3 \frac{2ae^{-ax_4}}{(1 + e^{-ax_4})^2}}{2\sqrt{1 - x_3 sigm(x_4)}} \right)}_{L_4(\bullet)} \dot{x}_4$$
$$= L_1(\bullet)\dot{x}_2 + L_2(\bullet)\dot{x}_3 + L_3(\bullet) + L_4(\bullet)\left(-\frac{1}{\tau_v} x_4 + \frac{i}{\tau_v} \right) \quad (3.35)$$

As seen from (3.35), the fact that the 3rd order derivative of the output $y = x_2$ has a nonzero coefficient for the input i means $\rho = n = 3$. Consequently, the system is full state feedback linearizable, and thus a controller for linearizing the system can be derived.

Define the following new coordinate variables:

$$\begin{aligned} \varepsilon_1 &= h(x) \\ \varepsilon_2 &= \dot{\varepsilon}_1 = L_f h(x) \\ \varepsilon_3 &= \dot{\varepsilon}_2 = L_f{}^2 h(x) \end{aligned} \tag{3.36}$$

Thus,

$$\varepsilon_1 = h(x) = x_2 \tag{3.37}$$

$$\varepsilon_2 = L_f h(x) = \frac{\omega_h}{\alpha} x_3 - \gamma \frac{\omega_h}{\alpha} x_2 \tag{3.38}$$

$$\begin{aligned} \varepsilon_3 &= L_f{}^2 h(x) \\ &= \left(-\omega_h{}^2 + \gamma^2 \frac{\omega_h{}^2}{\alpha^2} \right) x_2 + \left(-\frac{\omega_h{}^2}{\alpha} c_L - \gamma \frac{\omega_h{}^2}{\alpha^2} \right) x_3 + \omega_h{}^2 x_4 \sqrt{1 - x_3 sigm(x_4)} \end{aligned} \tag{3.39}$$

Using equations (3.36) to (3.39), the variables related to tracking error can be defined as

$$e=\begin{bmatrix}\varepsilon_1-r\\ \varepsilon_2-r^{(1)}\\ \varepsilon_3-r^{(2)}\end{bmatrix}$$

$$=\begin{bmatrix}x_2-r\\ \frac{\omega_h}{\alpha}x_3-\gamma\frac{\omega_h}{\alpha}x_2-r^{(1)}\\ \left(-\omega_h{}^2+\gamma^2\frac{\omega_h{}^2}{\alpha^2}x_2\right)x_2+\left(-\frac{\omega_h{}^2}{\alpha}c_L-\gamma\frac{\omega_h{}^2}{\alpha^2}x_2\right)x_3+\omega_h{}^2x_4\sqrt{1-x_3sigm(x_4)}-r^{(2)}\end{bmatrix} \quad (3.40)$$

r : reference of output

Next,

$$\dot{e}=A_Ce+B_c\left[\gamma(x)\left(u-\alpha(x)\right)-r^{(3)}\right] \quad (3.41)$$

$$\text{Where } A_c=\begin{bmatrix}0&1&0\\0&0&1\\0&0&0\end{bmatrix}\quad B_c=\begin{bmatrix}0\\0\\1\end{bmatrix}$$

For the controller,

$$u=\alpha(x)+\frac{1}{\gamma(x)}\left[\nu+r^{(3)}\right] \quad (3.42)$$

Where

$$\gamma(x)=\left(\omega_h{}^2\sqrt{1-x_3sigm(x_4)}+\frac{\omega_h{}^2x_4\left(-x_3\frac{2ae^{-ax_4}}{(1+e^{-ax_4})^2}\right)}{2\sqrt{1-x_3sigm(x_4)}}\right)\cdot\frac{1}{\tau_v}$$

$$\alpha(x) =$$

$$\frac{\left[\begin{array}{l}\left(-\omega_h{}^2+\gamma^2\frac{\omega_h{}^2}{\alpha^2}\right)\cdot\left(\frac{\omega_h}{\alpha}x_3-\gamma\frac{\omega_h}{\alpha}x_2\right)+\left[\begin{array}{l}\left(-\frac{\omega_h{}^2}{\alpha}c_L-\gamma\frac{\omega_h{}^2}{\alpha^2}\right)\\ +\left\{\frac{\omega^2{}_h x_4}{2\sqrt{1-x_3 sigm(x_4)}}\cdot\left(-sigm(x_4)\right)\right\}\end{array}\right]\\ \times\left(\alpha\omega_h x_4\sqrt{1-x_3 sigm(x_4)}-\alpha\omega_h x_2-\omega_h c_L x_3\right)\\ +\left\{\begin{array}{l}\omega^2{}_h\sqrt{1-x_3 sigm(x_4)}\\ +\frac{\omega^2{}_h x_4}{2\sqrt{1-x_3 sigm(x_4)}}\cdot\left(-x_3\frac{2ae^{-ax_4}}{(1+e^{-ax_4})^2}\right)\end{array}\right\}\cdot\left(-\frac{1}{\tau_v}x_4\right)\end{array}\right]}{\left(\omega_h{}^2\sqrt{1-x_3 sigm(x_4)}+\frac{\omega_h{}^2 x_4\left(-x_3\frac{2ae^{-ax_4}}{(1+e^{-ax_4})^2}\right)}{2\sqrt{1-x_3 sigm(x_4)}}\right)\cdot\frac{1}{\tau_v}}$$

From (3.41) and (3.42), it follows that

$$\begin{aligned}\dot{e} &= A_C e + B_c v \qquad \text{where } v = -Ke\\ &= \left[A_C - B_c K\right]\cdot e\end{aligned} \tag{3.43}$$

By the Routh-Hurwitz method, the condition for K is found such that the matrix $A_C - B_c K$ is Hurwitz.

$$k_3 > 0,\ -\frac{\left(k_1 - k_2 k_3\right)}{k_3} > 0 \text{ and } k_1 > 0 \tag{3.44}$$

Therefore, we choose

$$\begin{aligned} k_1 &= 2.5\times10^6 \\ k_2 &= 2\times10^5 \\ k_2 &= 1\times10^2 \end{aligned} \tag{3.45}$$

Using (3.42), (3.45) and $v=-Ke$, we obtain a feedback linearization based controller to control the angular velocity of the nonlinear system, and this controller is given by

$$u=\alpha(x)+\frac{1}{\gamma(x)}\left[-k_1e_1-k_2e_2-k_3e_3+r^{(3)}\right] \tag{3.46}$$

■ **Design of a controller for load pressure difference by feedback linearization theory**

By assuming $x_3=0$ in the first and second equations of (3.7), we can check if the internal states x_1 and x_2 are stable.

$$\begin{aligned} \dot{x}_1 &= \omega_{\max}x_2 \\ \dot{x}_2 &= -\gamma\frac{\omega_h}{\alpha}x_2 \\ \dot{x} &= \begin{bmatrix}\dot{x}_1\\ \dot{x}_2\end{bmatrix} = \begin{bmatrix}0 & \omega_{\max}\\ 0 & -\gamma\dfrac{\omega_h}{\alpha}\end{bmatrix}\begin{bmatrix}x_1\\ x_2\end{bmatrix} = Ax \end{aligned} \tag{3.47}$$

We verify the stability of the internal states of x_1 and x_2 using the matrix A.

$$\begin{aligned} &Det(\lambda I-A) \\ &=\left|\begin{bmatrix}\lambda & 0\\ 0 & \lambda\end{bmatrix}-\begin{bmatrix}0 & \omega_{\max}\\ 0 & -\gamma\dfrac{\omega_h}{\alpha}\end{bmatrix}\right| = \left|\begin{bmatrix}\lambda & -\omega_{\max}\\ 0 & \lambda+\gamma\dfrac{\omega_h}{\alpha}\end{bmatrix}\right| \end{aligned}$$

$$= \lambda^2 + \gamma \frac{\omega_h}{\alpha} \lambda = 0$$

$$\Rightarrow \lambda_1 + \lambda_2 = -\gamma \frac{\omega_h}{\alpha}, \quad \lambda_1 \cdot \lambda_2 = 0$$

$$\therefore \quad \lambda_1 < 0, \lambda_2 = 0 \text{ or } \lambda_1 = 0, \lambda_2 < 0$$

From the characteristic equation obtained from the determinant of $\lambda I - A$, we see that the internal states x_1 and x_2 are stable.

Therefore, we can develop a feedback linearizable SISO system using only x_3 and x_4.

$$\begin{aligned} \dot{x} &= f(x) + g(x)u \\ y &= h(x) = x_3 \end{aligned} \tag{3.48}$$

Where

$$f(x) = \begin{bmatrix} f_1(x) \\ f_2(x) \end{bmatrix} = \begin{bmatrix} \alpha\omega_h x_4 \sqrt{1 - x_3 sigm(x_4)} - \alpha\omega_h x_2 - \omega_h c_L x_3 \\ -\frac{1}{\tau_v} x_4 \end{bmatrix}, g(x) = \begin{bmatrix} g_1(x) \\ g_2(x) \end{bmatrix} = \begin{bmatrix} 0 \\ \frac{1}{\tau_v} \end{bmatrix}$$

x_3 (non-dimensional load pressure difference) is the output of interest.

The dimension n of the system is 2, and therefore we need to find the 2nd order derivative of y

$$y^{(1)} = \dot{x}_3 = \alpha\omega_h x_4 \sqrt{1 - x_3 sigm(x_4)} - \alpha\omega_h x_2 - \omega_h c_L x_3 \tag{3.49}$$

$$
\begin{aligned}
y^{(2)} &= \underbrace{\left(\alpha\omega_h \sqrt{1 - x_3 sigm(x_4)} - \frac{\alpha\omega_h x_4}{2\sqrt{1 - x_3 sigm(x_4)}} \cdot x_3 \cdot \frac{2ae^{-ax_4}}{(1+e^{-ax_4})^2} \right)}_{L_1(\bullet)} \dot{x}_4 \\
&\quad + \underbrace{\left(-\frac{\alpha\omega_h x_4 sigm(x_4)}{2\sqrt{1 - x_3 sigm(x_4)}} - \omega_h c_L \right)}_{L_2(\bullet)} \dot{x}_3 - \underbrace{\alpha\omega_h}_{L_3(\bullet)} \dot{x}_2 \\
&= L_1(\bullet) \cdot \left(-\frac{1}{\tau_v} x_4 + \frac{i}{\tau_v} \right) + L_2(\bullet)\dot{x}_3 - L_3(\bullet)\dot{x}_2
\end{aligned}
\tag{3.50}
$$

Since $\rho = n = 2$, the system is full state feedback linearizable. Thus, we are able to design an input-output linearizing state feedback controller.

The controller design procedure is the same as that for the cases of angular displacement and velocity.

Thus, the feedback linearization based controller for load pressure control can be obtained as:

$$
u = \alpha(x) + \frac{1}{\gamma(x)} \left[-k_1 e_1 - k_2 e_2 + r^{(2)} \right] \tag{3.51}
$$

Where

$$
e = \begin{bmatrix} \varepsilon_1 - r \\ \varepsilon_2 - r^{(1)} \end{bmatrix} = \begin{bmatrix} x_3 - r \\ \alpha\omega_h x_4 \sqrt{1 - x_3 sigm(x_4)} - \alpha\omega_h x_2 - \omega_h c_L x_3 - r^{(1)} \end{bmatrix}, \quad K = \begin{bmatrix} 5 \times 10^5 \\ 1.25 \times 10^3 \end{bmatrix}
$$

r : reference of output

3.3.3 Feedback linearization based controller for nonlinear system

Based on the equations (3.3), (3.5) and K, we can design the feedback linearization based controllers to control the angular displacement, velocity and load pressure of the nonlinear system.

As shown from the following schematic, the controller designed by feedback linearization method requires quantities (e.g., $sigm(x_4)$, $\sqrt{(1\text{-}x_3 sigm(x_4))}$, x_4, x_3, x_2 and x_1) calculated from the states of the nonlinear system. According to the reference and output type, our designed controller generates the desired control signal and sends it to the nonlinear system.

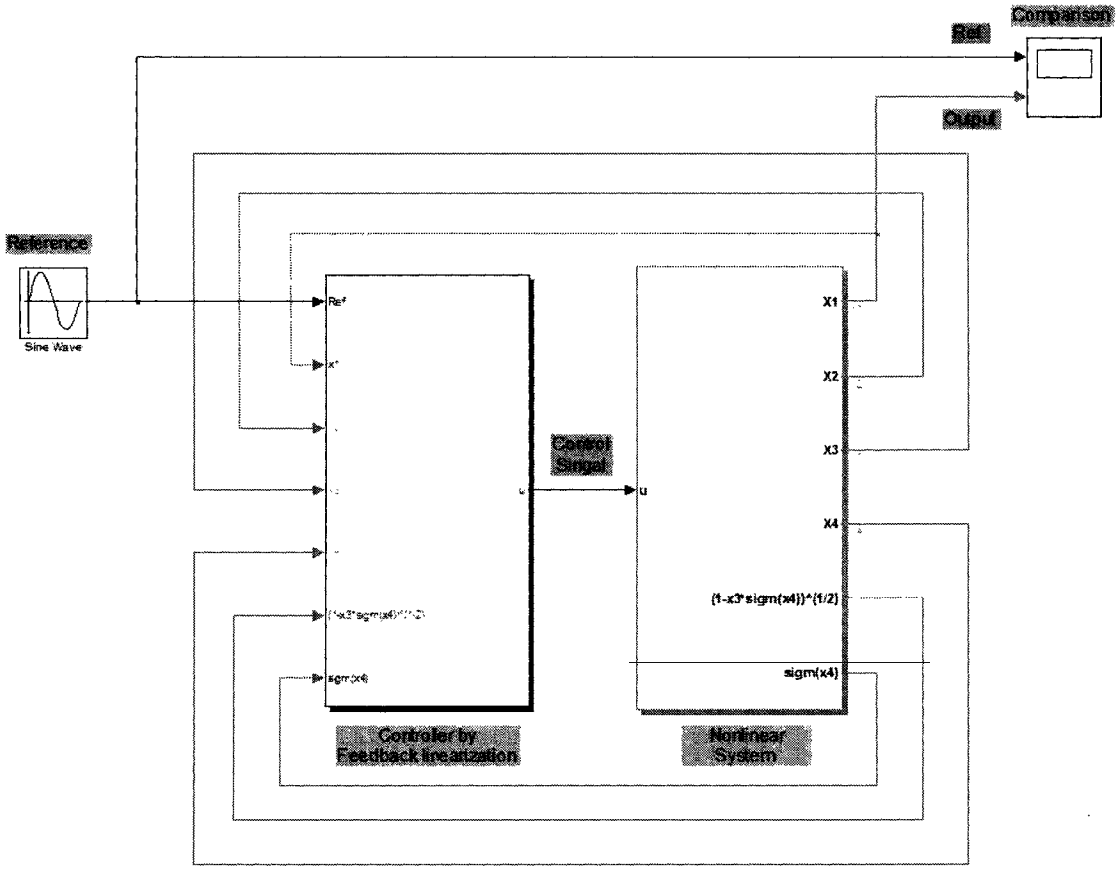

Figure 30 Design of feedback linearizable system

The performance of this controller is validated using MATLAB/Simulink based simulation. All reference types for each output for simulation are the same as the ones in 3.2.4 for equivalent comparison with the performance of the PID controllers for the nonlinear system.

However, we omit the case of a constant reference for velocity and load pressure difference. Because the constant output reference causes the actuator to rotate infinitely in one direction, numerical overflows may occur during real-time implementation.

Using a comparative analysis of the simulation results with the two controllers (i.e., PID controller and feedback linearization based controller), we will verify that the feedback linearization approach greatly contributes to the improvement in closed-loop performance in terms of accuracy and response rate for the nonlinear system.

■ **Simulation results**

▪ **Angular displacement**

▫ Comparison of performance between feedback linearization based controller and PID controller for constant reference: 1 (unit step)

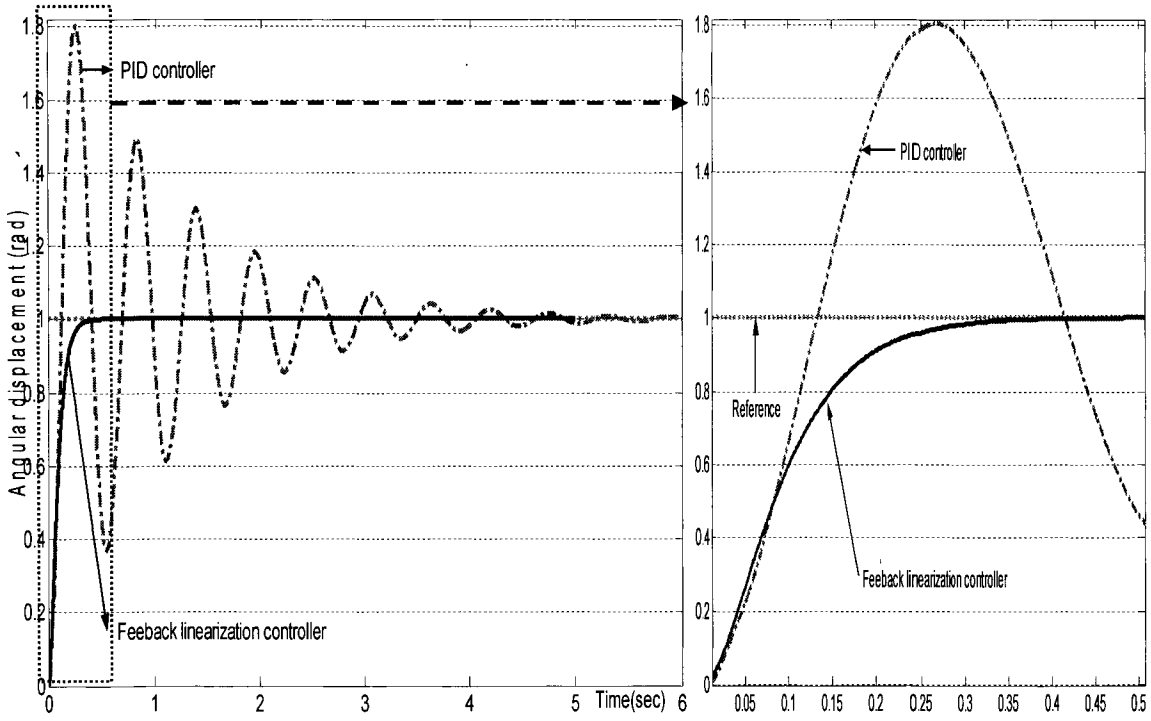

Figure 31 Comparison between feedback linearization based controller and PID controller for angular displacement control

To compare the performance of the feedback linearization based controller with the PID controller for angular displacement, we plot the simulation results of the two controllers together in the same figure.

As seen in Figure 31, the PID controller shows a large overshoot and oscillations for about 6 sec and slow settling to the constant reference, while the feedback linearization based controller shows high performance for angular displacement control. The superior

performance of the feedback linearization based controller can be verified by magnifying the data from the early part of the simulation. The required time of 0.4 sec to reach the reference shows the fast response rate, and the absence of overshoot and quick settling show the high accuracy of the controller.

▫ Response of feedback linearization based controller for sinusoidal reference: $1 \cdot \sin \pi t$

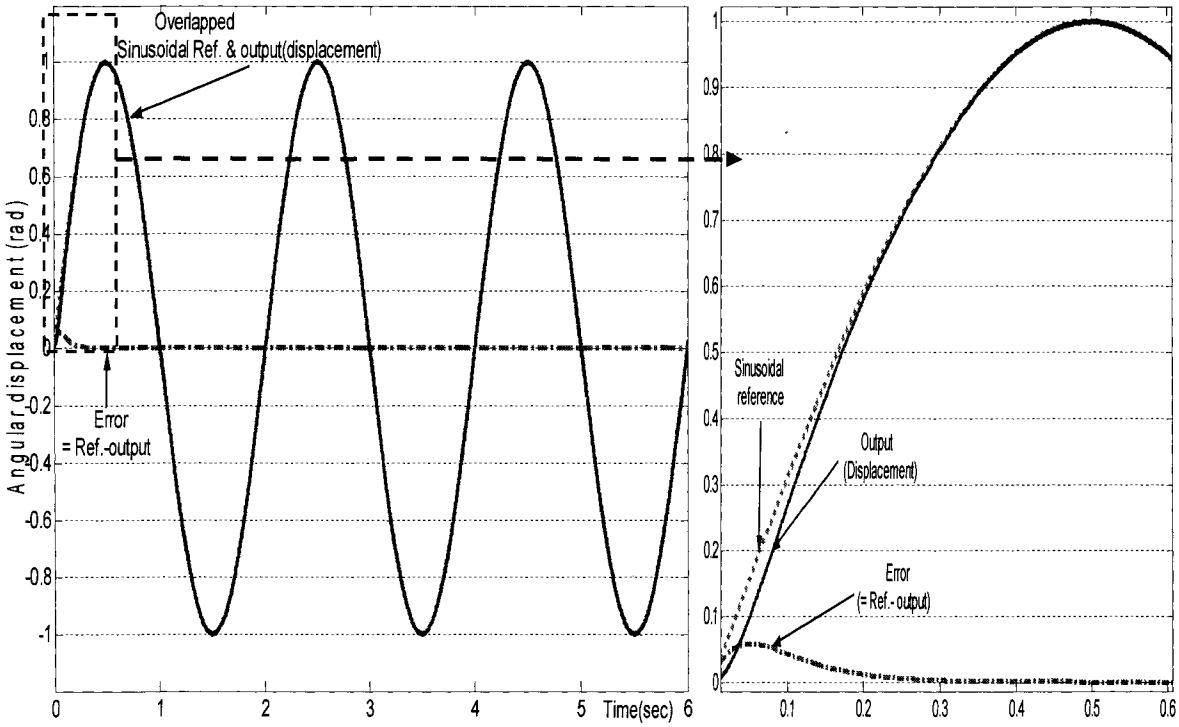

Figure 32 Sinusoidal response of feedback linearization based controller for angular displacement control

The response rate for the sinusoidal reference is very high (0.3 sec: to achieve steady-state). The output accurately tracks the reference after 0.3 sec, and the error between reference and output rapidly goes to zero. Based on these simulation results, we see that the feedback linearization based controller for angular displacement provides high tracking precision and fast response with sinusoidal reference commands as well.

- Comparison of performance between feedback linearization based controller and PID controller for sinusoidal reference: $1 \cdot \sin \pi t$

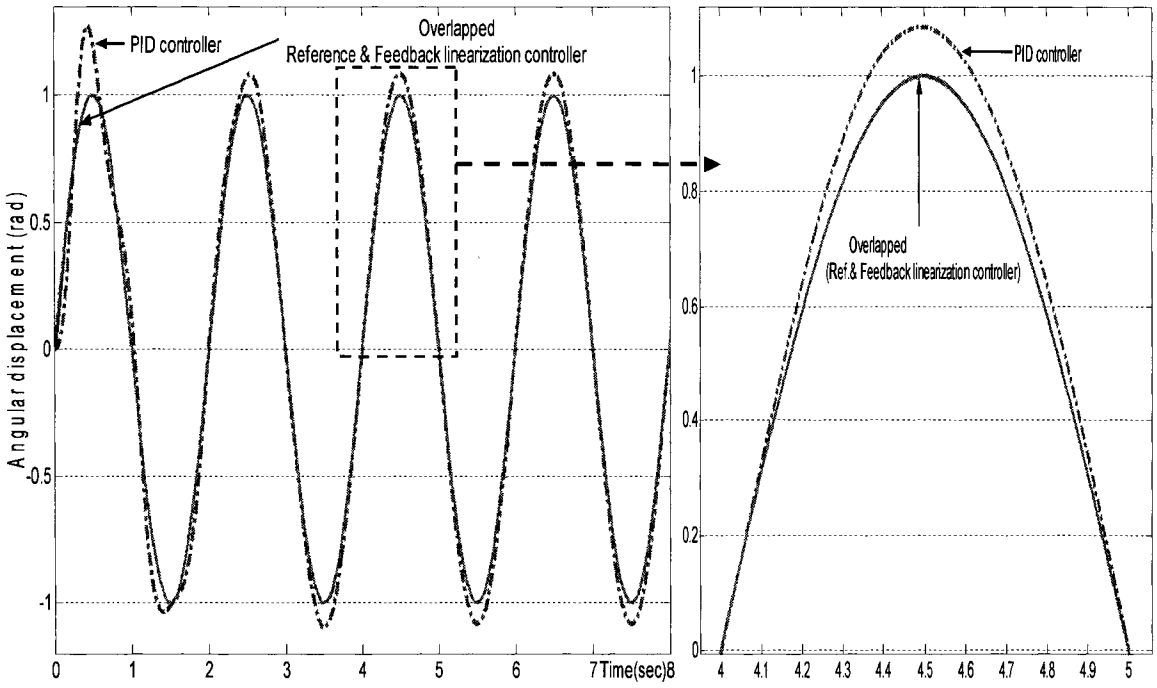

Figure 33 Comparison between feedback linearization based controller and PID controller for angular displacement control

The initial data plotted in Figure 33 shows the transient response of the system, and thus, we omit it for the following comparative analysis. We consider the steady-state section from 4 to 5 sec for detailed analysis. As seen from the enlarged figure on the right, the output of the system using the feedback linearized controller overlaps with the reference, while the output response using the PID controller presents a maximum error of $\pm$ 0.0826 between reference and output. The time (4 sec) for the PID controller to get to steady-state is longer than that (0.3 sec) of the feedback linearization based controller. These results clearly show the difference in performance and response rate between the two controllers.

- **Angular velocity**

  - Response of feedback linearization based controller for sinusoidal reference: $0.35 \cdot \sin \pi t$

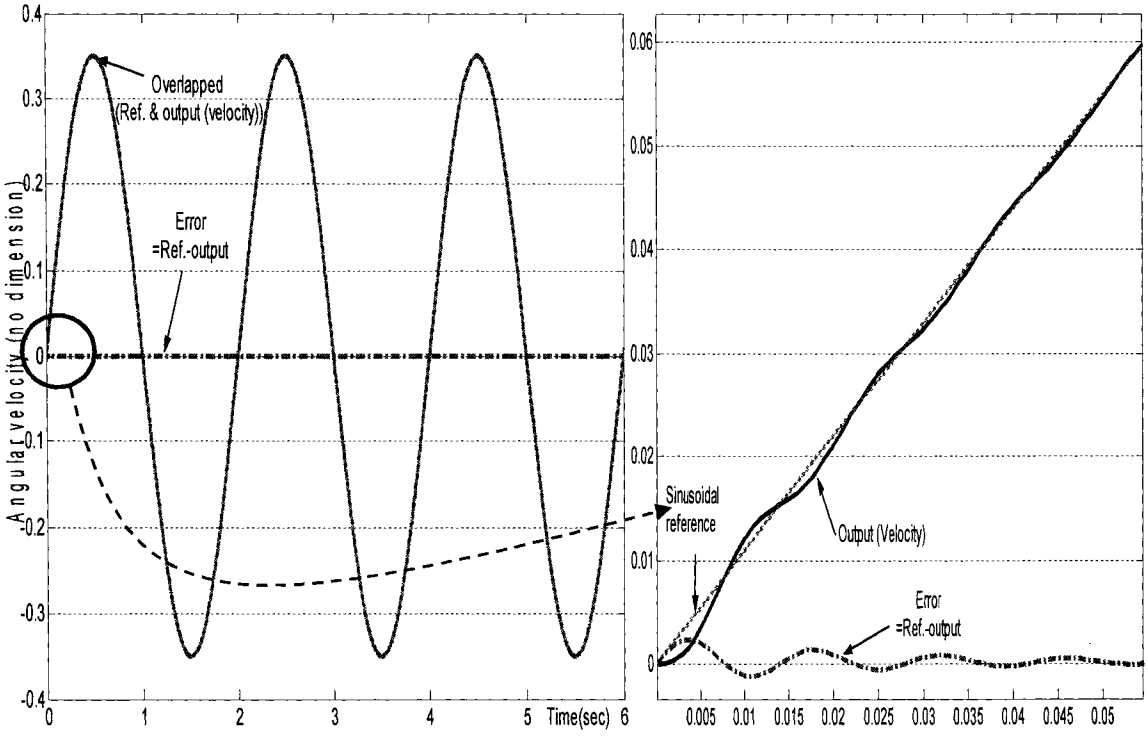

Figure 34 Sinusoidal response of feedback linearization based controller for angular velocity

The tracking response for the angular velocity output is much faster than that for angular displacement. After 0.05 sec, the output is exactly identical to the sinusoidal reference and the error is close to zero. The fast response and accuracy are remarkable, and these plots clearly show the superiority of the feedback linearization controller over the PID controller.

- Comparison of performance between feedback linearization based controller and PID controller for sinusoidal reference: $0.35 \cdot \sin \pi t$

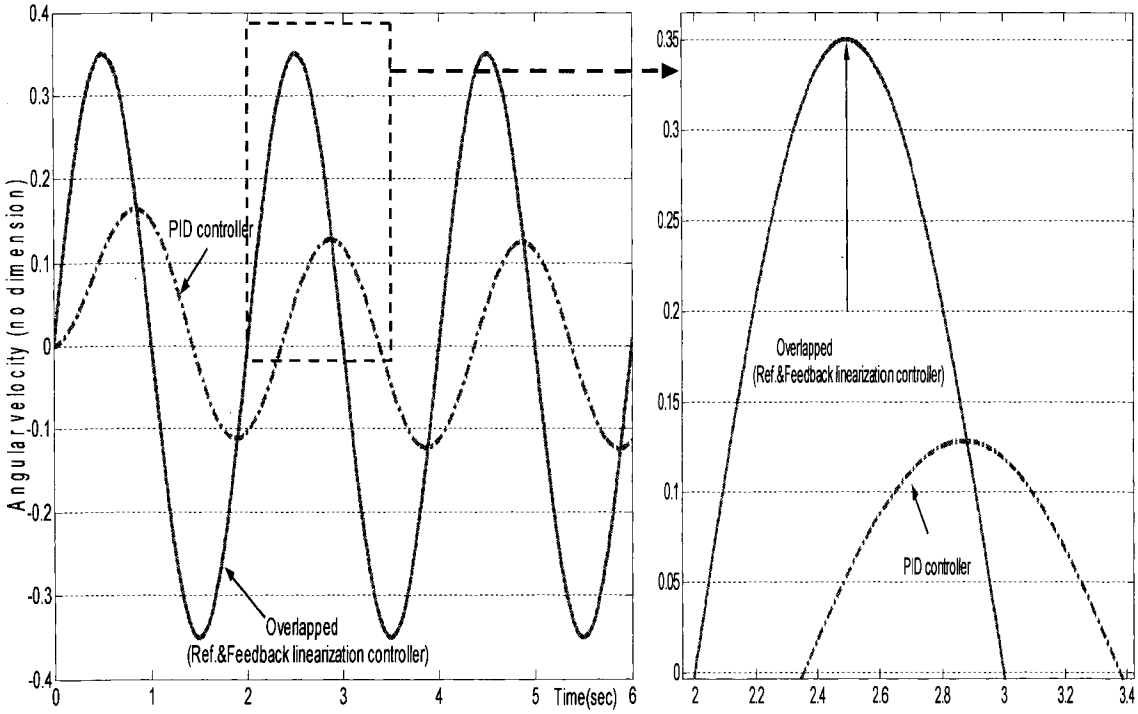

Figure 35 Comparison between feedback linearization based controller and PID controller for angular velocity control

The steady-state output (after the initial 2 sec) obtained using the PID controller shows a constant delay of 0.373 sec, and a maximum error of ± 0.323 between the sinusoidal reference and the output, whereas the output response obtained with the feedback linearization controller tracks the reference without any delay or error. Therefore, we can conclude that the controller designed using feedback linearization theory overcomes the performance limitations of the PID controller for angular velocity control in the nonlinear system.

- **Load pressure difference**

▫ Response of feedback linearization based controller for sinusoidal reference:

$0.2 \cdot \sin \pi t$

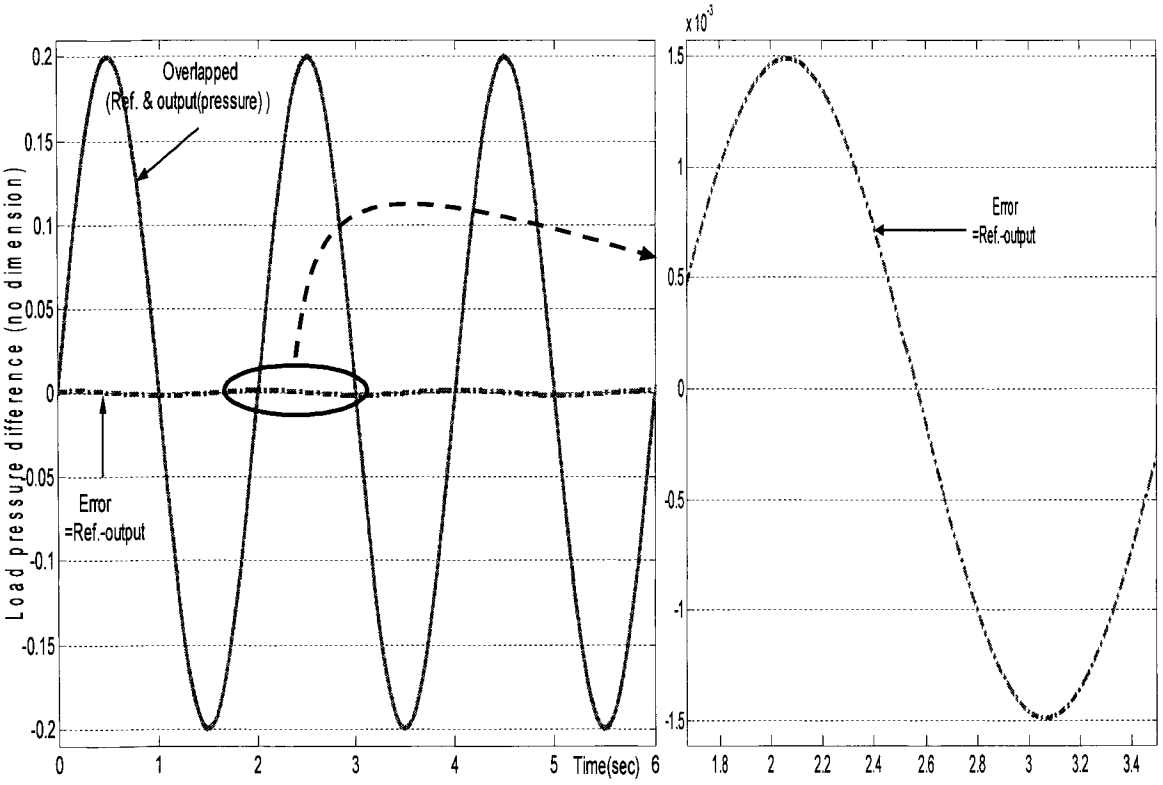

Figure 36 Sinusoidal response of feedback linearization based controller for load pressure control

Although the output is not perfectly identical to the sinusoidal reference (i.e., the error varies periodically in the form of a sine wave with a maximum value of $\pm 1.5 \times 10^{-3}$ as shown from the right side of Figure 36), this error is very small (0.75%). Besides, there is no delay. Consequently, the feedback linearization technique shows excellent performance for control of load pressure in the nonlinear system as well.

- Comparison of performance between feedback linearization based controller and PID controller for sinusoidal reference: $0.2 \cdot \sin \pi t$

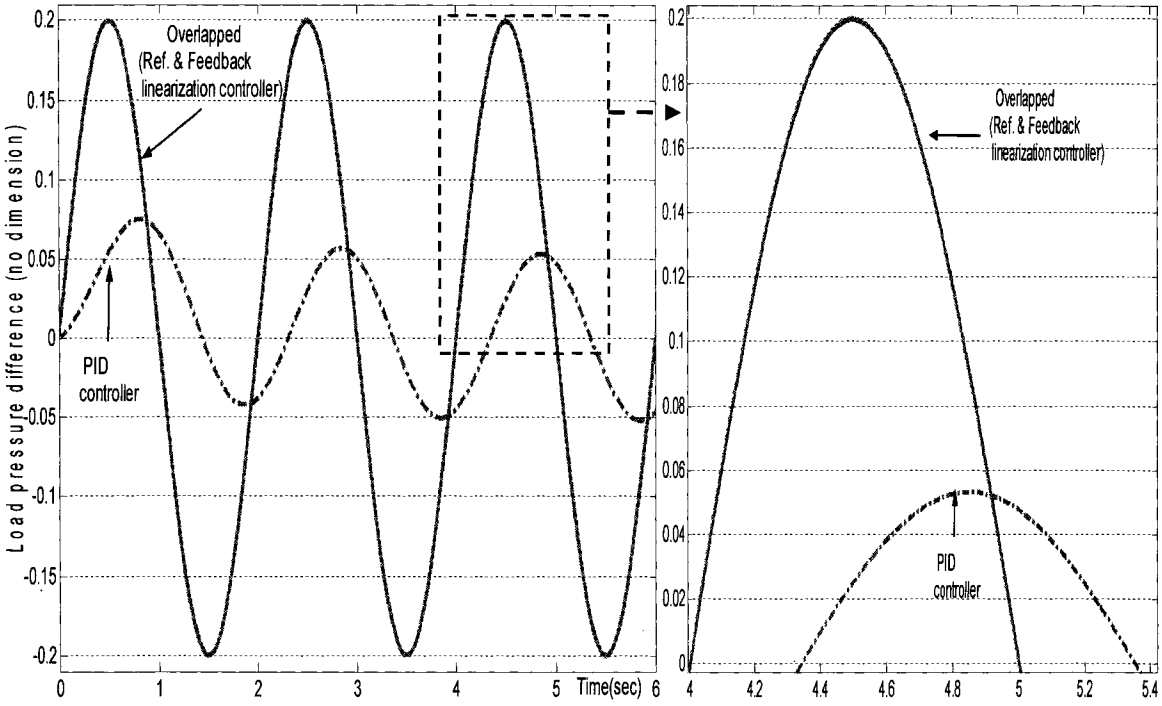

Figure 37 Comparison between feedback linearization based controller and PID controller for load pressure control

While the PID controller's output shows a delay of 0.34 sec and a maximum error of $\pm 1.813 \times 10^{-1}$ after 4 sec, the lack of delay and the extremely small error ($\pm 1.5 \times 10^{-3}$) using the feedback linearization based controller prove its suitability for load pressure control in the nonlinear system.

■ **Simulation results analysis**

The PID controller has advantages, but its limitations and deficiencies are exposed by the nonlinear dynamics of the hydraulic drive. To overcome these limitations, we introduced the theory of feedback linearization and applied it to the design of our control algorithms. Using simulation, we proved that this nonlinear controller has excellent tracking performance for angular displacement, velocity and load pressure control of the electro-hydraulic system.

However, experimental verification of this performance on the real physical system is also required, to prove the practical value of our feedback linearization based controllers. Experimental validation for this purpose will be described in the next chapter.

CHAPTER 4

REAL-TIME CONTROL AND COMPARATIVE STUDY

In this section, we describe the characteristics and functions of the LITP real-time system. This system is used for the experimental validation of the control algorithms developed in Chapter 3. Experimental tests using the LITP test-bench will also be used to perform a comparative analysis for the performance of each controller.

4.1 Introduction

In Chapter 3, we designed high performance controllers for angular displacement, velocity and pressure control of the nonlinear system based on feedback linearization theory. In particular, this nonlinear strategy provides us with a theoretical basis for the design of a high precision controller by addressing the dynamics of the nonlinear electro-hydraulic system.

While simulations using MATLAB/Simulink have shown promising results, we need to confirm these results through experimental validation on the physical hydraulic test-bench by implementing the controllers on a real-time system.

For conducting the real-time experiment, we use the LITP (Laboratoire d'intégration des technologies de production) test-bench with a commercial real-time system, namely, RT LAB. The LITP has chosen this system as a real-time platform due to the fact that it performs parallel and numerically accurate real-time processing using multi-processor systems, thus enabling us to implement complex controllers at high sampling rates. Additionally, it provides tools to simplify the modeling of dynamic systems like the electro-hydraulic drive for real-time simulation. These tools are based on MATLAB/Simulink with which we are already familiar, and thus special training for

real-time model design is not necessary. Lastly, it permits us to synchronously monitor experimental data and to modify the controller parameters at anytime during the experiment.

Because of these features, RT-LAB system has been used in a wide range of applications for the industry as well as academia, with many of these applications requiring high bandwidth and complex parallel computing.

In this chapter, we are going to introduce the methods, procedures and RT-LAB's key features for performing our experimental study. We will also provide data that shows the excellent performance of the feedback linearization based controller on the LITP test bench.

4.2 Experimental Method for real-time simulation

4.2.1 LITP test bench composition

As shown in Figure 38, the test bench of LITP for experimental simulation consists of the RT-LAB system and the electro-hydraulic system.

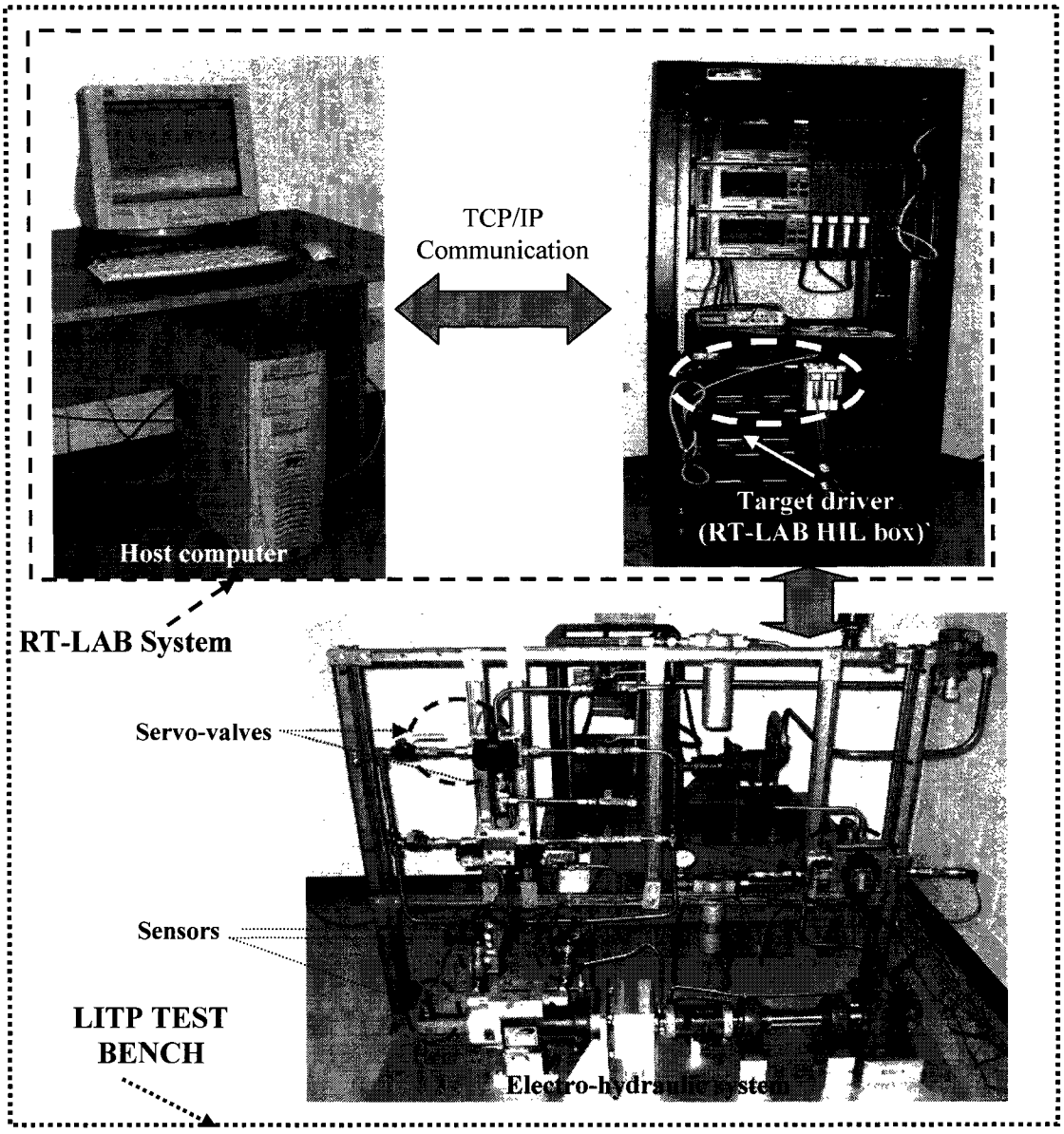

Figure 38 Composition of LITP test bench

The RT-LAB system consists of a host computer and a RT-LAB target driver.

The Windows/Intel host computer allows us to communicate with the real-time target (running the QNX operating system) of RT-LAB. Using this computer, we can design our simulation model, and run and control simulations on the real-time target.

On the RT-LAB target side, several microprocessors are connected via a high-speed communication network, using shared memory and the IEEE-1394/FireWire protocol. The target system can execute distributed simulations as a computation cluster. During the simulation, the communication with the host computer is achieved via TCP/IP. Figure 39 shows one RT-LAB computational node, which can be used as a single-target. The figure also shows two I/O Interface Cards. Slot #1, the analog input, reads the data (i.e., load pressure and angular velocity) measured by sensors in the hydraulic system, for our control computations.

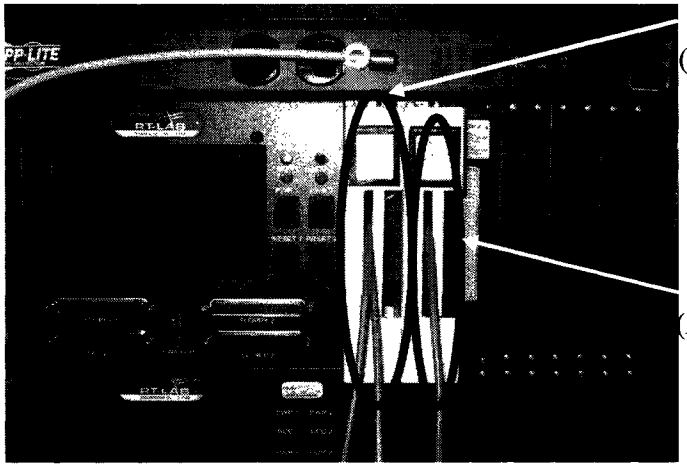

Figure 39 RT-LAB HIL box and I/O interface cards

As shown in Figure 39, the two lines of slot #1 are for receiving pressure and angular velocity data. Slot #2, the analog output, is used to send the two input signals to the plant (i.e., drive servo-valve command and load torque) from the RT-LAB target.

In the electro-hydraulic servo-system, as discussed in section 2.1, the most important components are the two servo-valves and three sensors. In the third picture in Figure 38, the servo-valve on the left governs the load pressure and the rotation of the actuator, the one on the right controls the torque load against the actuator's rotation. Accordingly, the left-side servo-valve is connected to the control input signal, while the right side servo-valve is driven by a constant input signal for torque load. It has a range of voltage from 0 V to 10 V. The orifice inside the right side servo-valve is normally closed if there is no input signal (i.e., 0 V) to it. Its opening area becomes larger and the load generated by hydraulic oil resistance gradually decreases as the input signal grows bigger. In other words, in the case of the maximum signal (i.e., 10 V), there is no resistance to rotation in the servo-system since the opening area of the right side servo-valve is at its maximum. Thus, to simulate T_L=0, we set the command voltage to this servo-valve to 10 V.

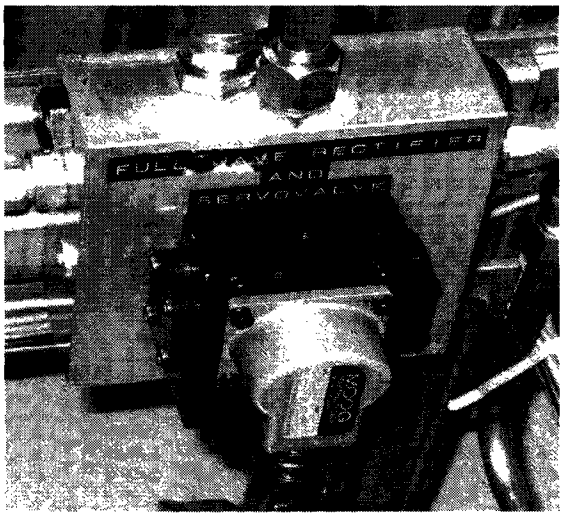

Figure 40 Servo-valve

Of the three sensors, two sensors are for measuring the pressure in each chamber of the servo-motor and the other sensor is for measuring the angular velocity of the actuator. The outputs of these sensors are analog voltages and we need to convert these voltage

signals into their corresponding physical quantities (i.e., pressure: N/m^2 and angular velocity: RPM) using the sensors' calibration factors.

These factors are provided in the sensor specification sheets as follows:

Relationship between volt and pressure unit : 1 V_{dc} $\rightarrow$ 2.06843×10^6 N/m^2 (4.1)

Relationship between volt and angular velocity unit : 1 V_{dc} $\rightarrow$ 240.5 RPM (4.2)

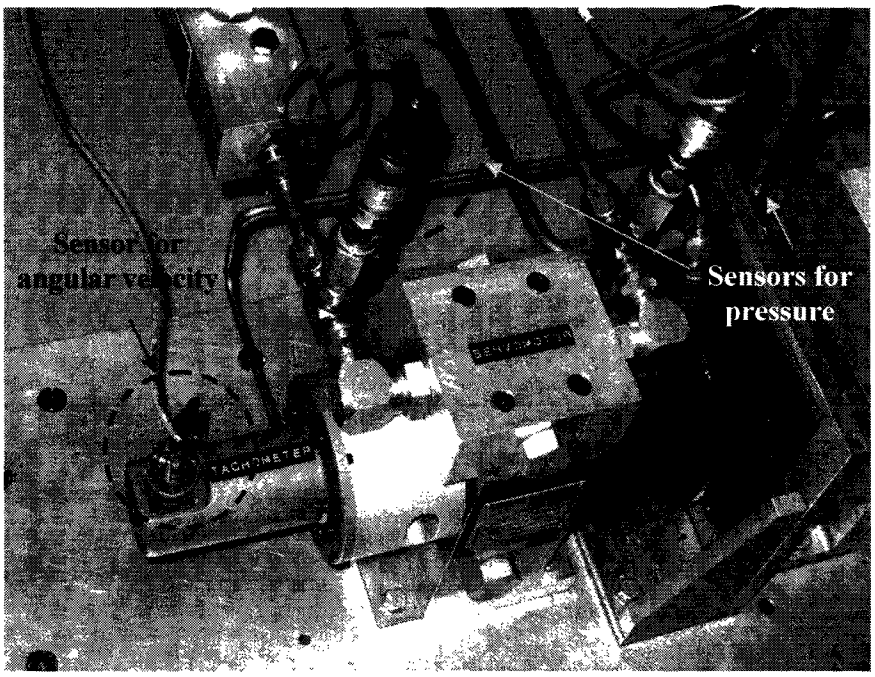

Figure 41 Sensors used for real-time experiment

4.2.2 Simulink model design using RT-LAB conventions

For preliminary design and off-line simulation of the complete system, we need to format our Simulink models using RT-LAB conventions. That is, the Simulink model

has to be divided into sub-systems, which must be named with a prefix in order to identify each function as noted from Figure 42.

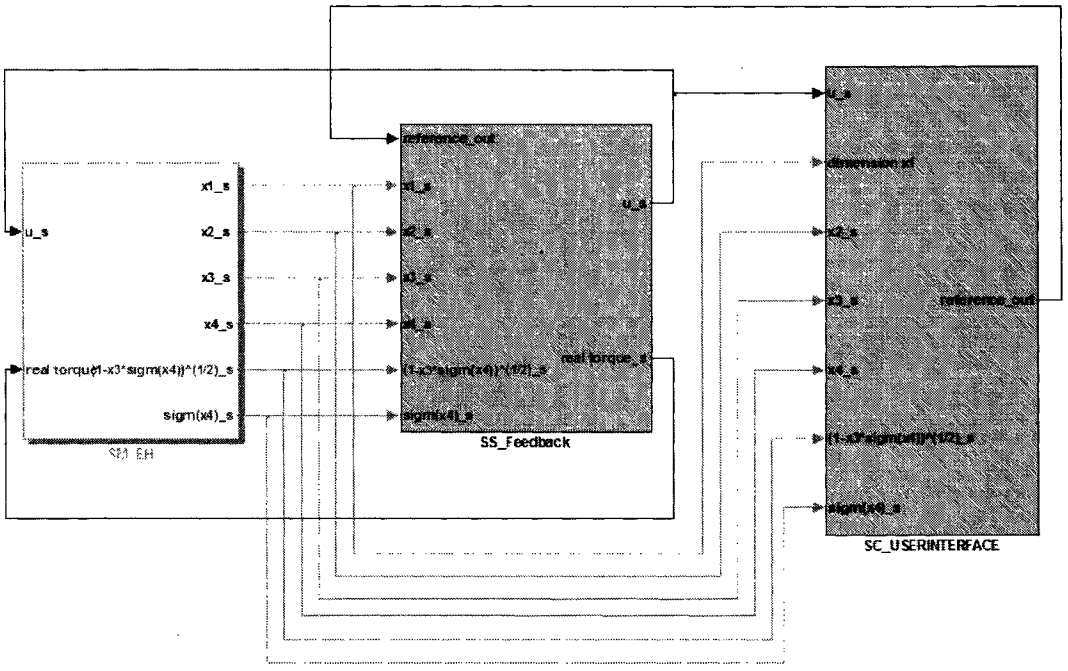

Figure 42 Simulink model separated into subsystems

Among the three subsystems present, the master system, having a prefix of SM_, contains the computational elements and is required in every RT-LAB Simulink model. In our model, SM_EH is a master subsystem and stands for the electro-hydraulic system (i.e., the plant).

SS_Feedback system is a slave subsystem with a prefix of SS_, and it represents the controller which receives data from the sensors and sends control signals to the servo-valve to induce the desired response in the plant.

SC_Userinterface is a console subsystem that contains all user interface blocks such as scopes and manual switches, but cannot contain the computation on which the real-time model relies.

■ **Characteristics of Master Subsystem (SM_EH)**

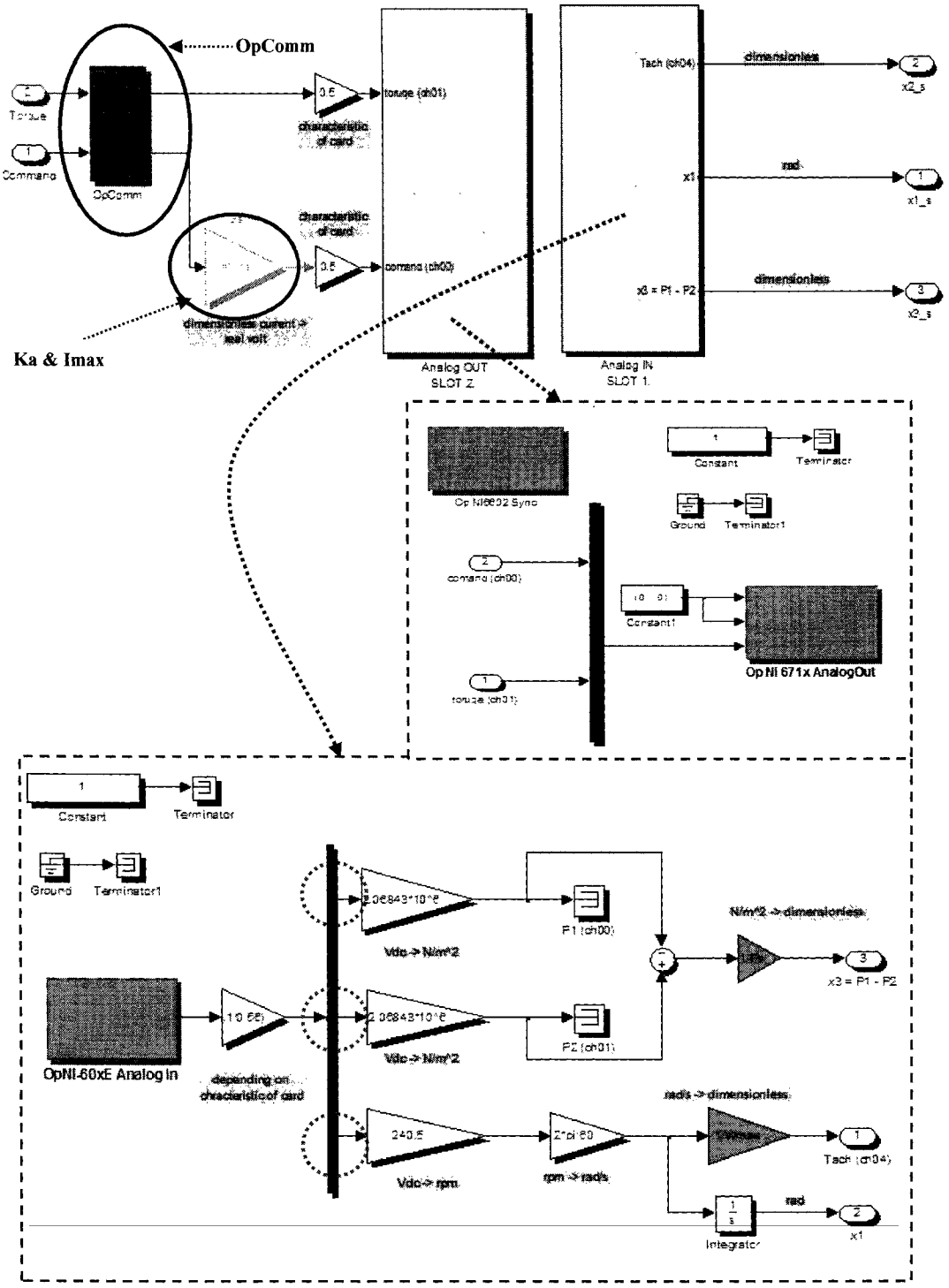

Figure 43 SM_EH subsystem

Using Figure 43, we describe the principal characteristics of the master subsystem.

First of all, in the topmost figure, we find the OpComm block that ensures synchronous communication between subsystems. All inputs to top-level subsystems must first go through an OpComm block before they can be used.

We can also see the servo-valve amplifier gain (K_a) and maximum servo-valve input current ($I_{\max}$) needed to convert the real voltage as a command into the dimensionless current (i) that we need in the 4th equation of our state space model (2.17). For that conversion, we use the following relationship:

$$\begin{aligned} V_{\text{dimension}} &= K_a \cdot I_{\text{dimension}} \\ &= K_a \cdot (i_{\text{dimensionless}} \cdot I_{\max}) \quad \text{where } i_{\text{dimensionless}} = \frac{I_{\text{dimension}}}{I_{\max}} \\ \therefore \quad \frac{i_{\text{dimensionless}}}{V_{\text{dimension}}} &= \frac{1}{K_a \cdot I_{\max}} \end{aligned} \tag{4.3}$$

The second and third figures show the Analog Out and Analog In blocks. Each block fulfills its respective function of I/O communication.

In addition, as indicated by the red dashed circles at the bottom of Figure 43, there are three sensor signal ports (two for pressure and one for angular velocity) for transmission of data measured by the sensors mentioned in section 4.2.1 (Figure 41). The equations for unit conversion associated with these three ports are given in equations (4.1) and (4.2). However, we note that there is no sensor measuring angular displacement in our real-time system. Thus, we have to calculate the angular displacement through the use of a numerical integrator in Simulink acting on the data measured by the angular velocity sensor.

■ **Characteristics of Slave Subsystem (SS_Feedback)**

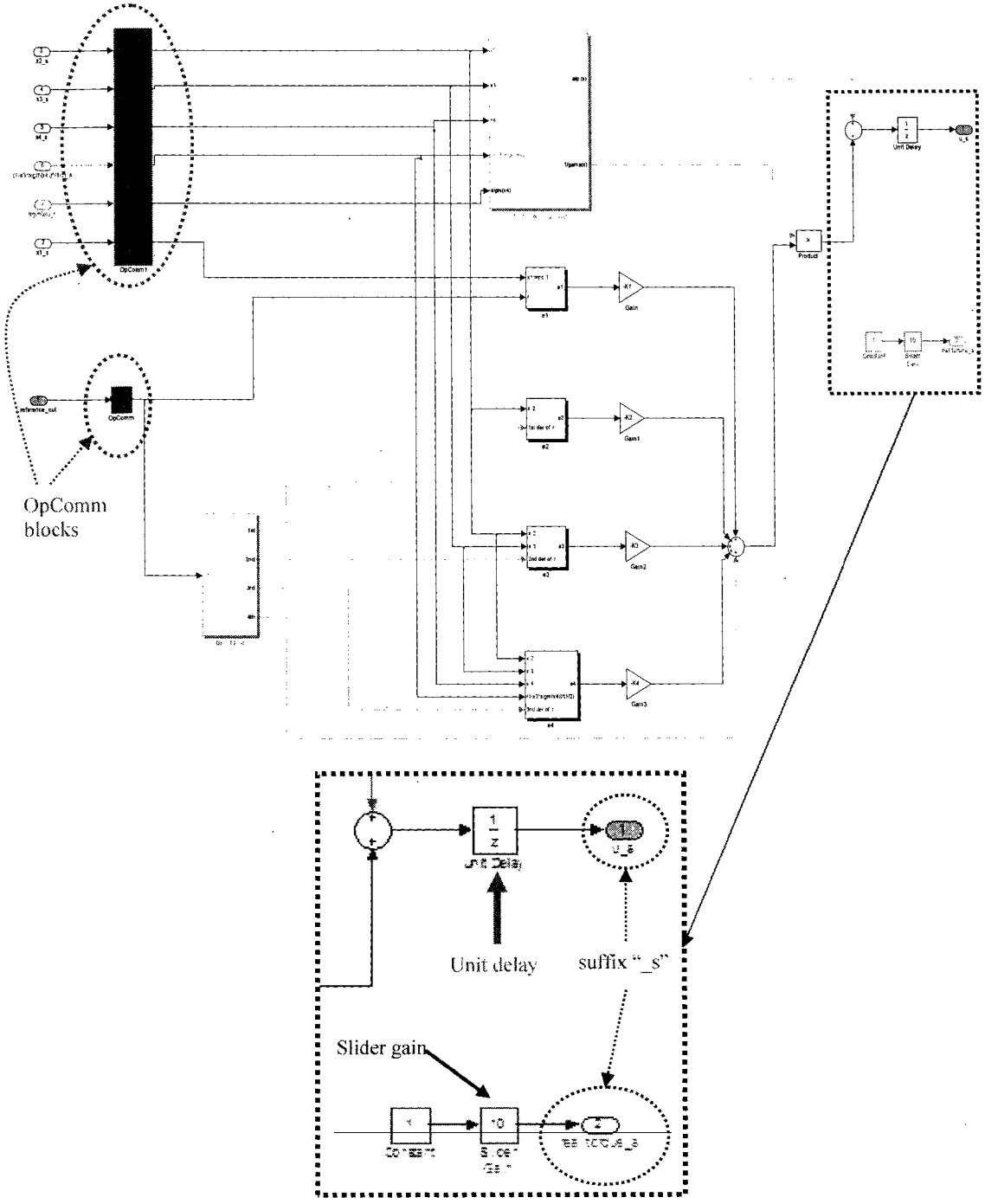

Figure 44 SS_Feedback subsystem

In Figure 44, we can see that there are two different OpComm blocks. The need for these two blocks can be explained by the OpComm placement rules which state that the SC subsystem runs asynchronously from the SM and SS subsytems. In other words, because the upper OpComm block is linked with ports that receive signals from the SM_EH subsystem and the lower OpComm block has a port that is connected to the SC_Userinterface subsystem, we have to use two distinct blocks.

Other important points can be found in the magnified part in Figure 44 as well.

In order to maximize parallel computation in RT-LAB, the slave and master subsystems must compute and send their outputs before they read their inputs. For this fucnction, RT-LAB prioritizes computation of slave or master outputs by identifying them with the suffix "_s" on the outport's name. Therefore, all outputs of SM and SS subsystem in our model have such a suffix "_s". The unit delay parameter is used in the Slave Subsystem and its function is to prevent a "deadlock" state.

As mensioned in section 4.2.1 in detail, the input signal for load torque has a range of voltage from 0V to 10V. For regulating that value of this input signal, a slider gain is used. However, in our simulation, we set the load torque to zero by fixing the input signal at 10V.

■ **Characteristics of Console Subsystem (SS_Userinterface)**

In this console subsystem, we use scopes to probe the control signal calculated by the SS_Feedback subsystem and the outputs (i.e., angular displacement, velocity and load pressure difference of servomotor) read by the SM_EH subsystem.

We also monitor the error of the feedback output with respect to the reference command signal, and thus check the controller's performance in terms of the tracking accuracy.

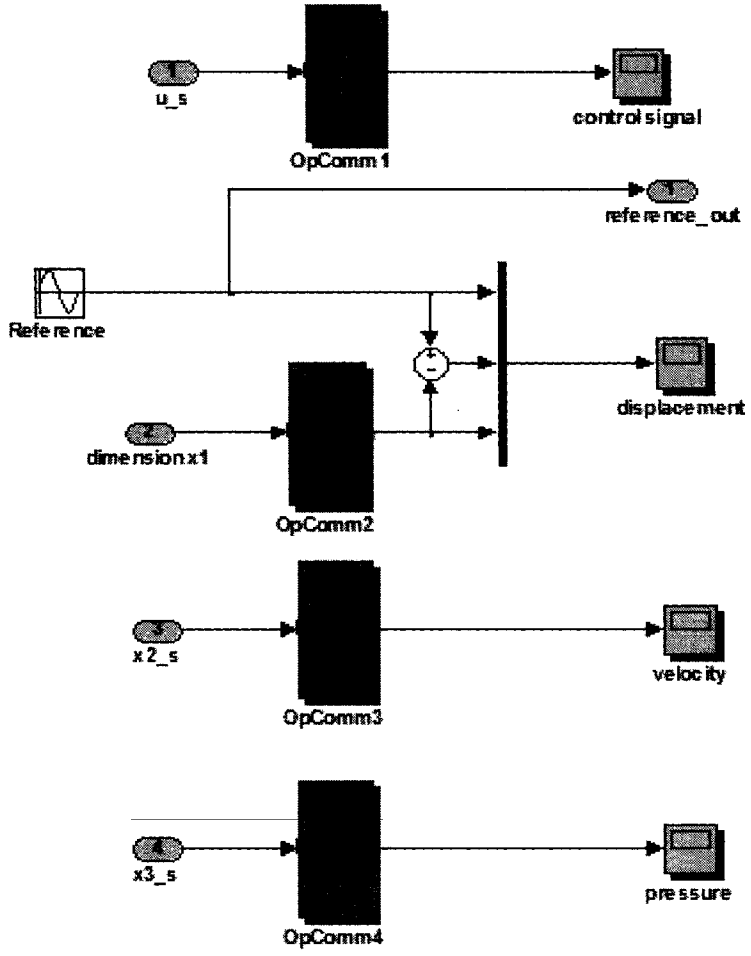

Figure 45 SC_Userinterface subsystem

4.2.3 Execution procedure of real-time simulation

In order to execute the simulation using the RT-LAB real-time system, we need to follow six steps using the Main Control console shown in Figure 46.

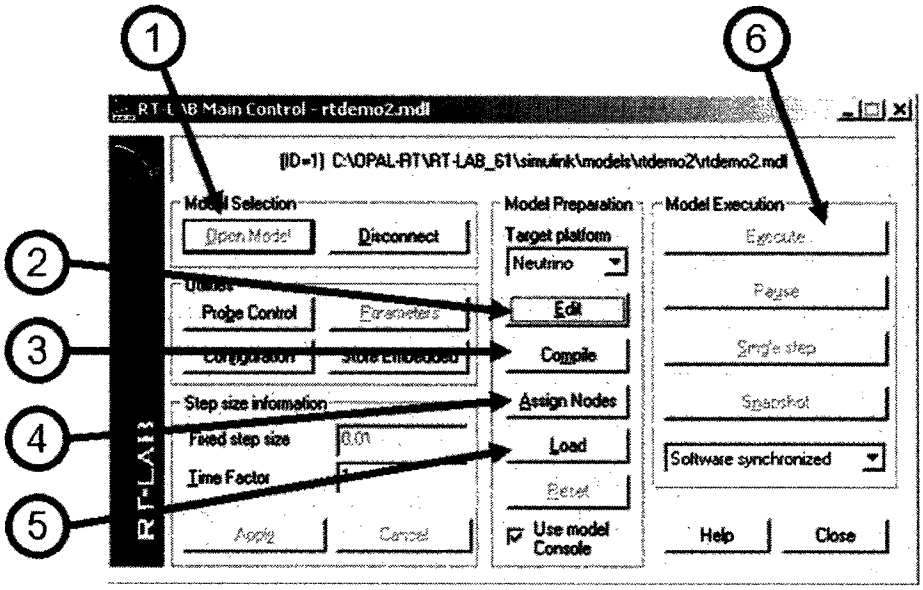

Figure 46 RT-LAB main control console

- Step 1: Opening the model designed in Simulink according to the RT-LAB convention, with the three required subsystems (Master, slave and console subsystem).
- Step 2: This step is optional because the edit mode is used whenever we need to modify the model.
- Step 3: Compilation which is performed by clicking the compile button. RT-LAB automates this process, which consists of the following tasks:
  - Separation of the original model into sub-models
  - Code generation for sub-models. Namely, RT-LAB generates the C code for the SM and SS (computation) subsystems.
  - Compilation of sub-model's C code

- Distribution of executables on desired target nodes

- Step 4: Assigning a subsystem to a specific target node by selecting appropriate physical node from the "Assign Nodes" dialog.
- Step 5: Transferring each computation subsystem to their assigned nodes using the FTP protocol. At the end of this loading process, we can see the automatically launched visualization window (left side of Figure 47) on the host PC. The appearance of this visualization window means that the subsystems are loaded and ready to run.

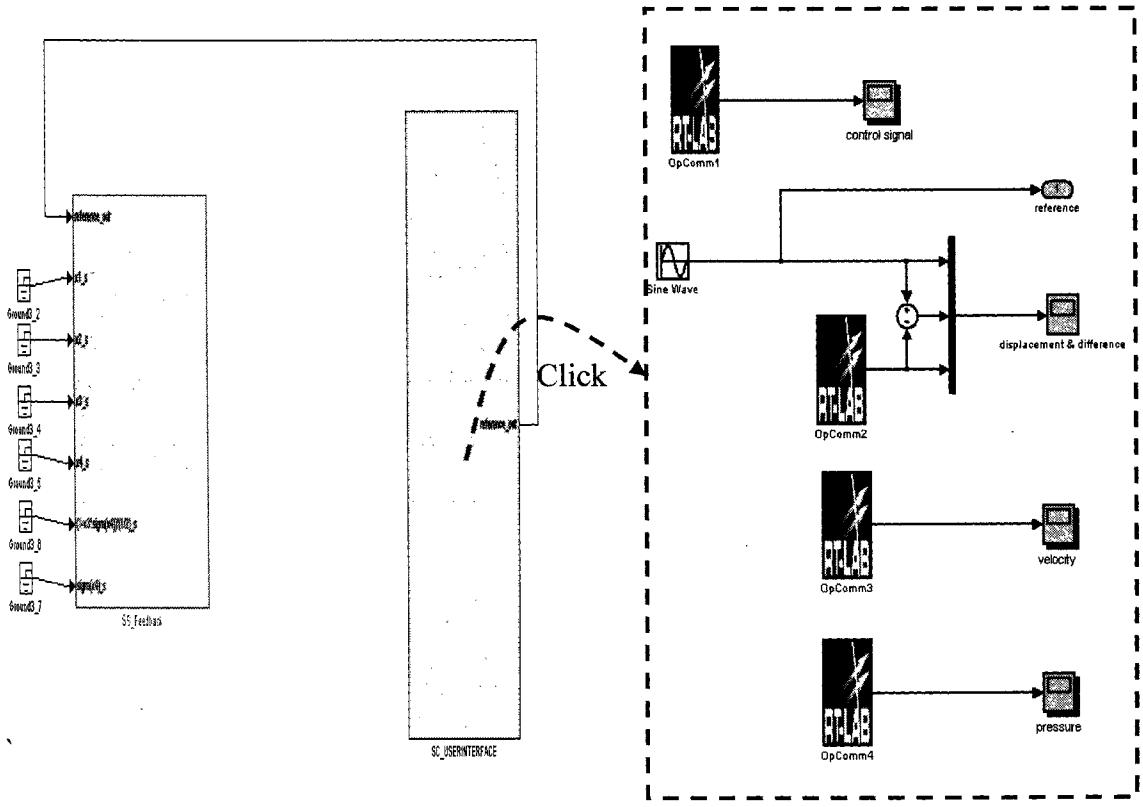

Figure 47 Automatically launched visualization

- Step 6: Execution of simulation.

During the execution process, if we click the SC_Userinferface block in Figure 47, we can see the console (the right side of Figure 47) generated by

RT-LAB. Using this console that displays the real-time data from the target, we can monitor our simulation results.

4.3 Real-time simulation using the LITP test bench

In section 3.3.3, we have verified the benefits of the feedback linearization based controller for the nonlinear hydraulic system by comparing it with the PID controller. But this verification was based on numerical simulation using MATLAB/ Simulink and so, we need to move to real-time simulation using the LITP test bench in order to prove that the feedback linearization based controller can be used in practical and physical applications.

For our real-time simulation, we adopted the Dormand Prince integration method as the solver in Simulink with a fixed time step of 0.001sec. All conditions of the real-time simulation, including all output references, are the same as the ones used in our previous MATLAB/Simulink based simulation.

Using a comparative analysis of the real-time simulation results between the feedback linearization based controller and the PID controller, we can assess the benefits of our chosen nonlinear strategy.

4.3.1 Model validation using real-time simulation

The first step in performing our experimental tests is a model validation which enables us to check how well our mathematical model (Figure 5) represents the dynamics of real hydraulic system. Since the feedback linearization based controller and PID controller were designed in conformity with this model, it is meaningless to apply these controllers to the real system for simulation if this model is not representative of the real system.

For the model validation using real-time simulation, we combine the real hydraulic system (SM_EH) in Figure 43 with the mathematical model (SS_Modeling) and conduct the open-loop real-time simulation as shown in Figure 48. During the simulation, we synchronously compared each output (i.e., angular displacement, velocity and differential pressure) from the SM_EH and SS_Modeling subsystems for the same input signals with a control input signal of $1 \cdot \sin 3\pi$ volt and torque load signal of 10 V (i.e., zero load). The reason why we chose a comparatively high frequency of 3π *rad / s* for the control input is to reduce experimental errors induced by internal friction in the real system.

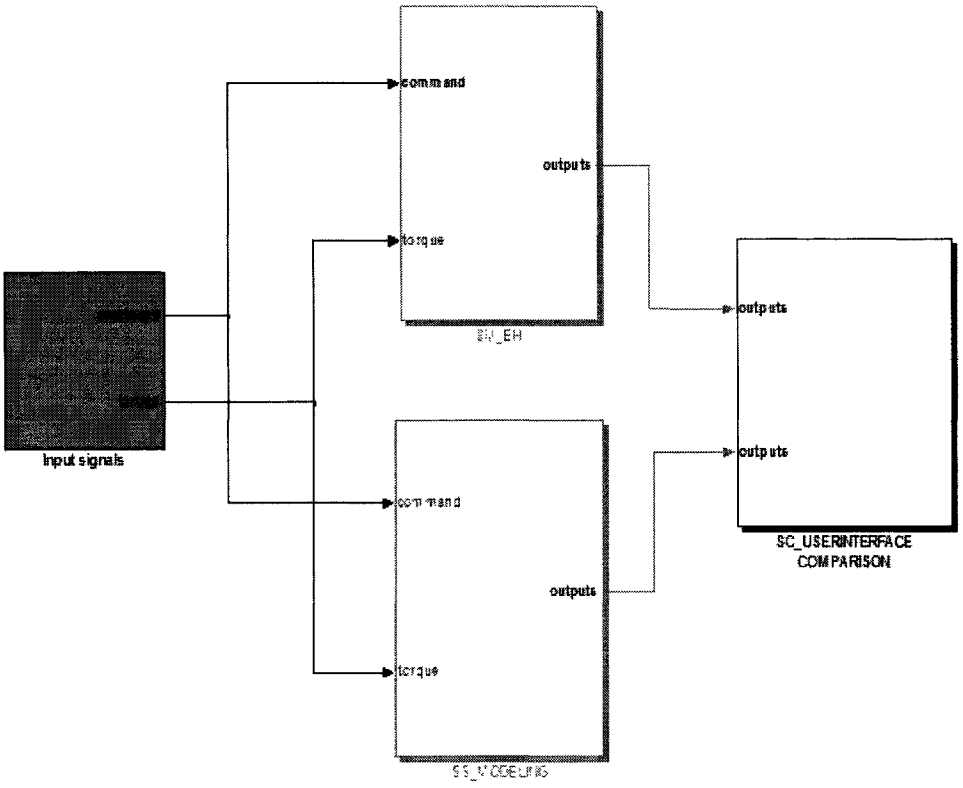

Figure 48 Schematic of Open-loop real-time simulation for model validation

■ Validation results

▪ Angular displacement

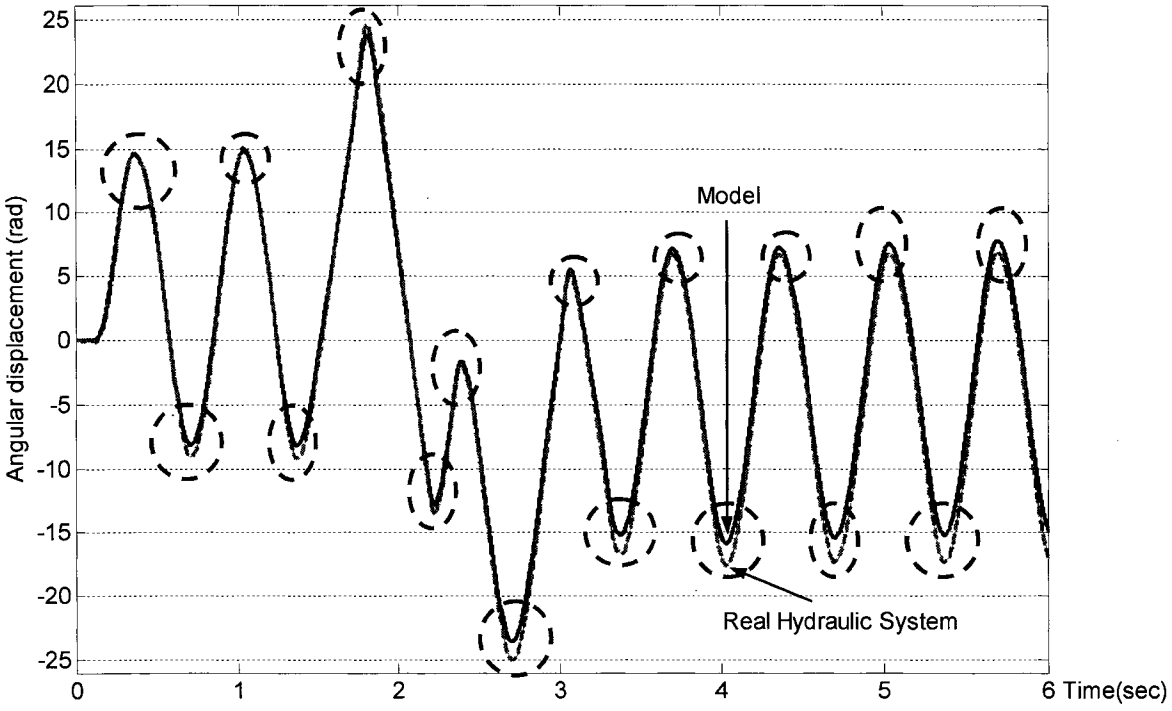

Figure 49 Comparison of angular displacement between mathematical model and real hydraulic system

From Figure 49, we see that both the model and the real system show well correlated outputs for angular displacement after 3 sec, and the maximum error (dashed circles) between each output is about 10%. As mentioned in section 4.2.2, we have to calculate the angular displacement by numerically integrating the angular velocity because of the absence of an angular displacement sensor in the real-time hydraulic system. Thus, it is possible that the error that we see in the model is due to the numerical integration.

Based on the data presented above, we can conclude that the mathematical model represents the real hydraulic system well for angular displacement.

- **Angular velocity**

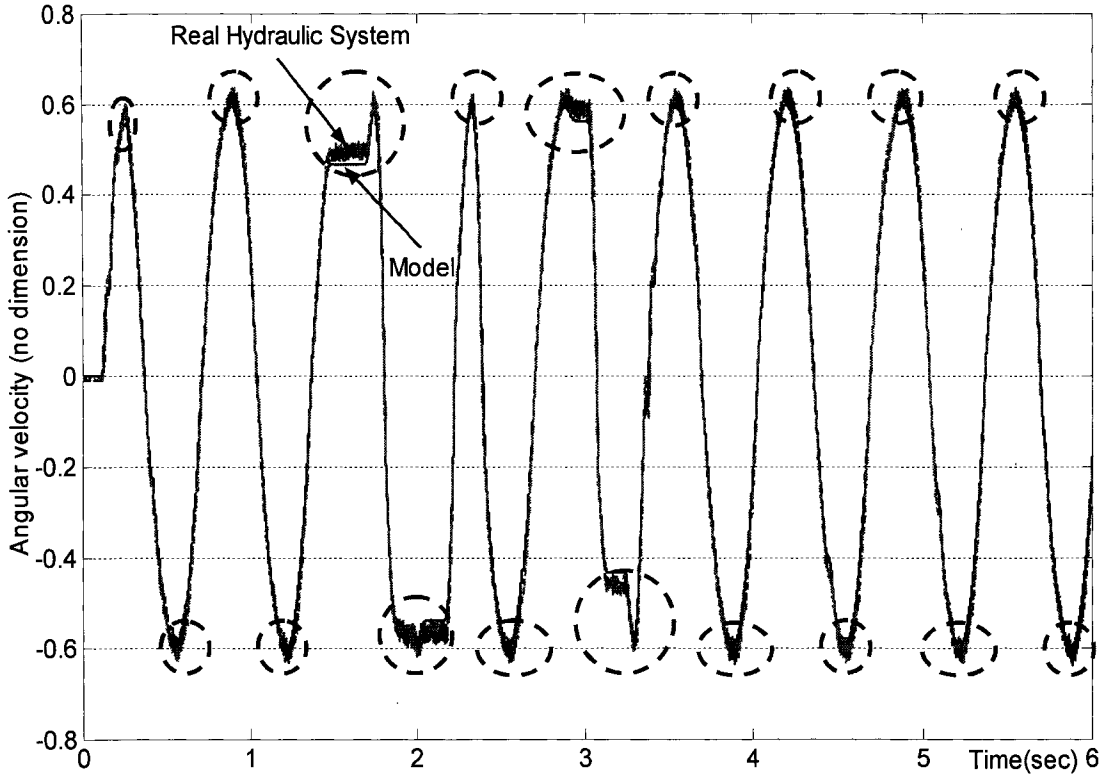

Figure 50 Comparison of angular velocity between mathematical model and real hydraulic system

From Figure 50, we can easily see that the outputs for angular velocity for the mathematical model and the real hydraulic system almost coincide with each other, and produce a symmetric sinusoidal wave with amplitude of 0.6. Since this output is obtained directly from the velocity sensor in the real-time system, the simulation result is very reliable. Therefore, this result enables us to state that this model represents the real hydraulic system's angular velocity characteristic accurately.

An interesting point to note is that we observe a disturbance whenever the actuator changes its rotational direction during the simulation. We believe that this disturbance occurs because of the rotational inertia of the actuator and a temporary pressure

fluctuation induced by the change in the load pressure's direction. The time when this disturbance occurs coincides with the time when the maximum error is observed in Figure 49 and Figure 51, and thus, we can surmise that the errors observed for all three outputs are caused by the fluctuations due to the directional change mentioned above.

- **Load pressure difference**

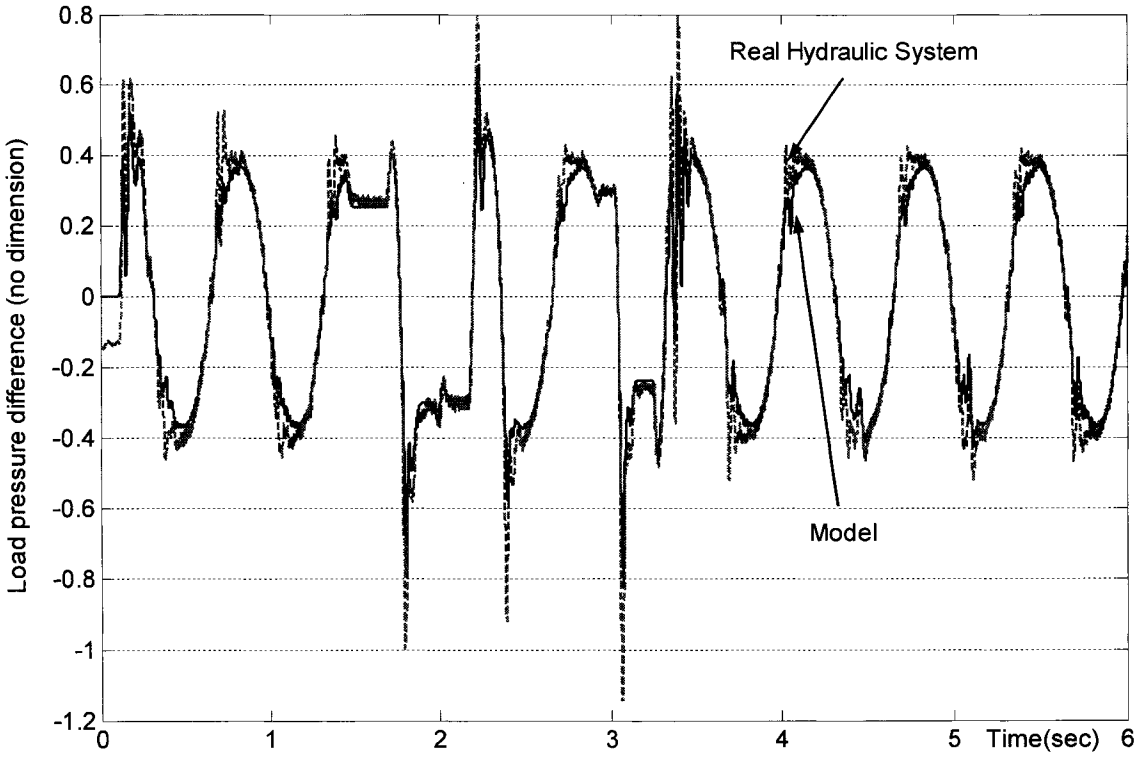

Figure 51 Comparison of load pressure difference between mathematical model and real hydraulic system

From the Figure 51, we see that after 3.5 sec, the outputs of the model and the real system are very much alike and show a regular and symmetric pattern within limits of ± 0.4. The output data is measured directly using two pressure sensors, and the data shown above indicates that the mathematical model accurately represents the real hydraulic system in terms of load pressure difference.

■ **Validation results analysis**

The open-loop simulation results presented above show that the state space model that we developed accurately represents the dynamics of the real hydraulic system for angular displacement, angular velocity and load pressure difference. This validation provides us with a solid basis for applying the PID and feedback linearization based controllers, which were designed according to the mathematical model, to the real-time system for our experimental tests.

4.3.2 Experimental testing of controllers

In order to comprehensively assess whether feedback linearization control brings performance improvements in terms of accuracy and response for controlling angular displacement, velocity and load pressure of the real hydraulic system, as compared to PID control, it is imperative that we analyze the results from the experimental tests for several reference commands. These commands are listed below.

- Cases of reference for angular displacement
  - Case 1-1: $1 \cdot \sin \pi t$ (Sinusoidal reference: base reference)
  - Case 1-2: $1 \cdot \sin 2\pi t$ (Double frequency)
  - Case 1-3: $2 \cdot \sin \pi t$ (Double amplitude)
  - Case 1-4: 1 (Constant reference: base reference)
  - Case 1-5: 2 (Double constant reference value)

- Cases of reference for angular velocity
  - Case 2-1: $0.35 \cdot \sin \pi t$ (Sinusoidal reference: base reference)
  - Case 2-2: $0.35 \cdot \sin 2\pi t$ (Double frequency)
  - Case 2-3: $0.7 \cdot \sin \pi t$ (Double amplitude)

Here, we omit the case of constant reference for angular velocity. A constant reference creates rotation in only one direction and can lead to a numerical overflow error in the angular displacement calculation.

- Cases of reference for load pressure difference

  Case 3-1: $0.2 \cdot \sin \pi t$ (Sinusoidal reference: base reference)

  Case 3-2: $0.2 \cdot \sin 2\pi t$ (Double frequency)

  Case 3-3: $0.3 \cdot \sin \pi t$ (1.5 times base amplitude)

Unlike the cases of angular displacement and velocity, we use a 1.5-times increase in amplitude because a large change of pressure can stress the system's mechanical components. As in the case of velocity, the one-sided action of pressure induced by a constant output reference also causes the actuator to rotate in one direction, and for the same reason given above, we omit this case.

■ **Simulation results**

▪ **Angular displacement**

▫ Comparison of Feedback linearization based controller and PID controller (Case 1-1)

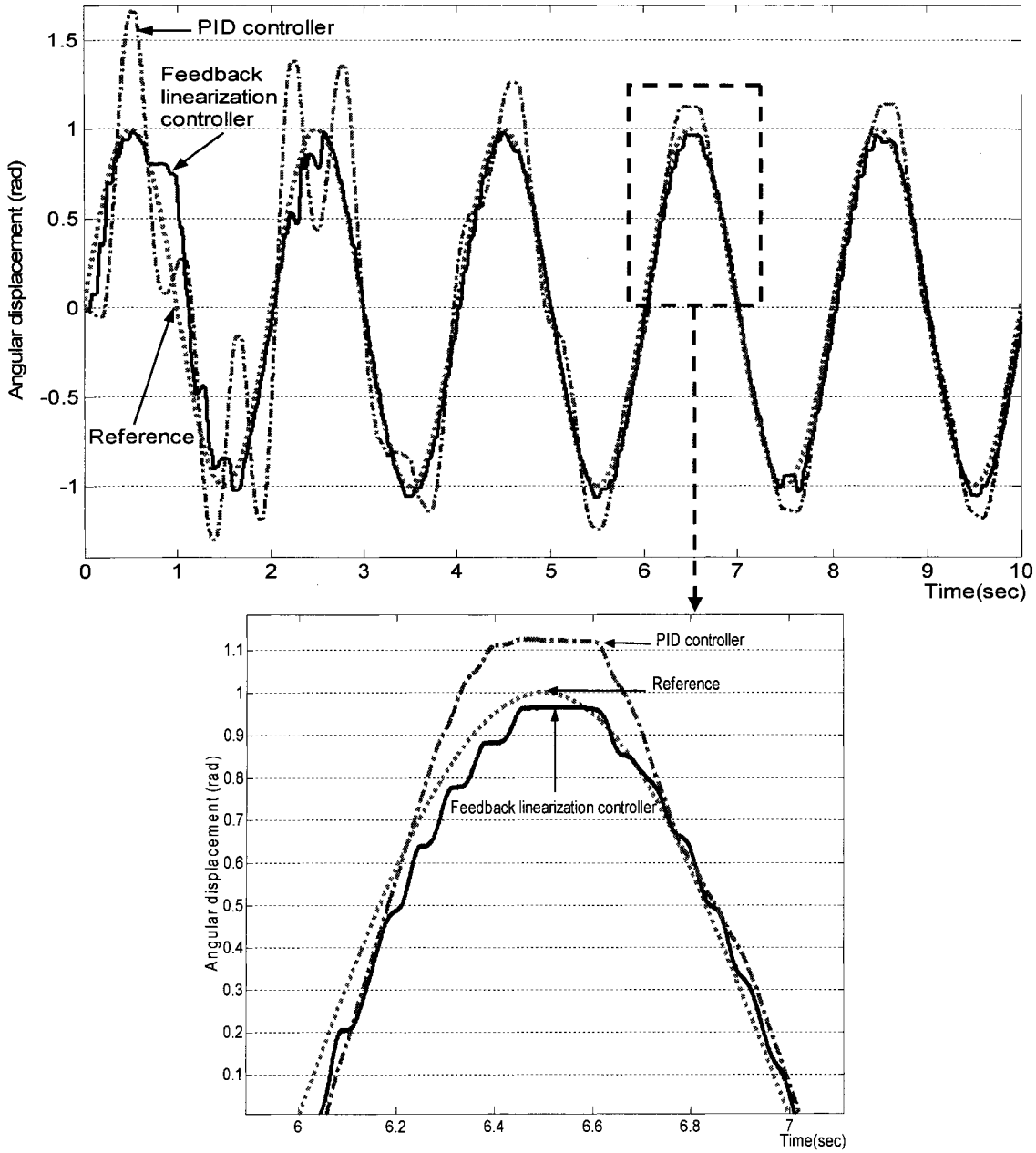

Figure 52 Comparison of real-time simulation results between feedback linearization based controller and PID controller (Case 1-1)

▫ Comparison of each controller's error (Case 1-1)

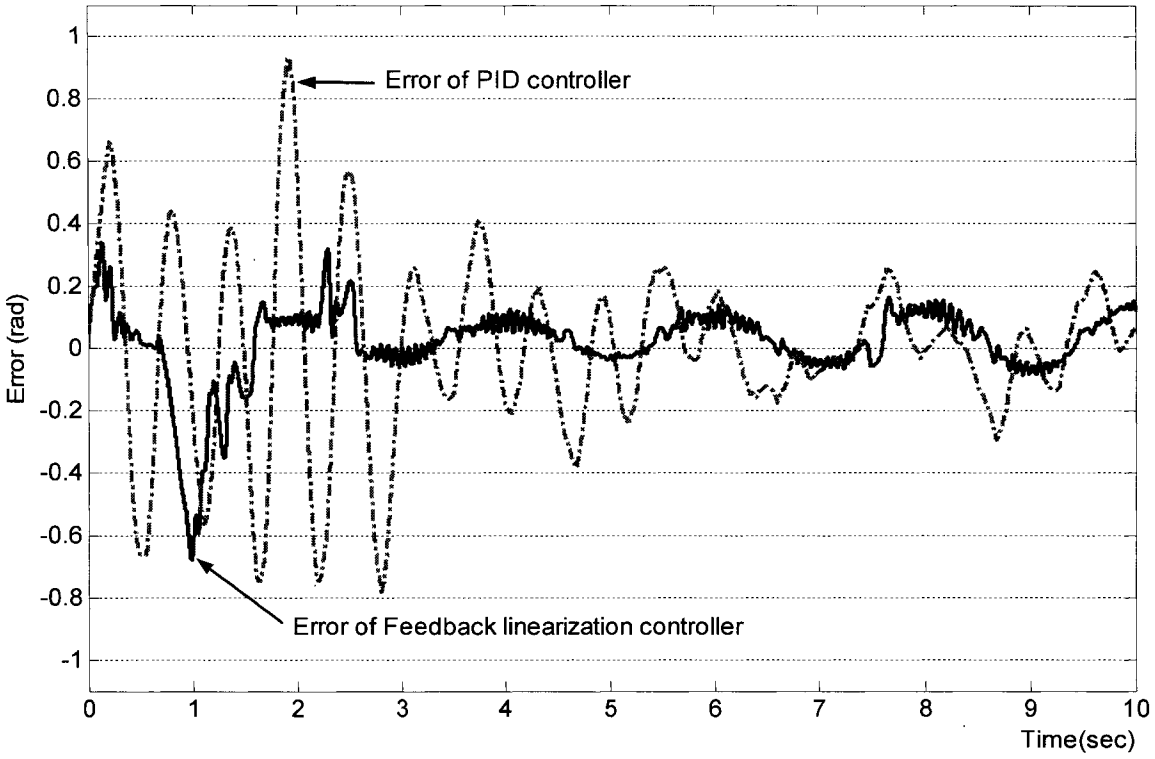

Figure 53 Error comparison of feedback linearization based controller and PID controller (Case 1-1)

From Figure 52, we see that after 2.58 sec, the output transient of the feedback linearization based controller settles, and we have its periodic error with a maximum of $+0.157$ and a minimum of -0.085, as seen in Figure 53.

In contrast to the results obtained using the PID controller, which show a slower response (time to achieve steady-state: 6 sec) and lower tracking precision (periodic error with a maximum $+0.25$ and minimum -0.29), we see that the data for the controller based on feedback linearization theory shows better tracking control for angular displacement control.

▫ Comparison of control signals between the two controllers (Case 1-1)

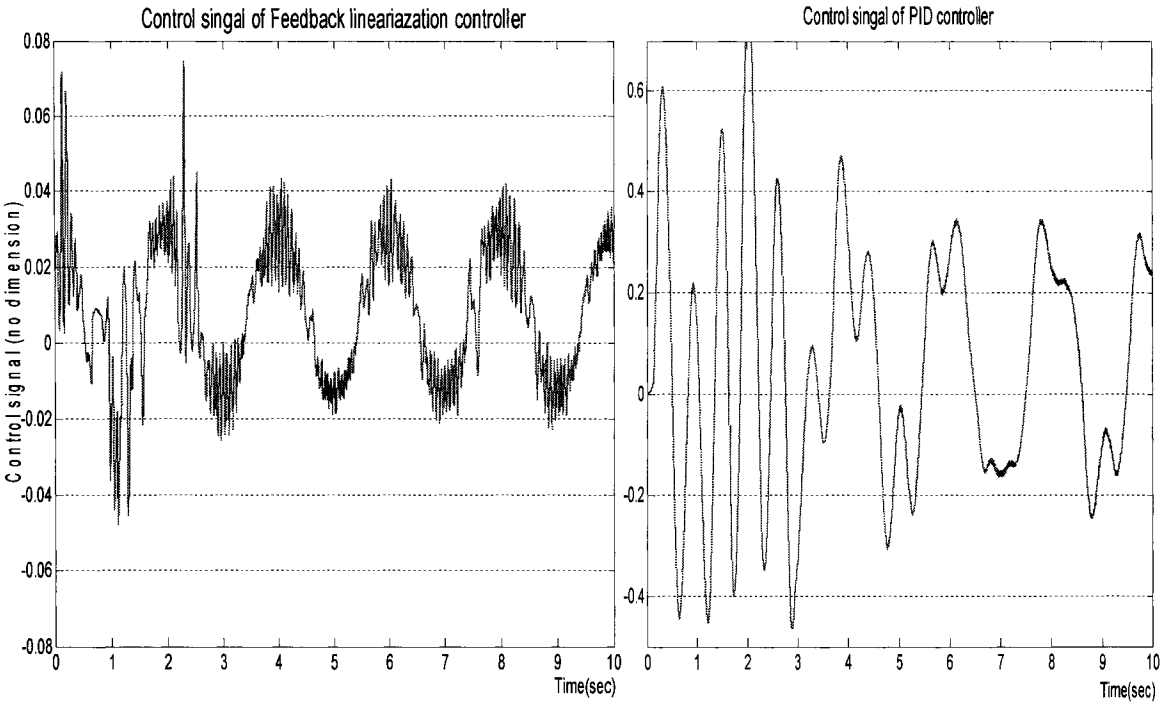

Figure 54 Comparison of control signals between the two controllers (Case 1-1)

From the comparison in Figure 54, we observe that the feedback linearization based controller generates a more symmetric and low-amplitude control signal than the PID controller, and thus improves the accuracy and the response rate of the system by minimizing overshoot and transient oscillations.

▫ Comparison of Feedback linearization based controller and PID controller (Case 1-2)

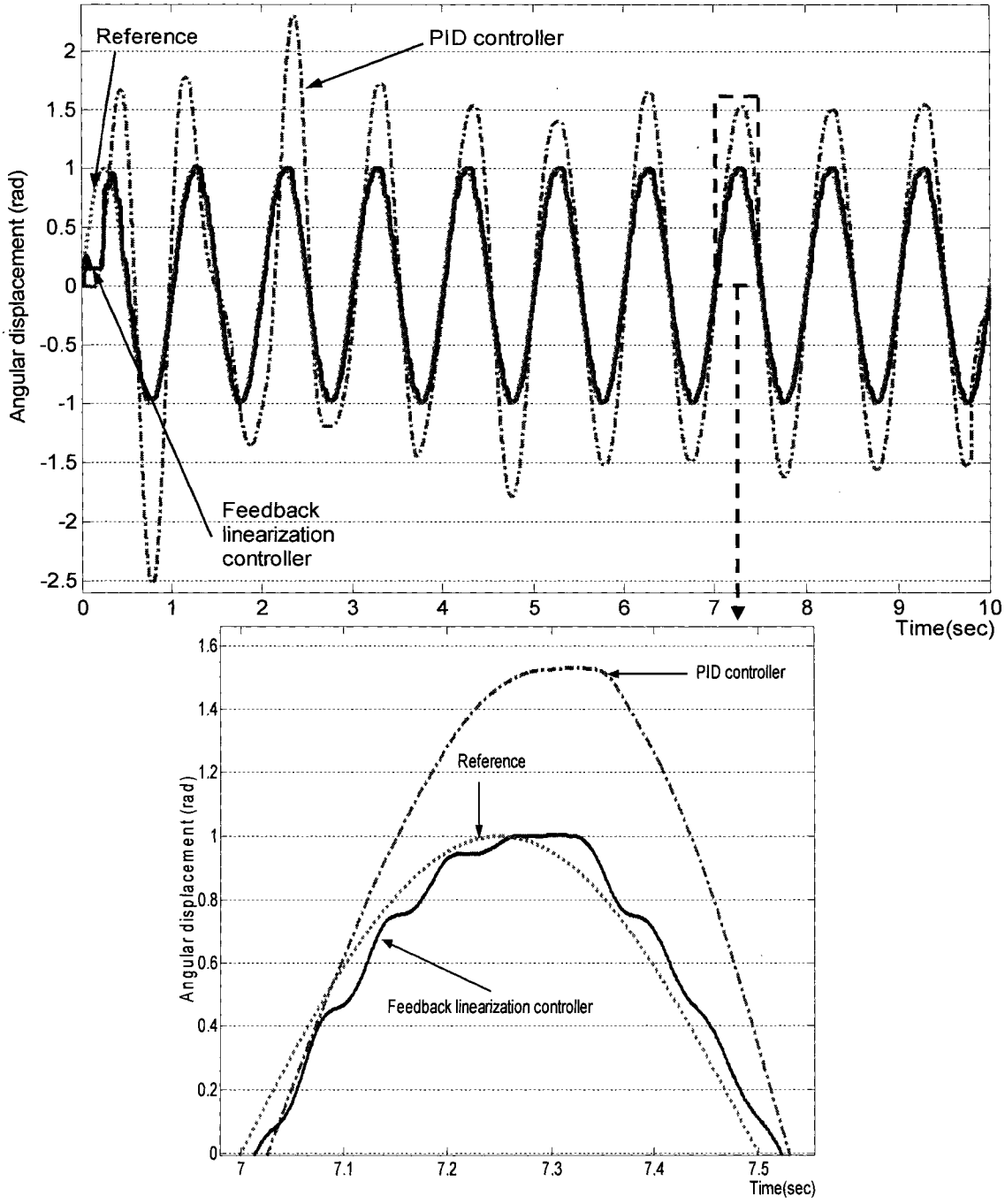

Figure 55 Comparison of real-time simulation results between feedback linearization based controller and PID controller (Case 1-2)

▫ Comparison of each controller's error (Case 1-2)

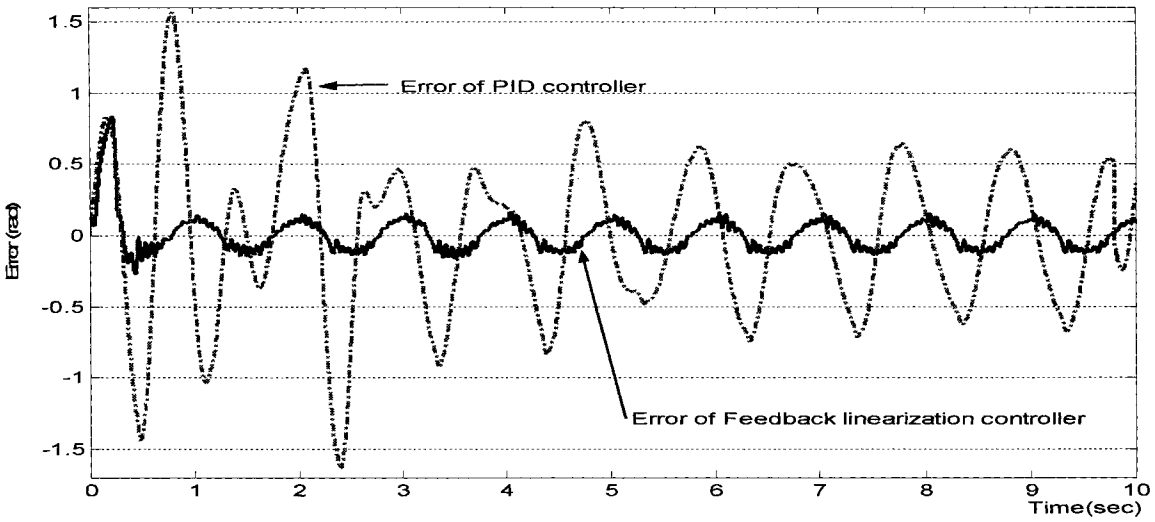

Figure 56 Error comparison of feedback linearization based controller and PID controller (Case 1-2)

As seen in Figure 55, after 0.5 sec, the feedback linearization based controller provides a quicker and less oscillatory response to the reference command than in case 1-1. The error between the reference and the output is within a maximum value of +0.15 and a minimum value of −0.13 which is almost the same as that of the feedback linearization based controller in case 1-1. We also see that for the feedback linearization based controller, the response rate increases as the frequency of the angular displacement's reference increases.

On the other hand, the doubling in frequency causes the error of the PID controller to increase (i.e., case 1-1: error at maximum +0.25 and error at minimum −0.29 vs. case 1-2: error at maximum +0.6 and error at minimum −0.68) and also causes an increase in the time to reach steady-state (i.e., case 1-1: 6 sec vs. case 1-2: 7 sec).

Thus, we note that when we double the frequency of the output reference, the feedback linearization based controller provides faster response and higher accuracy for angular displacement control than the PID controller.

▫ Comparison of Feedback linearization based controller and PID controller (Case 1-3)

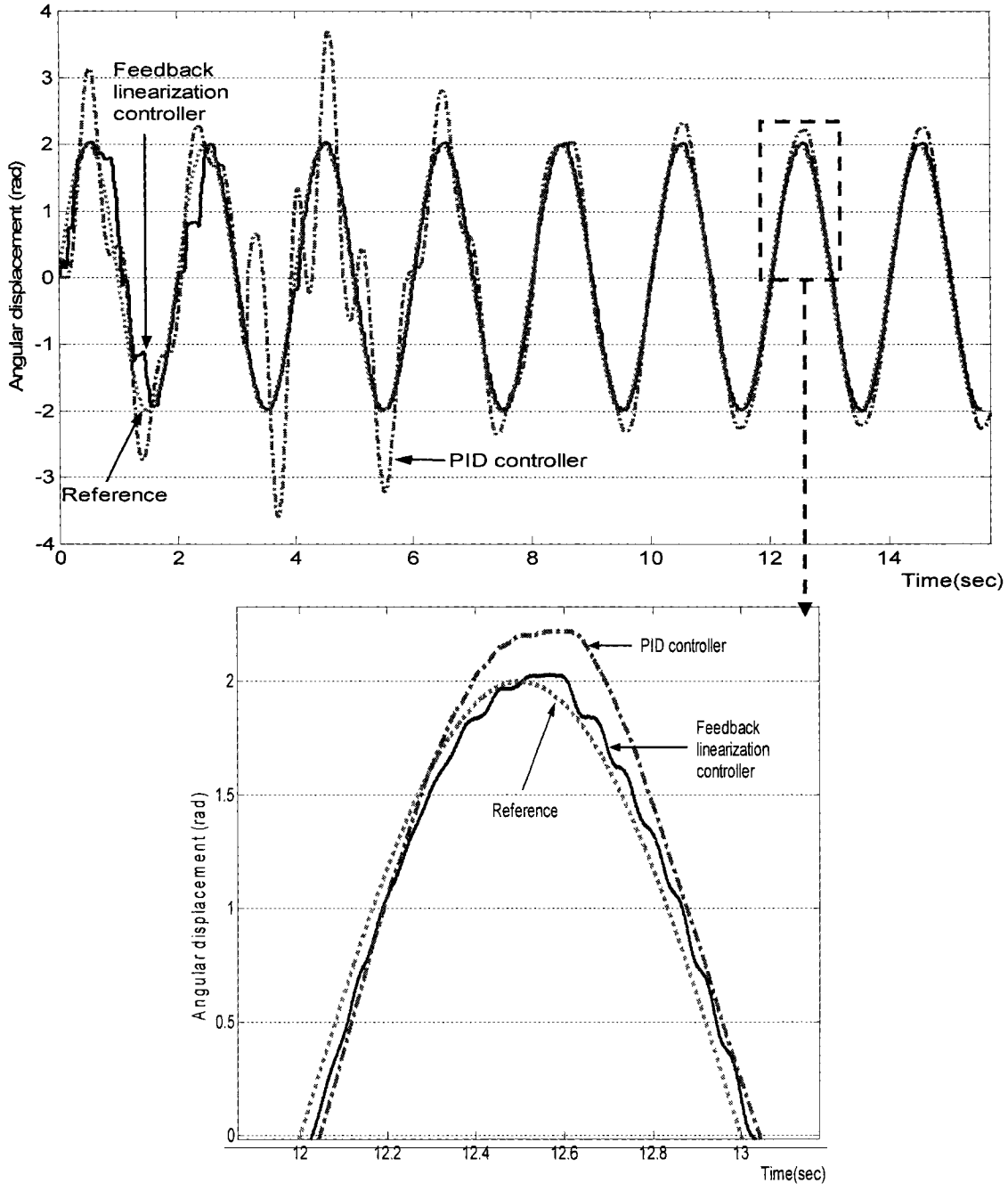

Figure 57 Comparison of real-time simulation results between feedback linearization based controller and PID controller (Case 1-3)

▫ Comparison of each controller's error (Case 1-3)

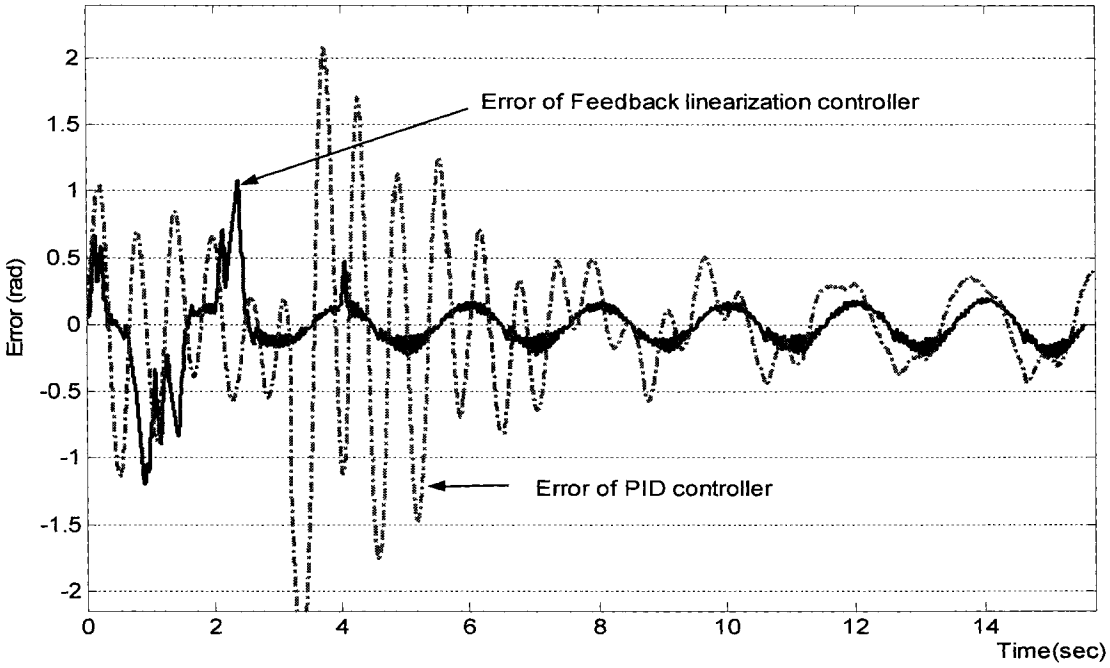

Figure 58 Error comparison of feedback linearization based controller and PID controller (Case 1-3)

For the feedback linearization based controller, the output closely tracks the reference after 2.65 sec and the error between reference and output is within the limits of +0.16 and −0.22. Even though the error increases very slightly and the response rate is a little slower compared with the results in case 1-1, we can consider this result to be similar to that of case 1-1. Therefore, doubling the amplitude of the displacement reference does not cause any distinctive change in the feedback linearization based controller's performance.

The doubling of the reference's amplitude lowers the response rate (i.e., case 1-1: 6 sec vs. case 1-3: 12 sec for the transient time) and precision (i.e., case 1-1: error at maximum +0.25 and error at minimum −0.29 vs. case 1-3: error at maximum +0.354 and error at minimum −0.429) of the PID controller compared with the results of case 1-1. Based on the performance of the two controllers (PID and feedback linearization controller), we can once again infer that the feedback linearization based controller has

superior performance when compared to the PID controller for angular displacement control when we double the amplitude of the reference command.

▫ Comparison of Feedback linearization based controller and PID controller (Case 1-4)

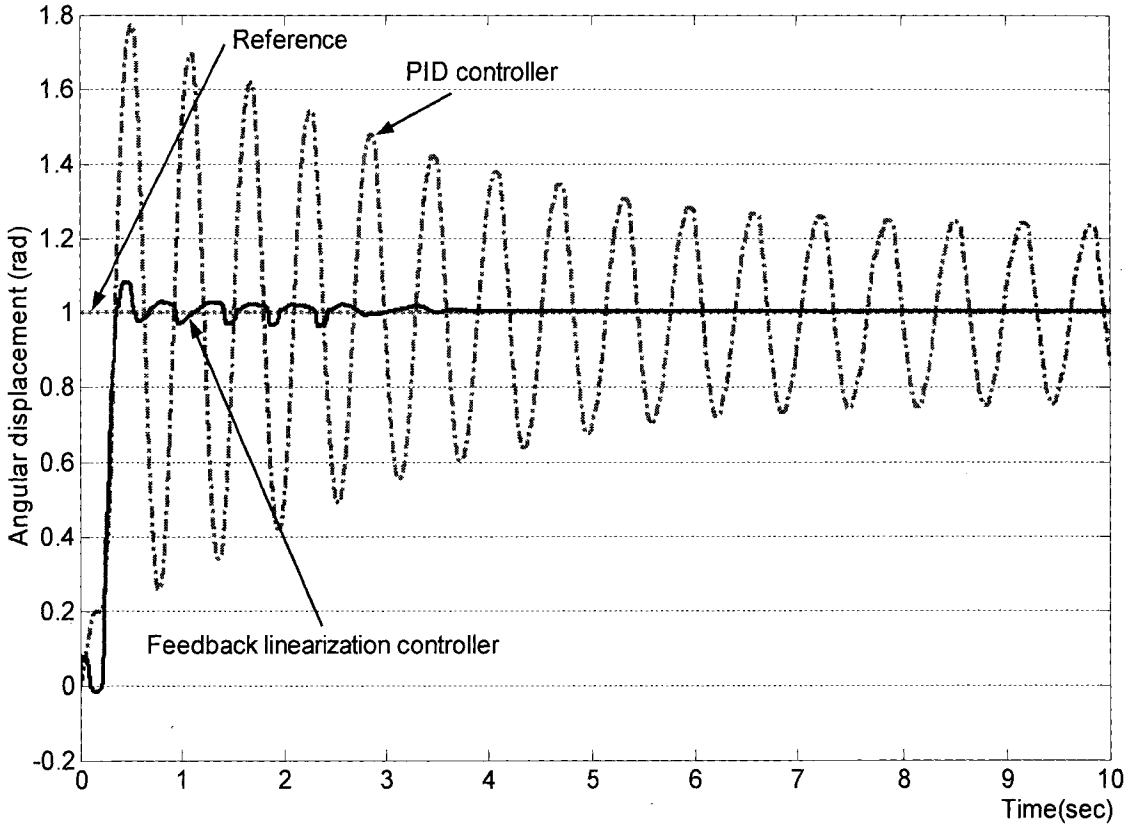

Figure 59 Comparison of real-time simulation results between feedback linearization based controller and PID controller (Case 1-4)

In the case of constant reference, the output with the feedback linearization based controller exactly tracks the reference after 4 sec.

But the PID controller output shows a transient oscillation for approximately 8 sec and the maximum error is ± 0.25. Thus, for the case of a constant reference, we are once again able to show that the feedback linearization based controller provides better tracking performance than the PID controller.

▫ Comparison of Feedback linearization based controller and PID controller (Case 1-5)

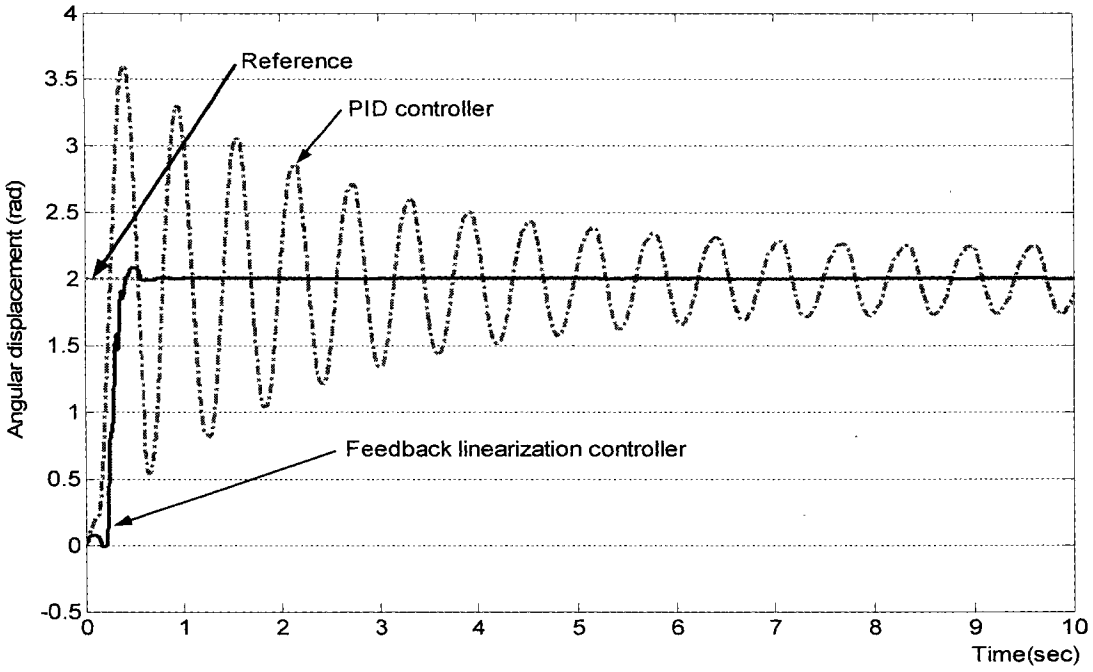

Figure 60 Comparison of real-time simulation results between feedback linearization based controller and PID controller (Case 1-5)

Comparing this result to case 1-4, we notice that doubling the constant reference value creates a faster response for the feedback linearization based controller (Figure 60), with the output and reference coinciding with each other after 1 sec. This response rate is faster than that (i.e., transient time to reference: 4 sec) of case 1-4.

On the other hand, the PID controller shows a sinusoidal oscillation for about 8 sec and a maximum error of ± 0.25 as in case 1-4. Thus, doubling the constant reference does not influence the performance of the PID controller.

Having shown that the feedback linearization based controller has significantly better performance than the PID controller for angular displacement control of the rotational hydraulic system, we now perform an experimental comparison of these two controllers for angular velocity control.

▪ **Angular velocity**

▫ Comparison of Feedback linearization based controller and PID controller (Case 2-1)

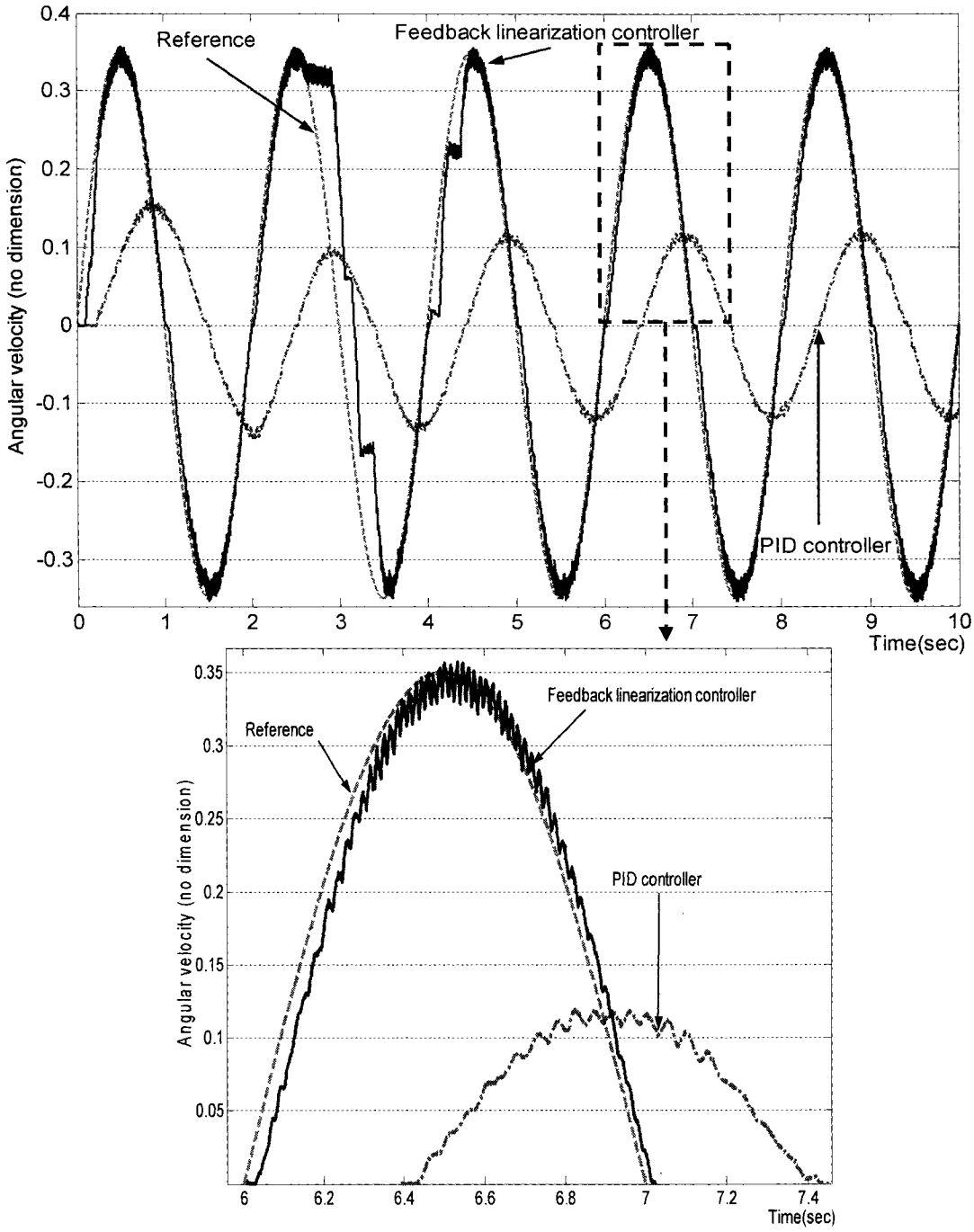

Figure 61 Comparison of real-time simulation results between feedback linearization based controller and PID controller (Case 2-1)

▫ Comparison of each controller's error (Case 2-1)

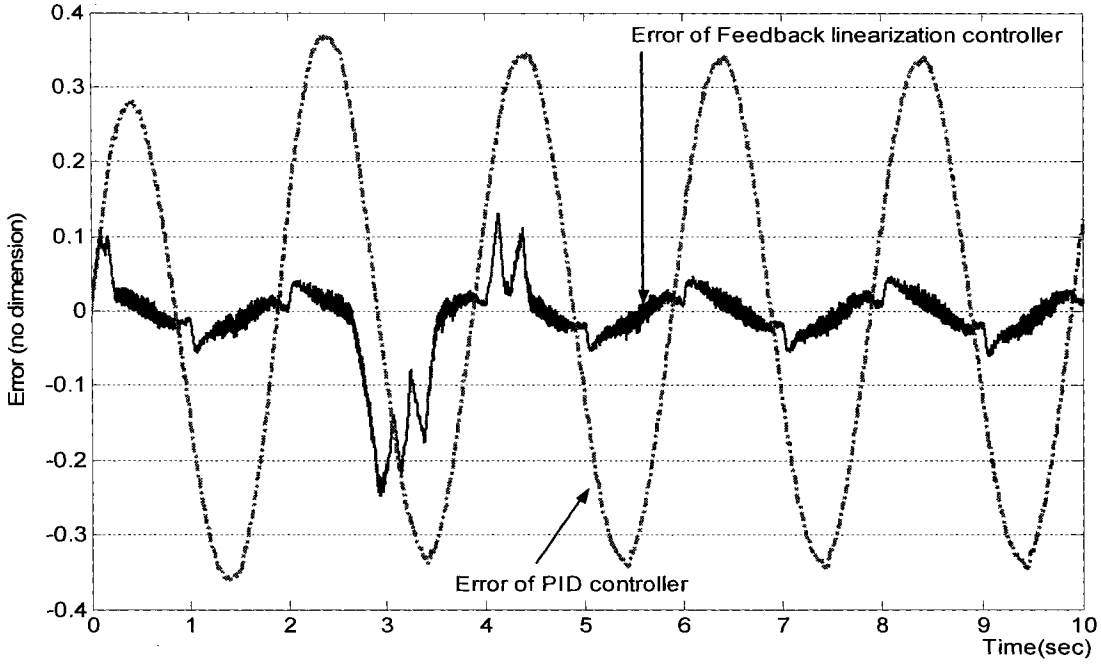

Figure 62 Error comparison of feedback linearization based controller and PID controller (Case 2-1)

From Figure 61 and Figure 62, the output of the feedback linearization based controller follows its reference very closely, with an error at the maximum of +0.04 and an error at the minimum of -0.05 after 0.3 sec, except for the interval between 2.5 and 4.5 sec where we see some unexpected fluctuations. This output error (as a percentage) for angular velocity is much smaller than the error for the case of angular displacement control. This difference may be attributed to the fact that the angular velocity is directly measured using a sensor while the angular displacement is obtained by calculation.

When we consider the slow response (i.e., PID: 5 sec vs. Feed.: 0.3 sec for the time to reach steady-state), the inaccuracy (i.e., PID: error of maximum +0.342 and minimum −0.345 vs. Feed.: error of maximum +0.04 and minimum -0.05) and the delay (i.e., PID: 0.5 sec vs. Feed.: 0 sec) of the PID controller, it is evident that the feedback linearization based controller is superior to the PID controller for angular velocity control of the rotational hydraulic drive.

▫ Comparison of control signals between the two controllers (Case 2-1)

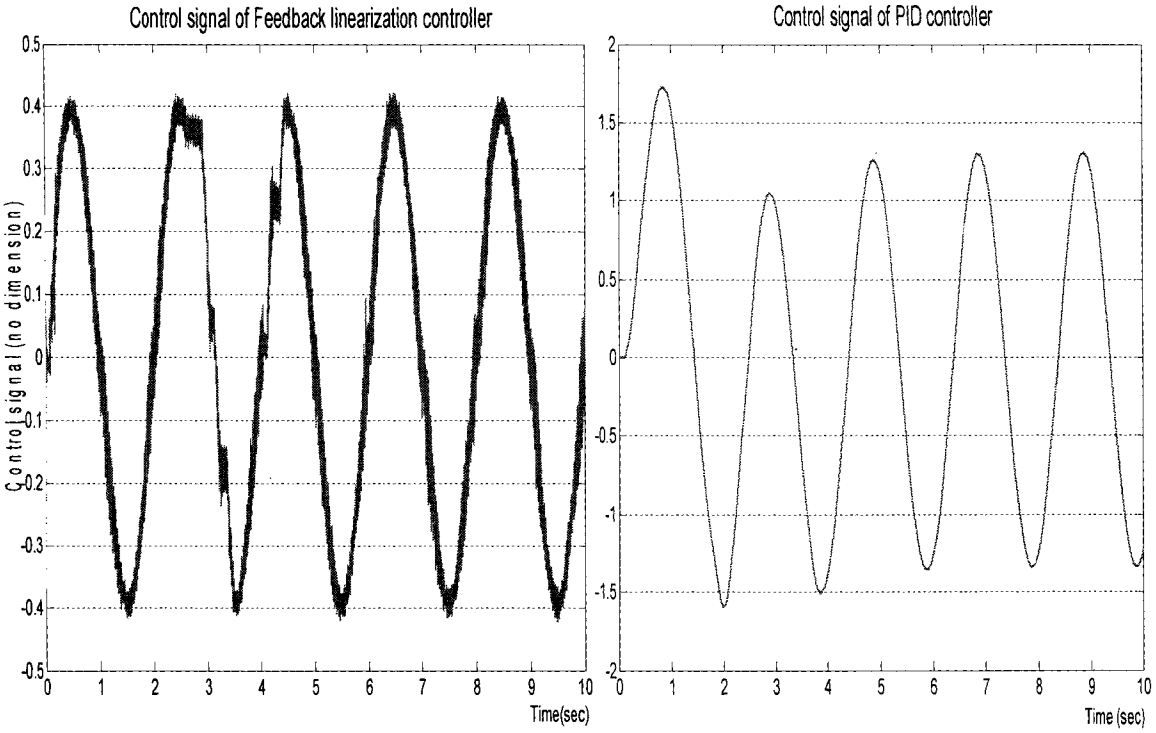

Figure 63 Comparison of control signals between the two controllers (Case 2-1)

From the figures above, we note that the feedback linearization based controller provides a lower amplitude signal with a shorter transient, leading to better transient performance.

▫ Comparison of Feedback linearization based controller and PID controller (Case 2-2)

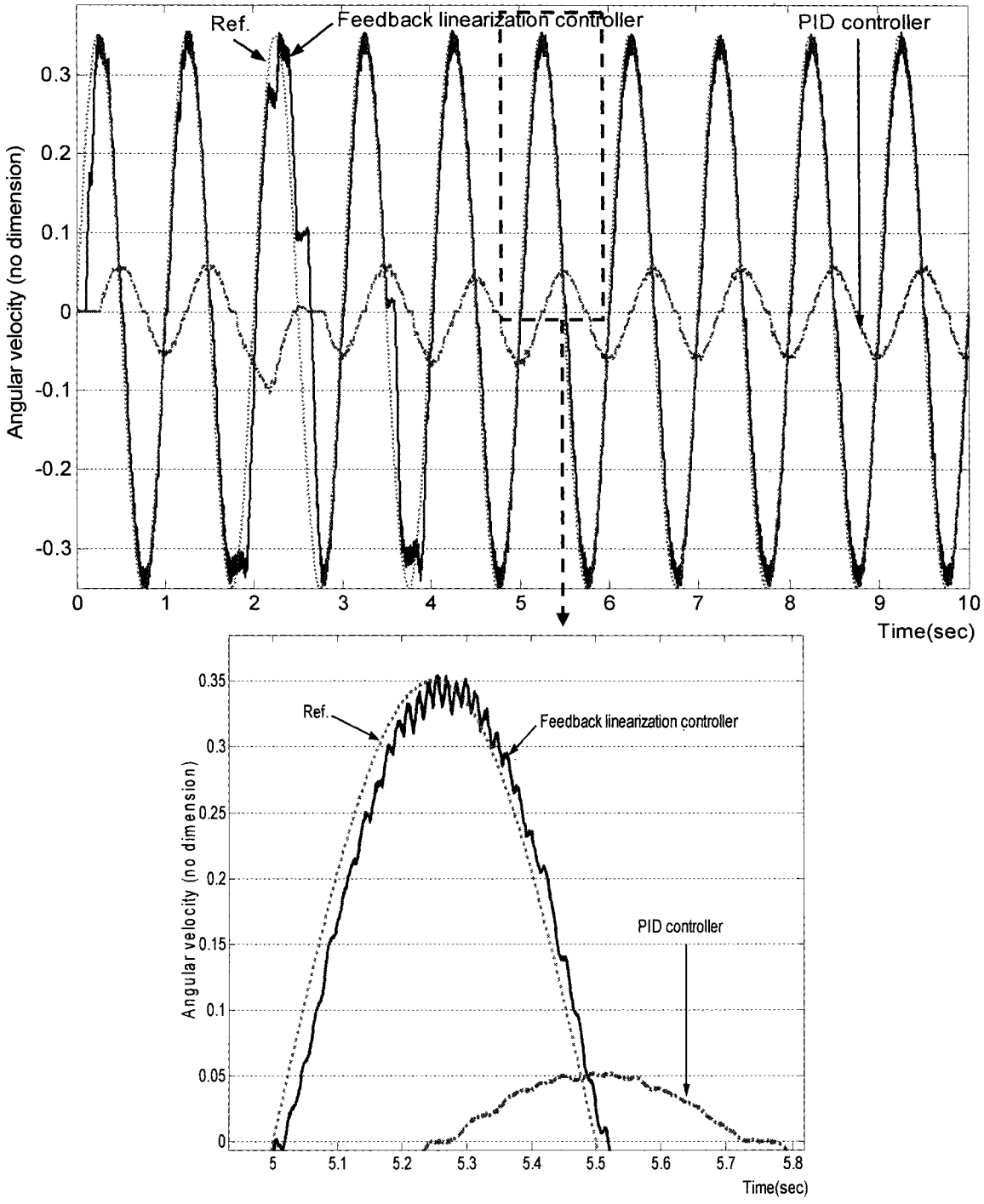

Figure 64 Comparison of real-time simulation results between feedback linearization based controller and PID controller (Case 2-2)

▫ Comparison of each controller's error (Case 2-2)

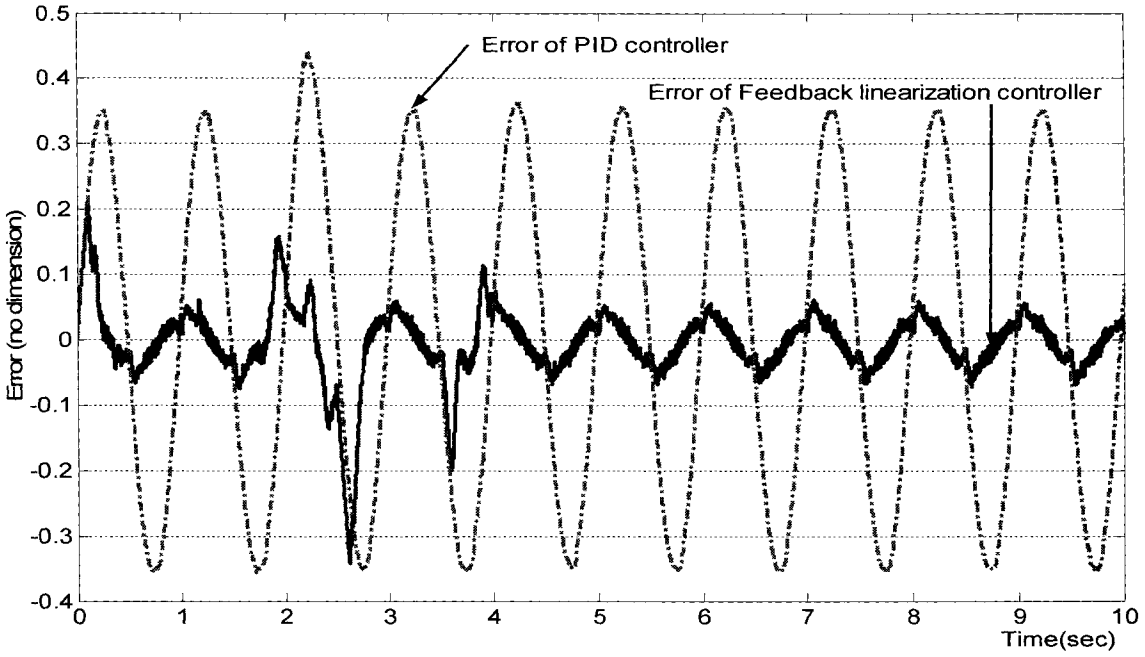

Figure 65 Error comparison of feedback linearization based controller and PID controller (Case 2-2)

In comparison with case 2-1, the feedback linearization based controller for angular velocity control yields satisfactory results without any noticeable change, even when the frequency of the reference signal is changed. The response rate and range of error are nearly identical to those in case 2-1.

This change in the frequency of the reference does not cause any remarkable change to the PID controller's accuracy (i.e., case 2-1: error at maximum +0.342 and error at minimum −0.345 vs. case 2-2: error at maximum +0.352 and error at minimum −0.352) and response time (case 2-1: 5 sec vs. case 2-2: 5 sec) either.

▫ Comparison of Feedback linearization based controller and PID controller (Case 2-3)

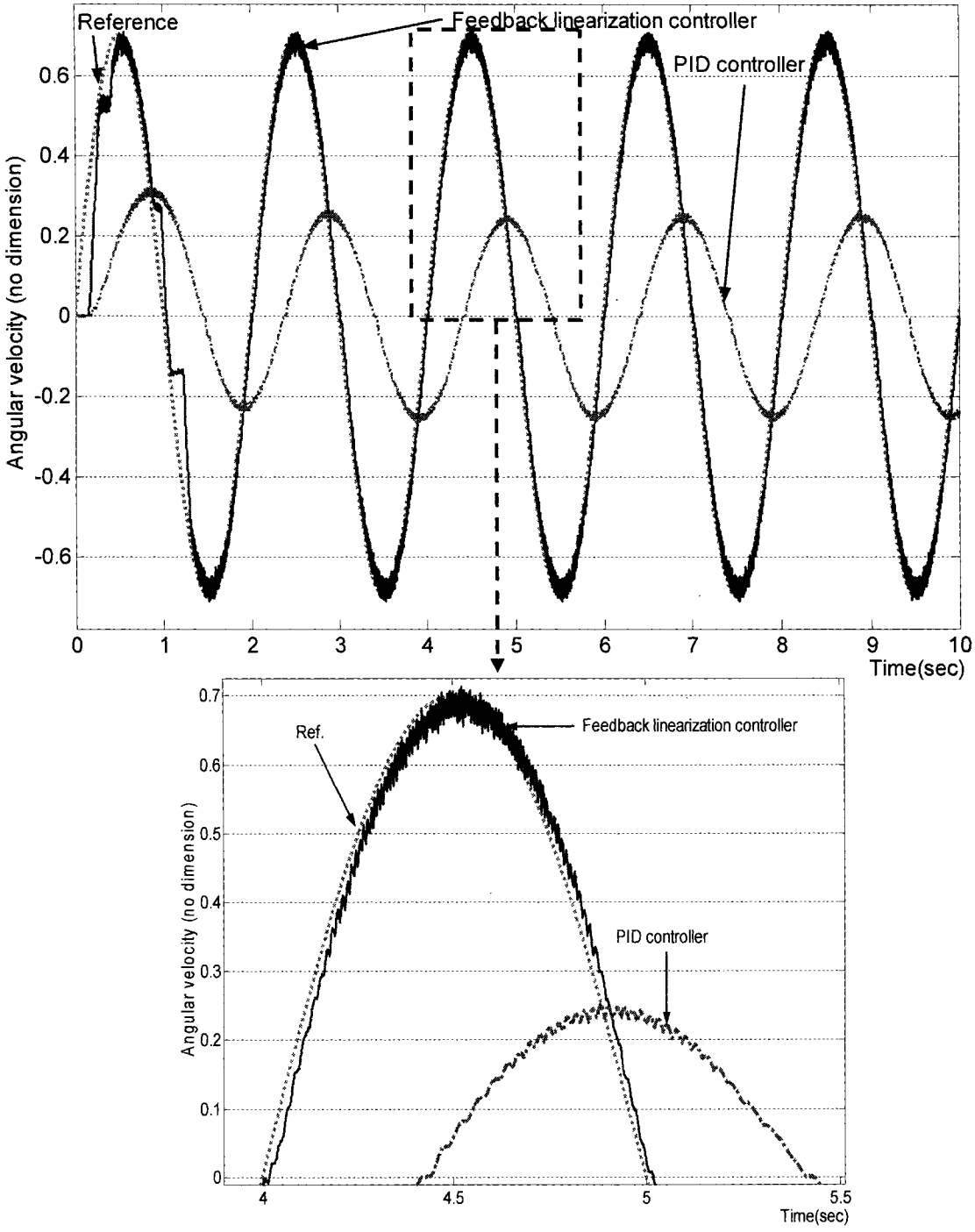

Figure 66 Comparison of real-time simulation results between feedback linearization based controller and PID controller (Case 2-3)

▫ Comparison of each controller's error (Case 2-3)

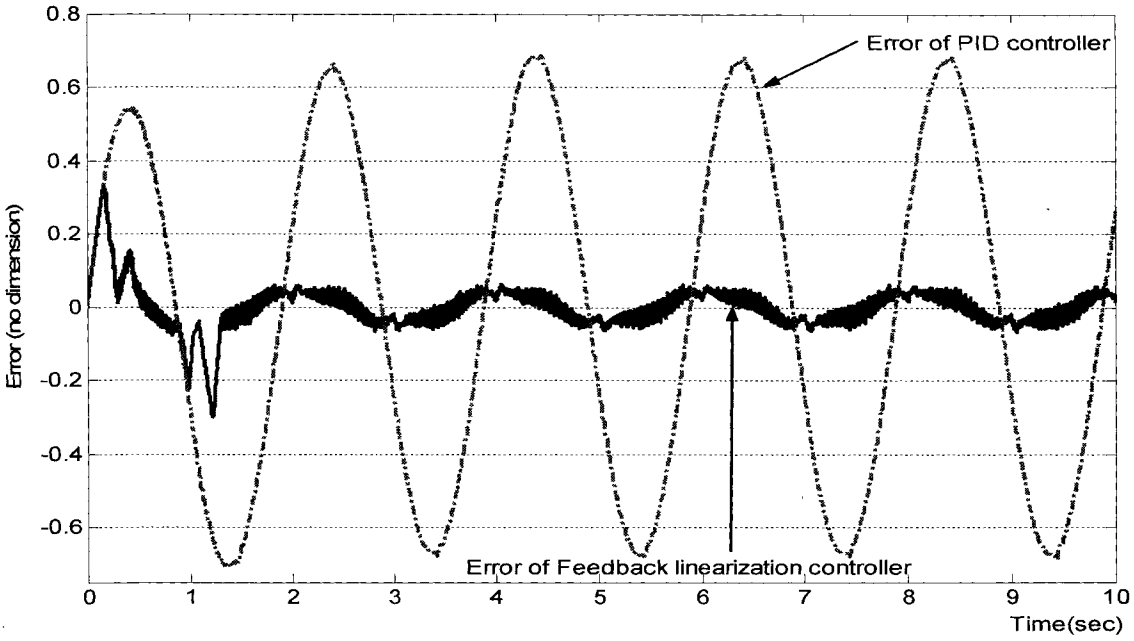

Figure 67 Error comparison of feedback linearization based controller and PID controller (Case 2-3)

Comparing the results above with those of case 2-1, we note that doubling the reference's amplitude does not induce any notable change in terms of response rate and precision for the feedback linearization based controller.

For the same reference condition change, the output error of the PID controller increases by a factor of two approximately (i.e., case 2-1: error at maximum +0.342 and error at minimum −0.345 vs. case 2-3: error at maximum +0.68 and error at minimum −0.68). The response time of the PID controller is almost the same in both case 2-1 and case 2-3. Thus, the change in the reference's amplitude lowers the accuracy of the PID controller.

By comparing the performance of each controller (PID and feedback linearization based controller), we note that the feedback linearization based controller has higher tracking performance for angular velocity control than the PID controller in the case of output reference with the amplitude doubled.

- **Load pressure difference**

  - Comparison of Feedback linearization based controller and PID controller (Case 3-1)

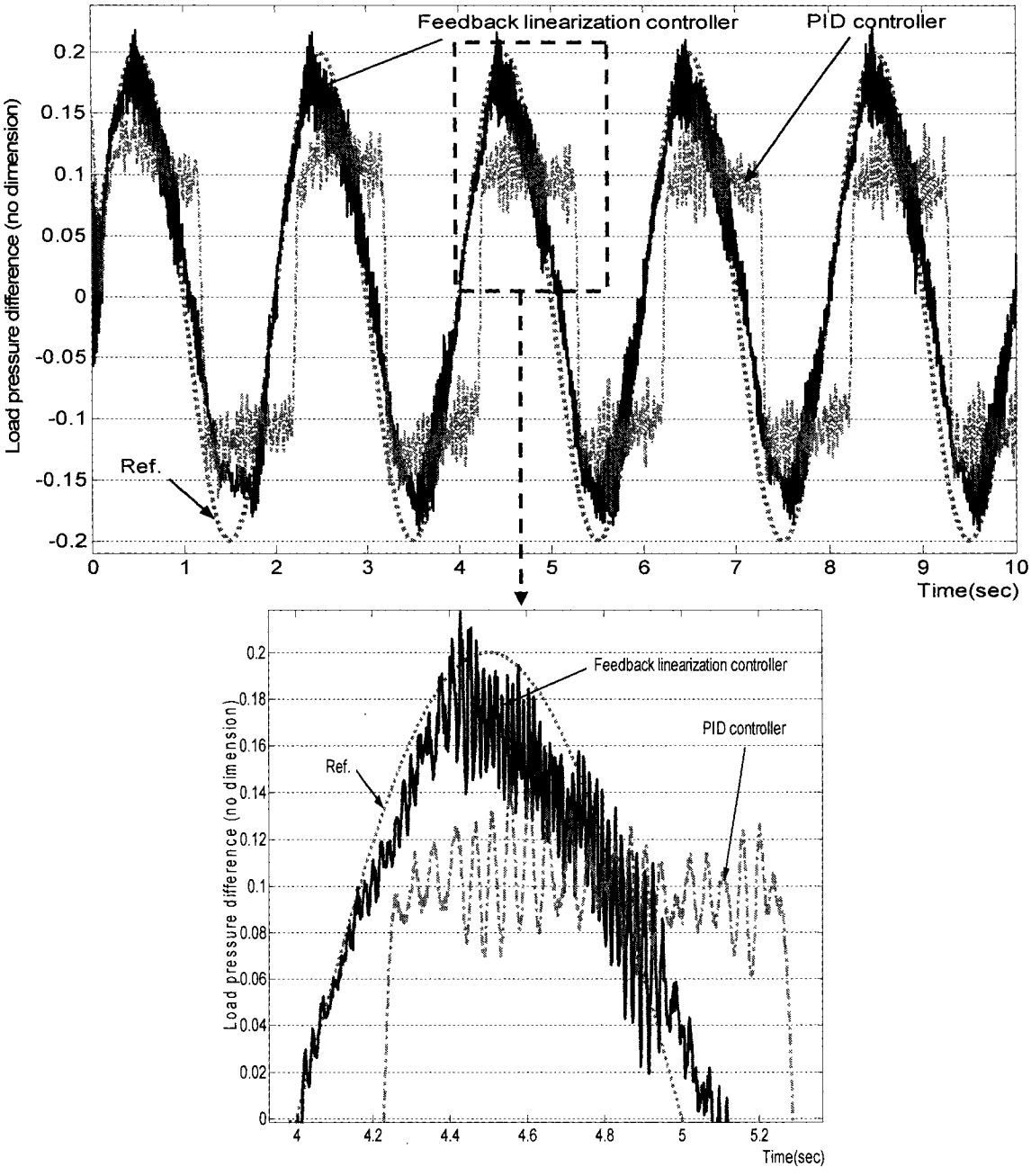

Figure 68 Comparison of real-time simulation results between feedback linearization based controller and PID controller (Case 3-1)

▫ Comparison of each controller's error (Case 3-1)

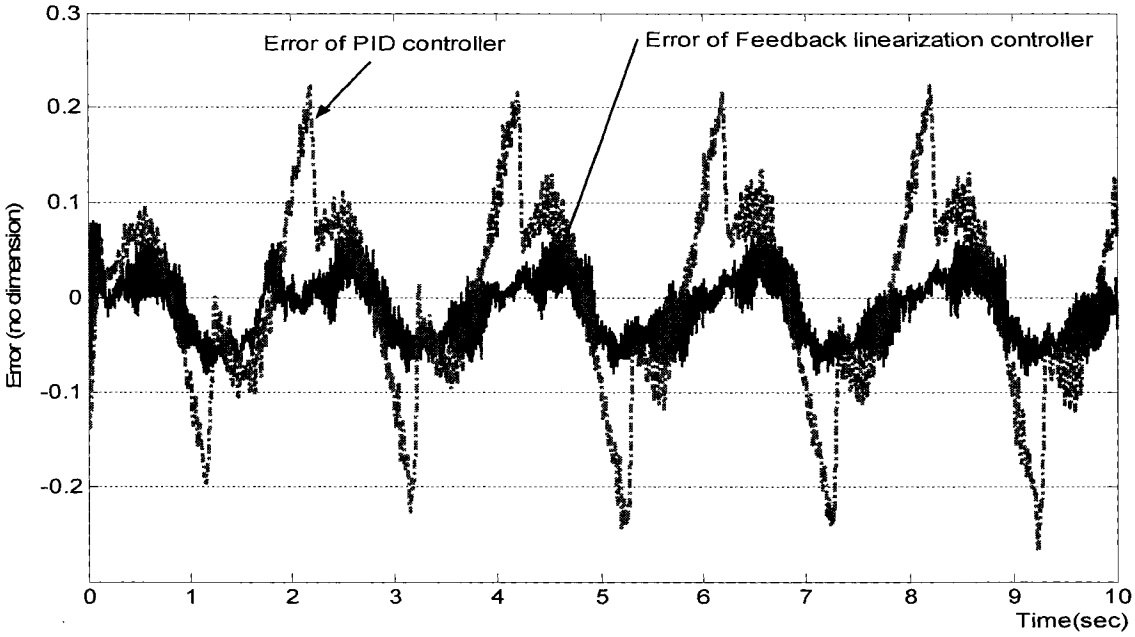

Figure 69 Error comparison of feedback linearization based controller and PID controller (Case 3-1)

In Figure 68, we notice that although we achieve effective tracking of the load pressure reference, there is noticeable high frequency jitter. This phenomenon can be explained by the fact that many factors (e.g., friction, mechanical dynamics, and viscosity of oil) affect pressure control, and thus, precise pressure tracking cannot be achieved easily in the real hydraulic system.

As shown in Figure 68 and Figure 69, our controller designed using feedback linearization theory provides quick response and high precision (i.e., error range: ± 0.05).

By comparing the control performance of the feedback linearization controller and the PID controller for load pressure control, we observe that the PID controller for pressure control results in a delay of 0.3 sec and an error range of $-0.24 \sim +0.225$, while the feedback linearization controller shows negligible error and delay .

▫ Comparison of control signals between the two controllers (Case 3-1)

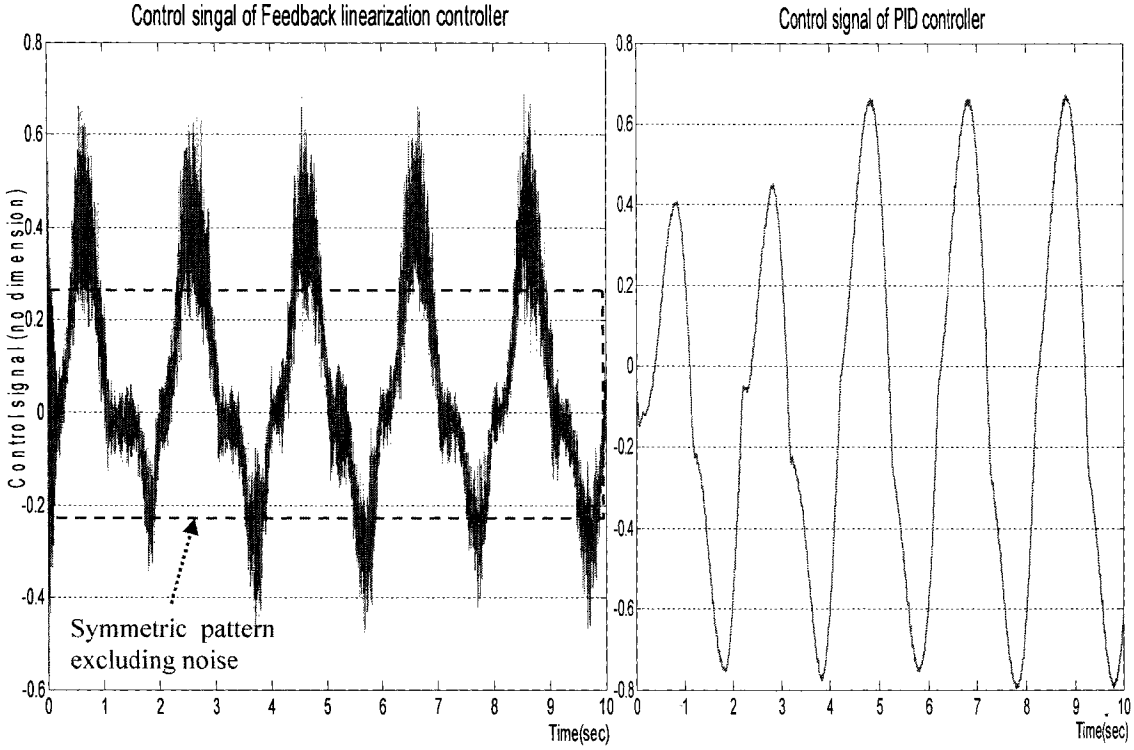

Figure 70 Comparison of control signals between the two controllers (Case 3-1)

The control signals generated by the two controllers are compared in Figure 70 and we note that if we neglect the high-frequency jitter in the control signal generated by the feedback linearization controller, it is steady with little variation in amplitude as opposed to the control signal generated by the PID controller.

▫ Comparison of Feedback linearization based controller and PID controller (Case 3-2)

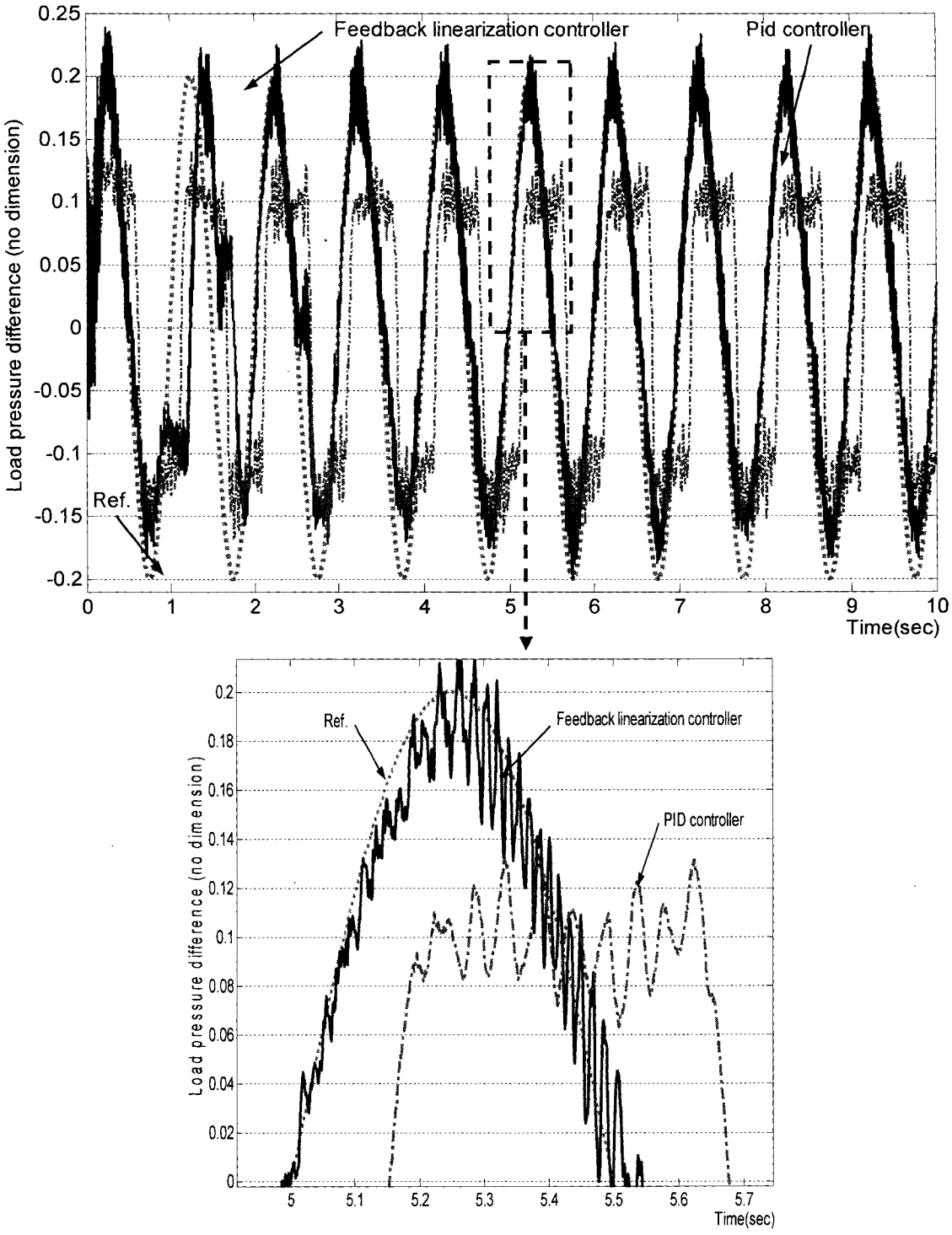

Figure 71 Comparison of real-time simulation results between feedback linearization based controller and PID controller (Case 3-2)

▫ Comparison of each controller's error (Case 3-2)

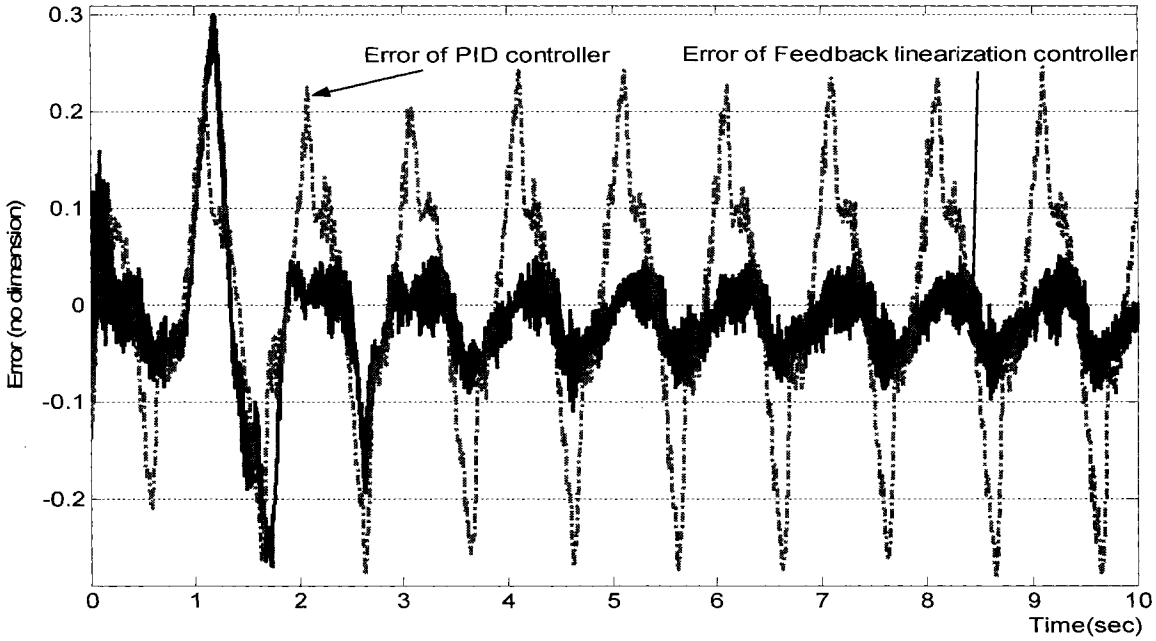

Figure 72 Error comparison of feedback linearization based controller and PID controller (Case 3-2)

In Figure 71 and Figure 72, we see that doubling the frequency of the output reference does not affect the response rate and error range of the feedback linearization controller when compared to case 3-1, except for a brief transient between the seconds 1 and 2. Thus, the feedback linearized controller provides good tracking performance of load pressure at higher frequencies.

For the PID controller we see that the delay in the output decreases to half that of case 3-1 (i.e., case 3-1: 0.3 sec vs. case 3-2: 0.15 sec) and the error range increases slightly (i.e., case 3-1: $-0.24 \sim +0.225$ vs. case 3-2: $-0.273 \sim +0.242$).

Once again, the performance of the feedback linearization controller is better than that of the PID controller.

▫ Comparison of Feedback linearization based controller and PID controller (Case 3-3)

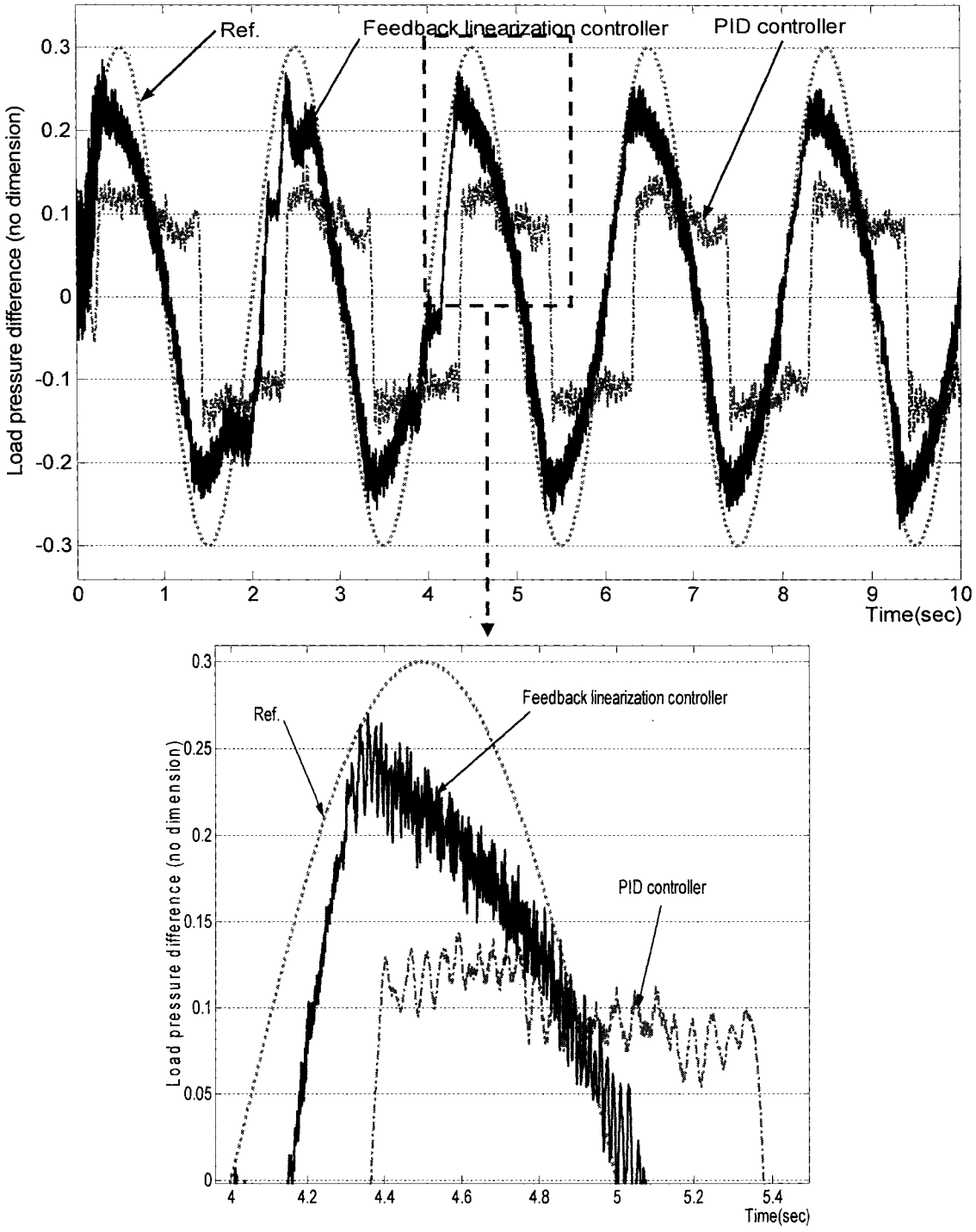

Figure 73 Comparison of real-time simulation results between feedback linearization based controller and PID controller (Case 3-3)

▫ Comparison of each controller's error (Case 3-3)

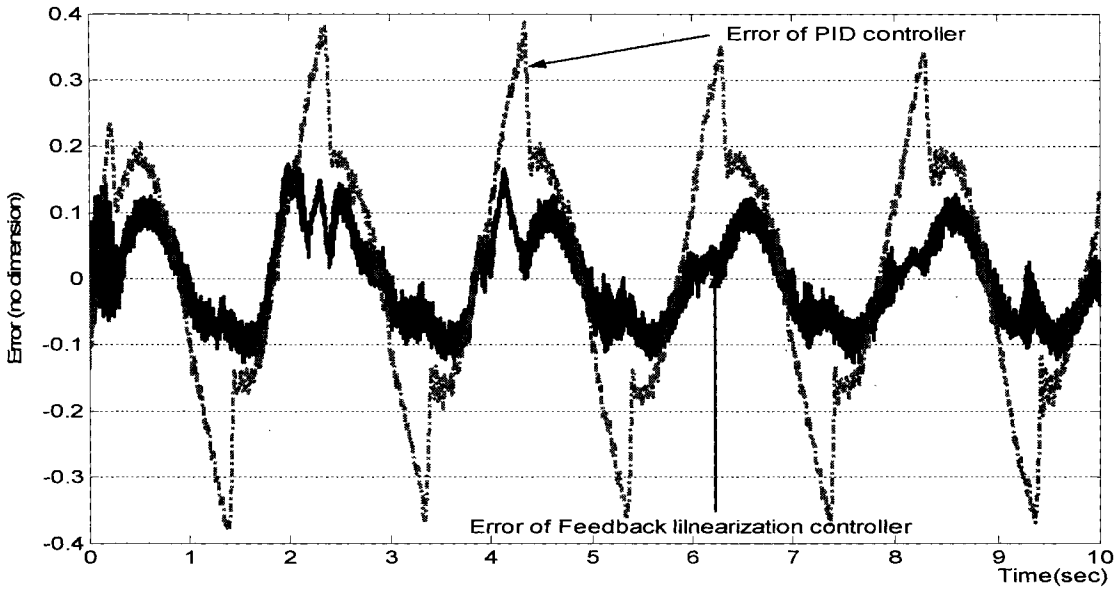

Figure 74 Error comparison of feedback linearization based controller and PID controller (Case 3-3)

In this case we increase the pressure reference's amplitude by a factor of 1.5. From Figure 74, we note that the output error of the feedback linearization based controller between reference and output is double that of case 3-1 (i.e., case 3-1: ±0.05 vs. case 3-3: ±0.1).

With the 1.5 times increase of reference amplitude, the PID controller shows a slightly longer delay (i.e., case 3-1: 0.3 sec vs. case 3-3: 0.4 sec) and an increased error range (i.e., case 3-1: −0.24 ~ +0.225 vs. case 3-3: −0.36 ~ +0.354), compared to case 3-1.

Based on the data plotted in Figures 73 and 74, we can conclude that the feedback linearized controller provides significantly better load pressure control performance than the PID controller for the real hydraulic system.

■ **Simulation results analysis**

The simulation results of feedback linearization based controller for each reference type are summarized in the following tables.

Table VI

Response of feedback linearization based controller for angular displacement control

Reference condition		Base	Double frequency	Double amp. (or ref. value)
Sinusoidal reference	Error range	-0.085 ~ +0.157	-0.13 ~ +0.15	-0.22 ~ +0.16
	Time to achieve steady-state	2.58 sec	0.5 sec	2.65 sec
Constant reference	Error range	0	N/A	0
	Time to achieve steady-state	4 sec	N/A	1 sec

Table VII

Response of feedback linearization based controller for angular velocity control

Sinusoidal reference condition	Base	Double frequency	Double amp.
Error range	-0.05 ~ +0.04	-0.055 ~ +0.06	-0.05 ~ +0.05
Time to achieve steady-state	0.3 sec	0.3 sec	0.3 sec

Table VIII

Response of feedback linearization based controller for load pressure control

Sinusoidal reference condition	Base	Double frequency	Double amp.
Error range	-0.05 ~ +0.05	-0.05 ~ +0.05	-0.1 ~ +0.1
Time to achieve steady-state	≅ 0 sec	≅ 0 sec	≅ 0 sec

For the sinusoidal cases of angular displacement, the error ranges are almost the same despite the variations in reference frequency and amplitude. The response is fastest when the frequency of the reference is doubled. For the constant reference case of angular displacement, the doubling of the reference value results in reduced time to reach steady-state.

Changes in the sinusoidal reference frequency and amplitude do not result in any distinctive changes in the error range and response time for angular velocity control.

In the case of pressure response, although the exact determination of the time to achieve steady-state is difficult due to the high frequency jitter, it is observed to be quite small. When the amplitude of the reference is doubled, the controller has the worst error range at twice the range observed in the other cases.

Compared with the results of velocity and pressure, the angular displacement data shows lower accuracy and response rate for all reference commands. The fact that there is no sensor to measure angular displacement and the use of numerical integration may contribute to this observation.

Based on the various experimental results for angular displacement, angular velocity and pressure difference control for a range of reference commands, we can definitively state that the feedback linearization controller provides better tracking performance in all cases.

CONCLUSIONS

The goal of this research is to understand the nonlinear nature of hydraulic system, study how these dynamics lead to limitations in PID controller performance, and to design and implement controllers appropriate for displacement, velocity and pressure control of a hydraulic drive. Feedback linearization theory is introduced as a nonlinear technique to accomplish this goal in our study, and the controllers designed using this theory are validated using two methods, namely numerical simulation and experimental tests, and the performance of these controllers are compared to the performance of PID controllers.

Using Simulink simulation, we presented the limitations of PID control and the suitability of our selected theory for nonlinear system control. Next, we showed the superior performance of the feedback linearization based controller using real-time simulation on a test bench at LITP. For several types of reference commands, the feedback linearization based controller showed significantly better tracking performance in terms of response time and tracking error, when compared to a corresponding PID controller for the real hydraulic system.

From these comprehensive tests, we conclude that for hydraulic systems that have nonlinear characteristics, feedback linearization theory provides a powerful control strategy that clearly improves the tracking precision and response rate of the closed-loop system.

Our study is limited to the control of a rotational hydraulic drive. Therefore, the application of feedback linearization theory to the control of linear hydraulic cylinders or the control of more complex integrated rotational and linear drives may be considered as future extensions of this work. The results of this thesis are expected to make a practical contribution to various industrial hydraulic applications.

ANNEX 1

HYDRAULIC SERVO-SYSTEM PARAMETERS

Parameter	Value
τ_v	0.01 sec
$I_{\max}$	10 mA
K_a	0.1351 V/mA
J	0.004821 Nms^2
B	0.0766 Nms
$A_{v\max}$	7.94×10^{-6} m^2
ρ	867 kg/m^3
β	7.995×10^{8} N/m^2
C_L	9.047×10^{-13}(m^3/s)/(N/m^2)
C_d	0.61
V	1.354×10^{-4} m^3
P_s	8.73×10^{6} N/m^2
D_m	2.802×10^{-6} m^3/rad
T_L	0 Nm
Q_s	4.8601×10^{-4} m^3/s
ω_h	138.68 rad/s
$\omega_{\max}$	173.45 rad/s
α	4.7408
γ	0.5432
c_L	0.0770
t_L	0

ANNEX 2

PROGRAM IN MATLAB

- **Feedback linearization based controller for angular displacement, velocity and load pressure control**

```
J=0.004821; % inertia load
b=0.0766; % Viscous damping coefficient
Avmax=7.94*10^(-6); % maximum servo-valve opening
row=867;%  fluid mass density
be=7.995*10^(8); % fluid bulk modulus
Cl=9.047*10^(-13); % leakage coeff.
Cd=0.61; %flow discharge coeff.
V=1.354*10^(-4); %*(7)^(-1/2); % actuator chamber volume

Ps=8730000; % supply pressure
Qs=Cd*Avmax*(Ps/row)^(1/2); % maximum supply flow for finding Wmax
Dm=2.802*10^(-6); % volumetric displacement of motor (m^3/rad)


Zv=0.01; % servo-valve time contant.
Wh=(2*be*(Dm)^2/(J*V))^(1/2); % Hydraulic natural frequency
alp=J*Wh*Qs/(Ps*(Dm)^(2)); % inertia load factor(dimensionless)
cL=J*Cl*Wh/(Dm^(2)); % Leakage load factor
Wmax=Qs/Dm; % maximum angular velocity
r=b*Wmax/(Ps*Dm); % viscous load factor

Imax=10;     % maximum servo-valve input current
a=700; % factor of sigmoid function
tL=0; % dimensionless torque

% for angular displacement control
K1=2e+8; % for condition of K vector
```

```
K2=2e+7; % for condition of K vector
K3=5e+5; %for condition of K vector
K4=1e+2; %for condition of K vector

y1=-(K2-K3*K4) % for Routh-Hurwitz
y2=(K1*K4^2+K2*(K2-K3*K4))/(K2-K3*K4) % for Routh-Hurwitz

A=1; % amplitude of sinusoidal reference
B=pi; % frequency of sinusoidal reference

% for angular velocity control
K1=2.5e+6; % for condition of K vector
K2=2e+5; % for condition of K vector

y1=-(K1-K2*K3) % for Routh-Hurwitz

A=0.35; % amplitude of sinusoidal reference
B=pi; % frequency of sinusoidal reference

% for load pressure control
K1=5e+5; % for condition of K vector
K2=1.25e+3; % for condition of K vector

A=0.2; % amplitude of sinusoidal reference
B=pi; % frequency of sinusoidal reference
```

REFERENCES

[1] Mohamed A Ghazy, *"Variable structure control for electrohydraulic position servo system,"* IECON Proceedings (Industrial Electronics Conference), vol. 1, pp. 2194-2198, 2001.

[2] V. N. a. D. A. Miroslav M., *"Position control of an electro hydraulic servo system using sliding mode control enhanced by fuzzy PI controller,"* Mechanical Engineering, vol. 1, pp. 1212-1230, 2002.

[3] Hong Sun and George T.-C. Chiu, *"Nonlinear observed based force control of Electro-hydraulic actuators,"* Proceedings of the American Control Conference, San Diego, California, June 1999.

[4] Takahiro S. and Kendo U., *"Gain-scheduled velocity and force controllers for electrohydraulic servo system,"* Electrical Engineering in Japan, vol. 146, pp. 65-73, 2004.

[5] Rui Liu and Andrew Alleyne, *"Nonlinear Force/Pressure tracking of an electro-hydraulic actuator,"* Transactions of the ASME, vol. 122, pp. 232-237, 2000.

[6] Mihailo Jovanovic, *"Nonlinear Control of an Electrohydraulic Velocity Servo system,"* Proceedings of the American Control Conference Anchorage, May, 2002.

[7] I. Ursu, F. Popescu, *"Backstepping control synthesis for position and force nonlinear hydraulic servoactuators,"* 10th International Conference on Applied and Industrial Mathematics, Pitesti, Romania, October 11-13, 2002.

[8] Kaddissi C. J.-P. Kenné and M. Saad, *"Position Control of an Electro-Hydraulic Servosystem - A Non-Linear Backstepping Approach,"* ICINCO (2) -International Conference on Informatics in Control, Automation and Robotics, 2004.

[9] J. Chiriboga, Thein, May-Win L., Misawa, Eduardo A., *"Input-output feedback linearization control of a load-sensing hydraulic servo system,"* IEEE Conference on Control Applications - Proceedings, pp. 910, 1995.

[10] R. M. H. C. a. K. H. L. S. LeQuoc, *"Tuning electrohydraulic servovalve to obtain high amplitude ratio and low resonance peak,"* The journal of fluid control, vol. 20, pp. 30-47, 1990.

[11] Z. Yongqian, LeQuoc, S. and Saad, M., *"Nonlinear fuzzy control on a hydraulic servo system,"* Proceedings of the 1998 American Control Conference (IEEE Cat. No.98CH36207), Philadelphia, PA, USA, 1998.

[12] C. A. Rabbath, H. Desira, and K. Butts, *"Effective modeling and simulation of internal combustion engine control systems,"* Proceedings of the American Control Conference, vol. 2, pp. 1321, 2001.

[13] Y. Sugahara, T. Endo, H.-O. Lim, and A. Takanishi, *"Control and experiments of a multi-purpose bipedal locomotor with parallel mechanism,"* Proceedings - IEEE International Conference on Robotics and Automation. Arlington, VA: Institute of Electrical and Electronics Engineers Inc., vol. 3, pp. 1326, 2003.

[14] A. L. B. A. Tsourdos, Brian A. White, *"Fight control design for a missile. An approximate feedback linearization approach,"* Proceedings of the 7th Mediterranean Conference on Control and Automation. Haifa, Israel, June 2-30, 1999.

[15] A. Alleyne and R. Liu, *"A simplified approach to force control for electro-hydraulic systems,"* Control Eng. Pract. (UK), vol. 8, pp. 1347, 2000.

[16] W. Anderson, *Controlling electrohydraulic systems*: M. Dekker, 1988.

[17] T. L. Chern and Y. C. Wu, *"Design of integral variable structure controller and application to electrohydraulic velocity servosystems,"* IEE Proc. D, Control Theory Appl. (UK), vol. 138, pp. 439, 1991.

[18] B. Friedland, *Control system design*: McGraw-Hill, 1986.

[19] E. A. P. a. R. Guenther, *"Control of a servopneumatic drive with friction compensation,"* 1st FPNI-PhD Symp. Hamburg, pp. 117-127, 2000.

[20] A. Guesalaga, *"Modelling end-of-roll dynamics in positioning servos,"* Control Eng. Pract. (UK), vol. 12, pp. 217, 2004.

[21] M. Hamdan and G. Zhiqiang, *"A novel PID controller for pneumatic proportional valves with hysteresis,"* Conference Record of the 2000 IEEE Industry Applications Conference. Thirty-Fifth IAS Annual Meeting and World Conference on Industrial Applications of Electrical Energy (Cat. No.00CH37129). vol.2, pp. 1198, 2000.

[22] Y. B. He, P. S. K. Chua, and G. H. Lim, *"Performance analysis of a two-stage electrohydraulic servovalve in centrifugal force field,"* Trans. ASME, J. Fluids Eng. (USA), vol. 125, pp. 166, 2003.

[23] J. E. Johnson, *Electrohydraulic servo systems*, 2nd ed: Penton IPC., 1977.

[24] O. Keles and Y. Ercan, *"Theoretical and experimental investigation of a pulse-width modulated digital hydraulic position control system,"* Control Eng. Pract. (UK), vol. 10, pp. 645, 2002.

[25] H. K. Khalil, *Nonlinear systems*, 3rd ed: Prentice Hall, 2002.

[26] M. B. K. Krstic, Ioannis Bouquiner; Kokotovic Petar V, *Nonlinear and adaptive control design*: J. Wiley and Sons, 1995.

[27] P. Y. Li, *"Dynamic redesign of a flow control servovalve using a pressure control pilot,"* Trans. ASME, J. Dyn. Syst. Meas. Control (USA), vol. 124, pp. 428, 2002.

[28] H. E. Merritt, *Hydraulic control systems*: New York, N.Y.: J. Wiley and Sons, 1967.

[29] N. Niksefat and N. Sepehri, *"Robust force controller design for an electro-hydraulic actuator based on nonlinear model,"* Proceedings - IEEE International Conference on Robotics and Automation, vol. 1, pp. 200, 1999.

[30] N. Niksefat and N. Sepehri, *"Design and experimental evaluation of a robust force controller for an electro-hydraulic actuator via quantitative feedback theory,"* Control Eng. Pract. (UK), vol. 8, pp. 1335, 2000.

[31] N. S. B. Nise, *Control Systems Engineering*, 4th ed: Wiley, 2004.

[32] F. D. Norvelle, *Electrohydraulic control systems*: Prentice-Hall, 2000.

[33] K. Ogata, *Modern control engineering*, 4th ed: Prentice-Hall, 2002.

[34] M. C. Shih and C. K. Chen, *"An experimental study on the hydraulic oscillator position control by using the model-following optimal control method,"* Mechatronics (UK), vol. 2, pp. 375, 1992.

[35] S. M. Shinners, *Advanced modern control system theory and design*: J. Wiley and Sons, 1998.

[36] M. R. Sirouspour and S. E. Salcudean, *"On the nonlinear control of hydraulic servo-systems,"* Proceedings - IEEE International Conference on Robotics and Automation, vol 2, p 1276-1282, 2000.

[37] I. Ursu, F. Popescu, & Ursu, F, *"Control synthesis for electrohydraulic servo mathematical model,"* 11th International Conference on Applied and Industrial Mathematics. Oradea, Romania, May 29-31, 2003.

[38] G. W. Younkin, *Industrial servo control systems*, 2nd ed: New York, 2003.